Journal of Neonatal Surgery
ISSN(Online): 2226-0439
Vol. 14, Issue 32s (2025)
https://www.jneonatalsurg.com

OPEN ACCESS

Comparative Study Of Ct And 1.5 Tesla Mri In Quantitative Estimation Of Bone Mineral Density In Lumbar Spine

Ishant[1*], Raushan Kumar[2]

[*1]M.Sc. Research fellow, Department of Radiological and Imaging Techniques, College of Paramedical Sciences, Teerthanker Mahaveer University, Moradabad, Uttar Pradesh, 244001.

Email ID: sharmaishant2311@gmail.com

[2].Assistant Professor, Department of Radiological and Imaging Techniques, College of Paramedical Sciences, Teerthanker Mahaveer University, Moradabad, Uttar Pradesh, 244001.

Email ID: raushank.paramedical@tmu.ac.in

***Corresponding Author:**

Ishant

M.Sc. Research fellow, Department of Radiological and Imaging Techniques, College of Paramedical Sciences, Teerthanker Mahaveer University, Moradabad, Uttar Pradesh, 244001.

Cite this paper as: Ishant, Raushan Kumar, (2025) Comparative Study Of Ct And 1.5 Tesla Mri In Quantitative Estimation Of Bone Mineral Density In Lumbar Spine. *Journal of Neonatal Surgery*, 14 (32s), 993-1060.

ABSTRACT

The effectiveness of 1.5 Tesla magnetic resonance imaging (MRI) and quantitative computed tomography (QCT) for determining bone mineral density (BMD) in the lumbar spine of 44 patients (22 males, 22 females; mean age 46.02 ± 11.14 years) from Western Uttar Pradesh was compared in this prospective cross-sectional study, which was carried out at Teerthanker Mahaveer Hospital and Research Centre in Moradabad, India. Hounsfield Units (HU), QCT-derived BMD, and MRI signal intensities (T1-weighted, T2-weighted, gradient echo) among the L1–L5 vertebrae were among the measurements. Significant age-related differences ($p < 0.05$) were noted in T1, T2, HU, and QCT-BMD at particular lumbar levels, but no significant gender differences were reported in imaging parameters or BMD ($p > 0.05$). The sensitivity of MRI to bone marrow changes was demonstrated by Pearson correlation analysis, which revealed negative correlations between T1/T2 signal intensities and QCT-BMD and positive correlations between HU and QCT-BMD. 50% gender prediction accuracy was attained via binary logistic regression (100% for females, 0% for males). Despite drawbacks such geographical bias and small sample size, the results demonstrate MRI's potential as a radiation-free substitute for DEXA and validate CT's dependability for BMD evaluation. To improve diagnostic accuracy, future research should investigate larger cohorts and more sophisticated MRI techniques.

Keywords: *Bone Mineral Density (BMD), Lumbar Spine, Quantitative Computed Tomography (QCT),1.5 Tesla MRI, Hounsfield Units (HU), T1-weighted Imaging, T2-weighted Imaging, Gradient Echo (GRE), Osteoporosis, Osteopenia, DEXA (Dual-energy X-ray Absorptiometry), Age-related Differences, Gender Differences, Pearson Correlation, Binary Logistic Regression, Western Uttar Pradesh, Cross-sectional Study, Prospective Study, Imaging Parameters. Trabecular Bone, Cortical Bone, Radiation-free Imaging, Volumetric QCT, Single-slice QCT, Phantom Technique, Calcium, Phosphorus, Bone Marrow, MRI Signal Intensity, CT Reconstruction, Postmenopausal Women, Bone Health, FRAX (Fracture Risk Assessment Tool), T-score, Z-score, Estrogen, Testosterone, Spinal Deformities, PSS Analysis, Independent Sample t-test, One-way ANOVA.*

1. INTRODUCTION

Computed tomography is a modality used in the radiology department, which employs ionizing radiation to produce cross sectional images of an item.

1.1: HISTORY

In 1960's electric and music industries (EMI), who also owned the Abby road, studies used the Beatles concert to raise funds for the research of the first EMI Scanner. The primary credit for the invention of the CT scan goes to British engineer Sir Godfrey Newbold Hounsfield, although physicist Dr. Allan Cormack also made a significant contribution. When body.

section radiography first emerged in the early 1920s, the term "tomography" was coined. Later in 1935 Sir Grossman labelled tomography as a section

Watson in 1937 developed a technique in which the sections were cross-rational and it was referred to as transverse axial tomography. However, they were of little use in diagnostic radiology because of the images' lack of clarity and details. In addition to these advancements, a number of mathematical algorithms were being developed that were intended to reconstruct an object's image from multiple projections. Combining all the mentioned innovations in 1967, Hounsfield merged reconstruction techniques to tomography equipment and presented the world's first clinically useful CT Scan which was used for the imaging of Brain.

Several imaging techniques were employed in the early CT scans, such as placing the X-ray source inside the patient in some cases and placing it outside the patient in others, akin to an X-ray machine. In 1973 Hounsfield published his research in the British Journal of Radiology and named it Computerized Transverse axial scanning. In addition to this, the CT scan was also known by a number of other names, including Transmission Reconstructed Tomography, Computer Assisted Tomography, and Computerized Transaxial. Ultimately, the (RSNA) Radiological Society of North America trademarked the term "computed tomography," which became widely recognized. In 1972, EMI Lab introduced the first EMI scanner. For this invention, Sir Godfrey Hounsfield and Dr. Allen Cormack shared the 1979 Nobel Prize in Physiology and Medicine. [1]

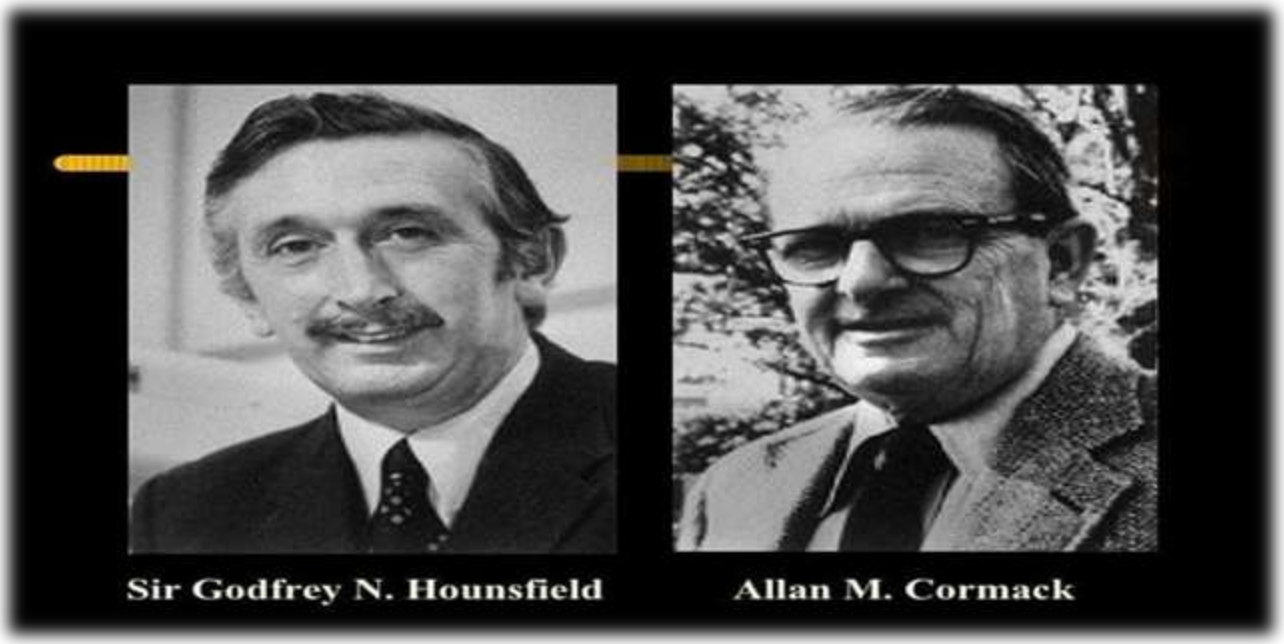

Figure 1.1: Godfrey Newbold Hounsfield(left) and Allan Macleod Cormack (Right)

PIONEER SCAN

On October 1, 1971, Dr. James Ambrose became the first physician to use the EMI scanner, which was still in its infancy. It took a day to acquire the data from the first scan of a female patient with a brain tumour. since the x-ray tube and detector had a one-degree rotational translation motion. A few more days will be needed later for the image reconstruction.

1.2: CT PRINCIPLE

The basic idea behind the CT modality is that it can determine the precise anatomical structure of a body part that can be recreated from multiple projections of that body part. This means that an object is scanned from various angles, and then an algorithm for reconstruction combines all of the projections from various angles to create an image.

This makes more sense when compared to X-ray projection. An x-ray source, an item to be scanned, and an image receptor are the three components of radiography. After being exposed from the tube, X-rays travel through the item and land on the image receptor, where they are processed to produce an X-ray image. This image is a 2D depiction since it was captured from a single projection, which only displays one dominating projection (AP, Lat., etc.).

In contrast, we take many projections during a CT scan rather than just one. An X-ray tube is rotated in a circular motion around the subject to accomplish this.

Together, the detectors and the X-ray tube catch the transmitted X-rays and transform them into signals. The quantity of these detectors varies from seller to vendor and from generation to generation.

Rotate-translate motion was a feature of previous generations of X-ray tubes, meaning that the aligned detector translates along the route after the X-ray tube has rotated. Later slip rings were added to CT scanners because this method was time-consuming. The X-ray tube, detector array, generator, and a few other important parts were connected to the slip ring once it was introduced. The X-ray tube and detector circle constantly around the patient while the slip ring rotates around them. The volumetric data collected because of this continuous data collecting shortened the scan duration and was subsequently processed by a reconstruction technique for multiplanar and three-dimensional representation.

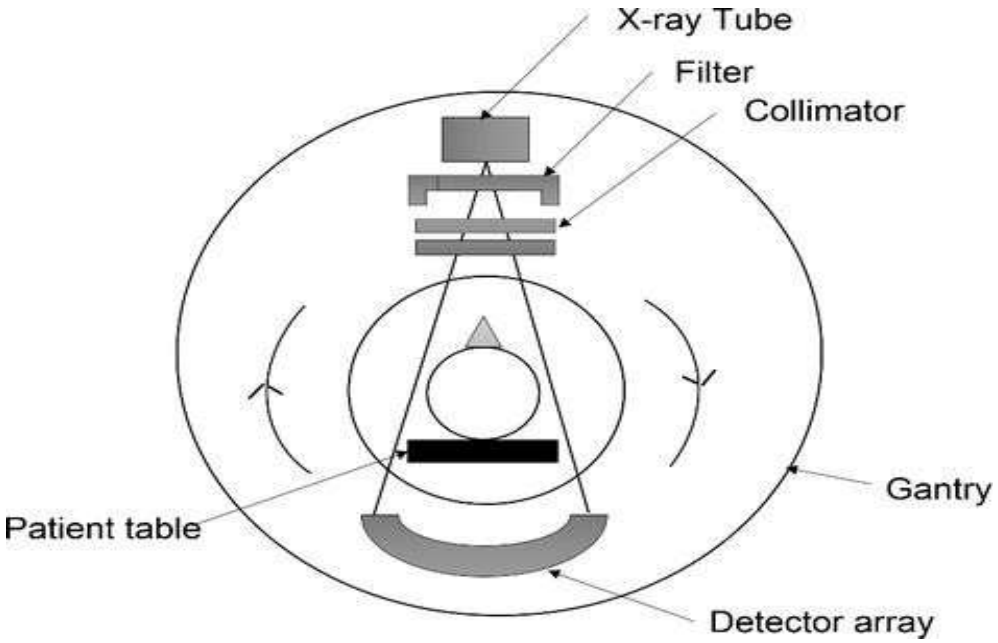

Figure 1.2: CT scan Principle

1.3: STEPS INVOLVED IN CT SCAN

1) Data Acquisition: The patient is positioned in the middle of the gantry during a CT scan, and the detection system gathers the transmitted X-rays from the patient. There are two methods for acquiring data: volumetric data acquisition, which is used in multi-detection CT scans, or slice-by-slice, which was used in conventional X-rays.

The X-ray tube and detector move simultaneously to gather data for each slice during the slice-by-slice collection process. The data is then transmitted to a computer system for reconstruction.

The patient sofa then moved, and data is collected once more. This process is repeated until the scan is finished.

However, a drawback of the typical unit is that anatomical features are overlooked because of patient movements because scan times are lengthy, which also causes stair step artifact.

For volume acquisition, the tube and detector moved continuously in a spiral motion, scanning the complete body area rather than slice by slice. The benefit of volumetric data for post-processing resulted from this.

2) CONVERSION OF LINEAR ATTENUATION COEFFICIENT IN CT NUMBER:

The linear attenuation coefficient (u), which is based on attenuation that happens when x-rays interact with materials, is the form of the data obtained from the detectors. This (p) is transformed into the CT number, a figure determined by the beam's composition, thickness, and quality. The linear attenuation, which is shown on the image as grayscale, is precisely proportional to these CT values. Each pixel has its own definition for this (p).

PIXEL - In the matrix, it is the smallest unit.

VOXEL - Volume data is contained in this tiny depiction of a tissue block.

MATRIX - It is a complete array of pixel configurations.

A picture with a large grayscale can be represented by converting (u) into a CT number.

Each substance has its own CT number: Air = -1000, bone = +1000, and water = 0.

The Hounsfield number (H) is another name for the CT number in honour of **Sir Hounsfield.**

3) IMAGE REPRESENTATION

Following the collection of the projected X-rays, a computer reconstruction technique converts them into digital images during the data acquisition process. These algorithms create the digital image and determine the linear attenuation coefficient. These are some of the reconstruction algorithms that are most frequently employed.

a. **Back projection:** It is among the simplest and most traditional methods for reconstructing images. This reconstructs the image by adding together all of the transmitted rays. Its inability to provide a crisp image of the object was its shortcoming, which is why clinical CT does not employ it. Additionally, it creates a star pattern when some of the high-density object's back-projected intensity reaches locations outside of it.

b. **Iterative reconstruction:** It is essentially a presumption that every point in the matrix is known and has the same value. This value is then added to the measured values until the two reach a mutually agreeable limit.

c. **Filtered back projection:** Convolution technique is another name for it. With the development of digital filters, it is identical to back projection except that the blurring effect and starlike pattern are eliminated. Following the completion of these reconstruction methods, the CT images are prepared for digital monitor display and can be saved and printed for further use.

Post Processing

Depending on the radiologist's needs, the gathered data can be rendered, remodelled, darkened, or brightened. There are various post-processing programs that aid in improving image diagnosis. Here are a few of the more widely utilized ones.

MPR (MULTI PLANAR RECONSTRUCTION): This allows the acquired data to be shown in axial, coronal, and sagittal planes.

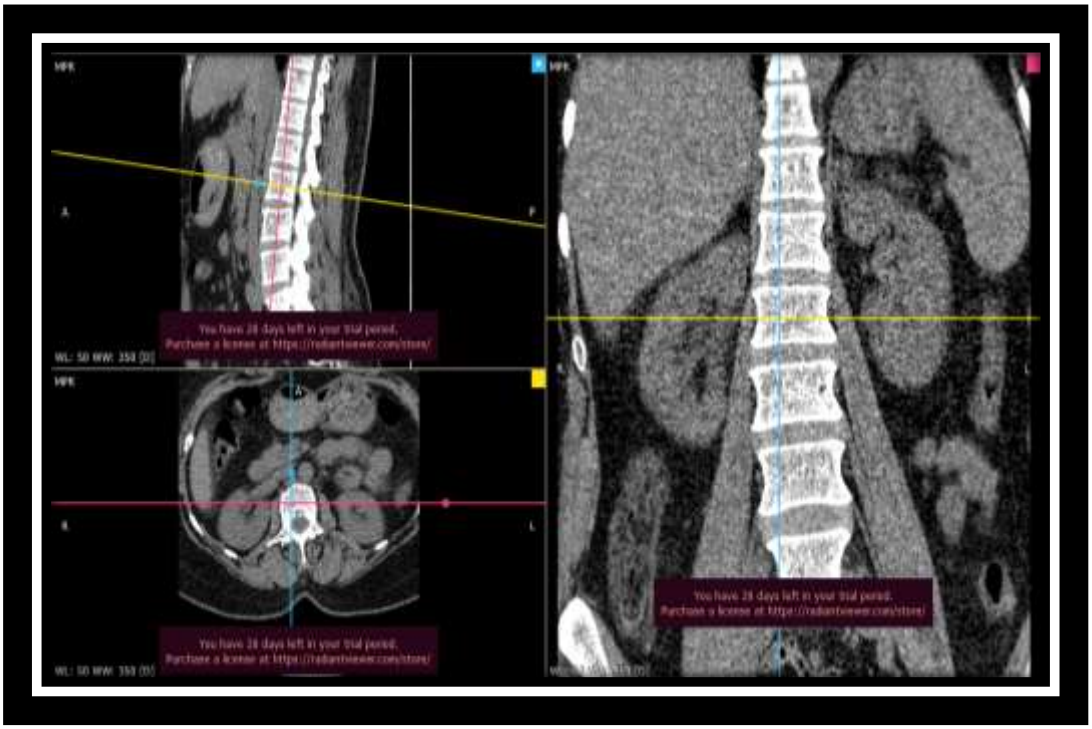

Figure 1.3: Representation of MPR

Maximum or minimum intensity projection - Only the tissue with the highest attenuation is seen in maximum intensity projection, which is helpful for evaluating calculi in various organs. On the other hand, because lowest intensity projection only displays low-density tissues, it is utilized to visualize soft tissues.

Surface rendering -This technique, which is sometimes referred to as shaded surface display, shows the organs' surfaces on the picture. Since only 10% of the collected data is needed for image reconstruction, this procedure is incredibly quick and simple. However, its lack of detail is a disadvantage.

Volume rendering- This method is highly useful for visualizing the correct anatomy of the organs and produces a 3D depiction of the chosen organ with considerably more detail. However, this method uses high-performance CPUs and a lot of data.

1.4: Bone: The bones that make up the human skeleton offer stiffness, house bone marrow, store various micronutrients, aid in posture, produce red blood cells, and perform a host of other tasks. Calcium and phosphate, which give bones their strength and density, are stored in the bone matrix. An adult has 206 bones in total, each with unique shapes, characteristics, locations, and other attributes. Ligaments hold these bones together.

These 206 bones are classified as 2 groups:

1) Axial skeleton
2) Appendicular skeleton.

The 80 bones that make up the axial skeleton are primarily found in the head and trunk. In contrast, the 126 bones that make up the appendicular skeleton are primarily responsible for the body's movements.

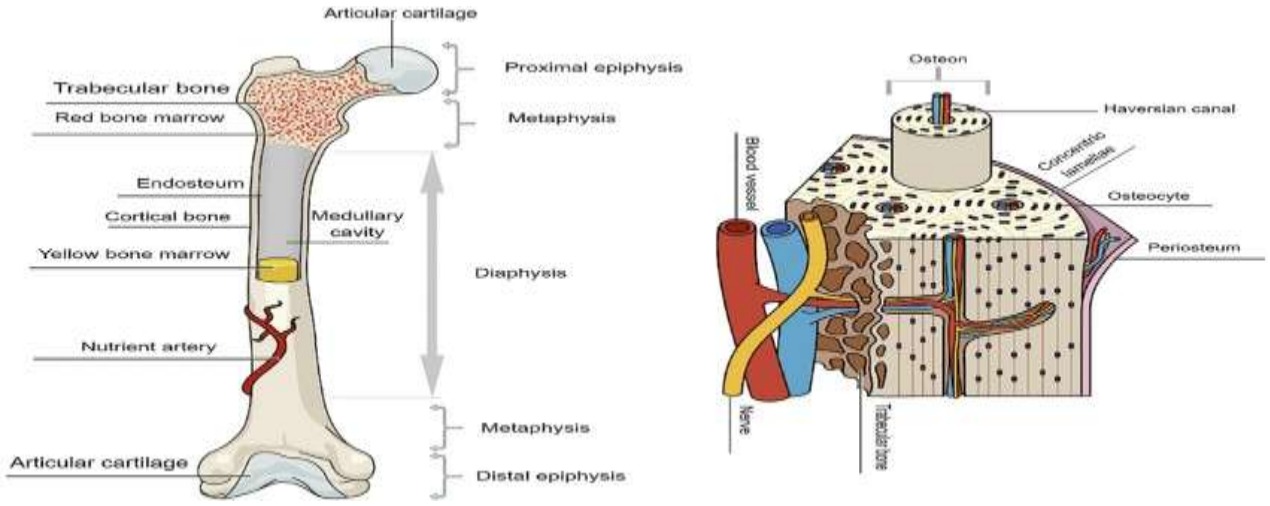

Figure 1.4: Representation of Structure of Long bone.

WHAT IS A BONE?

Osteocytes are found in a matrix of hardened collagen fibers that make up this connective tissue. With the exception of the articulating surfaces, the entire bone is covered in an outer layer of dense fibrous membrane called the periosteum. The compact bone (cortex) is the dense, rigid outer shell of the bone. The Cancellous region of the bone is occupied by red bone marrow, which is the site for hemopoiesis and is highly porous. The shaft of the long bone is hollow, known as the medullary cavity, and contains the yellow bone marrow. One kind of hyaline cartilage is this articulating cartilage. The osteocytes, which are in charge of preserving bone density and growth, are housed in a matrix made of collagen fibers.

36% organic, 36% inorganic and 28% water make up the bone matrix. Calcium and phosphorus are the inorganic components; collagen and non-collagenous organic materials make up the organic matrix of bone; osteocalcin is also present and aids in the binding of calcium to collagen during the mineralization process. With the exception of the hyoid, all bones are joined by a joint.

Classification of bone based on shape

1. Long bones
2. Short bones
3. Flat bones
4. Irregular bones
5. Sesamoid bones [4]

OSSIFICATION

The embryo's skeleton is primarily made up of hyaline cartilage and fibrous membranes. Ossification starts in the sixth week of embryonic development and lasts until adulthood. A compact bone appears as a slice of a tree with circles growing larger toward the edge when viewed at the microscopic level. It is composed of several tube-like structures known as the Haversian system or osteon.

The central canal of these osteons contains lymphatic, nerve, and blood vessels. A perforated canal connects the center canal to the others. Lamellae are parallel series-like structures found in the central canal of the bone. Osteocytes are housed in tiny spaces called lacunae that are present in this lamella. Canaliculi, which contain intestinal fluid to support the osteocytes, connect the lacuna to one another.

The spongy (cancellous) bone has trabeculae that house the osteocytes and are connected by canaliculi, giving the appearance of a honeycomb when viewed under a microscope. These canaliculi provide the intestinal fluid needed to support the osteocytes.

Bone is made up of various cells.

OSTEOBLASTS, OSTEOCYTES AND OSTEOCLASTS.

While osteocytes are found throughout the inside of the bone and are created by the fusing of single nucleus blood bone precursor cells, osteoclasts, osteoblasts, and bone lining cells are found on the surface of the bone.

A. OSTEOBLAST

Responsible for making new bone cells and repairing old bone cells. They do this by making a protein mixture Osteoid, and are mainly present in the periosteum and endosteum and centre of ossification (epiphyseal plate). They originate from mesenchymal stem cells.

B. OSTEOCYTES

When osteocytes mature, mature cells are produced that are found in the bone. They are found in the bone matrix, lamellae, and trabeculae and help to preserve bone tissue. The most prevalent kind of cells in completely developed bone tissue are these ones. They survive for as long as the bone is present, which is a very long time. It also participates in the process of bone remodelling and has the ability to desorb and resorb. Osteocytes remove calcium from the bone when the calcium level is too low. Diseases like osteoporosis and osteoarthritis are linked to the malfunction or early mortality of osteocytes.

C. OSTEOCLASTS

They aid in the upkeep, remodelling, and repair of bones by breaking down bone tissue. [5].

1.5 : BONE MINERAL DENSITY

One indicator of bone health is bone mineral density. It provides information on a person's bone health. This is accomplished by quantifying the mineral content of a certain bone volume. BMD calculates calcium and phosphorus, the two primary components of bone, to determine the health of the bone. The BMD levels in the body start to rise as puberty sets in and reach their peak in the third decade of life, depending on the age and sex of the individual.

The body begins to lose bone density as people age because hormones that are crucial for maintaining bone health, such as oestrogen in women and testosterone in men, decrease. Based on this outcome, the bone is classified as [3].

A)-NORMAL BONE

B)-OSTEOPENIA

C)-OSTEOPOROSIS

Figure 1.5: Representation of Normal Bone and Osteoporosis Bone.

OSTEOPENIA

When it comes to bone mineral density, osteopenia is a condition that implies the bones have begun to weaken and lose density. The bone continues to remodel throughout life, with new bone cells growing and old ones breaking down. However, as people age, the body begins to break down old bone cells more quickly than it produces new ones. The bone becomes weaker and loses mass. Osteopenia is the first stage of this decrease, which can eventually progress to osteoporosis. [6]

OSTEOPOROSIS

The word "osteoporosis" refers to the loss of bone density that causes the bone to become weaker and more prone to breaking. Because osteoporosis has minimal symptoms and the patient is unaware that they have it, it also falls under the category of silent disease. For postmenopausal and elderly women, the condition becomes more problematic. Because it encourages the formation of osteocytes, estrogen is essential for bone health, and women have a lack of it after menopause.

Estrogen receptors are found on many kinds of bone cells; this hormone dimerically attaches to certain acceptor sites known as the estrogen response (ERE). Target genes are stimulated as a result of this interaction, which aids in the bone cells' ability to react to the body's estrogen levels. It controls cytokines and proto-oncogenes that are known to be crucial for bone function, such as the differentiation of osteoclasts from other types of bone cells. While no clear correlation between estrogen shortage and bone health has been established, some research has shown that it causes an increase in osteoclasts. There is still a lot of research to be done.

Despite being a quiet illness, osteoporosis can cause symptoms such as loss of height, kyphosis, and excruciating back pain. These symptoms usually go undiagnosed until a slight fall occurs, which can also result in a fracture. These are a few typical risk factors for osteoporosis.

a) SEX- Osteoporosis is more common in women because estrogen levels decline after menopause. Men who are 60 years of age or older are more vulnerable.

b) AGE- As people age, their bodies begin to lose bone more quickly than new bone is formed, which can result in osteoporosis.

c) BODY SIZE- Women and men who are extremely thin are more vulnerable.

d) RACE- Compared to Africans, white males and white Asians are more vulnerable.

e) HORMONAL CHANGES - Osteoporosis risk is increased by low levels of estrogen in premenopausal women and testosterone in males.

f) DIET- The risk may also be increased by a diet low in calcium, vitamin D, severe dieting, and inadequate protein consumption.

g) Medication- Antiepileptic drugs, glucocorticoids, and other drugs are used to treat HIV, rheumatoid arthritis, and some forms of cancer.

h) Life style- Regular smoking, chronic alcohol consumption, and a lack of physical activity all raise the risk.

Keeping these risk factors in mind, old age people and postmenopausal women shall visit the doctor for diagnosis. For the diagnosis of osteoporosis the doctor performs some physical exams on the patient which include, checking the height and weight, checking the posture, way the patient walks and muscles stability. If the doctor is suspicious he/she refers the patient for a BMD (bone mineral density) test. This is the most common and best method of finding the density of the bone. DEXA (dual x-ray absorptiometry) is the modality usually used for the testing of BMD. As per the results of the DEXA scan, treatment is planned by the doctors. Once the patient gets osteoporosis it cannot be completely cured, the treatment focuses on preventing it from getting worse.

In most cases, treatment consists of :

Proper nutrition- The right amount of calories, calcium, vitamin D, protein, and a balanced diet are all necessary for this.

Dairy products, green leafy vegetables, broccoli, and other foods high in calcium and vitamin D should be consumed.

Vitamin D is essential for the intestinal absorption of calcium. After being in the sun, it becomes active in the skin. Foods high in vitamin D include fish oil and eggs.

600 IU of vitamin D and 1000 mg of calcium per day are necessary for an adult.

Life style -Bones can be strengthened by physical activity and exercise, however strenuous activities should be avoided as they can strain and shatter bones. In addition, quitting smoking and alcohol promotes better bone health.

Medication - The FDA has authorized a few drugs to treat osteoporosis.

Bisphosphonates- This medication helps treat osteoporosis by slowing down the loss of bone and preserving bone mass.

Calcitonin - This is a therapy for women who are unable to take other drugs.

Estrogen agonist/antagonist- Other names for the therapy include Tissue Selective Estrogen Complex (TSEC) and Selective Estrogen Receptor Modulator (SERM). Although they are not estrogen, they have actions similar to those of estrogen and aid in increasing bone density.

Estrogen and hormone therapy- Although a combination of estrogen and progestin is authorized to prevent osteoporosis, the risks and benefits are first observed because of possible adverse effects.

PTHnPand PTH- Both men and women can benefit from parathyroid hormone analog, which is a kind of parathyroid hormone that promotes bone density.

Rank Ligand (RANKL) inhibitor- This inhibitor aids in delaying the loss of bone.

Sclerostin Inhibitor- It inhibits the actions of proteins, promotes the growth of new bone cells, and reduces bone loss. [**7, 35**]

1.6: QCT (Quantitative computed tomography): Early radiography methods used single and dual energy photon absorptiometry, which employs a radionuclide source, to investigate the cortical morphometry of the 2nd Meta carpal of the non-dominant hand. In the 1980s, radionuclide sources were replaced by dual energy x-ray absorptiometry or DXA. which developed significant improvements in spatial and temporal resolution. With DEXA, only one minute per site is now used instead of the previous fifteen. Due to the reduced ionizing radiation in DXA and its application in pharmaceutical and epidemiological research, QCT was no longer utilized after the invention of the CT scanner. QCT has become more popular in musculoskeletal research as a result of improved software and reduced radiation levels in CT scanners.

Principle - In order to determine the linear attenuation coefficient with respect to the water HU (0), a CT scanner employs transmitted x-rays from the patient's body. Denser regions, such as bone, absorb more radiation and so have higher attenuation; their HU value is higher than that of soft tissue, which has lower density, low x-ray attenuation, and low HU values. This HU is now converted into bone mineral equivalent (mg/cm3) by using a phantom in the scan field of vision. An oval ROI was placed in the trabecular bone of the spine in the early CT scanners. However, as the technology advanced, 3D volumetric scans made it possible to analyze the hip as well.

Some specially designed peripheral CT scanners are specially used to measure BMD which are mobile, less expensive and have lower dose.

Phantom technique - Since the phantom contains different concentrations of materials with properties comparable to those of bone, it is employed as a reference for QCT in this case. The patient lays above the phantom, which is set up on the sofa. The attenuation measured may be translated from Hounsfield Unit to bone mineral equivalents in mg/cm3 (g/l) using regression of concentration and attenuation of the calibrated phantom. When fluid liquid phantoms (K2HP4) were first utilized, air bubbles formed in the solution because of fluid leaking or transpiring from the solution into the phantom's Perspex, making scanning challenging or imprecise. Later, hydroxyapatite, a solid material phantom, was used. Since many phantoms have been created, there hasn't been any discernible variation in the outcomes of the many phantom forms. European forearm phantoms (EFP) and European spine phantoms (ESP) are the most utilized for PQCT. The examination known as peripheral QCT frequently uses the non-dominant forearm. The region between the olecranon and the tip of the ulnar styloid is measured when the forearm is positioned prone inside the QCT gantry. In order to limit hand movement during scanning, a velcro strap is utilized.

Standard QCT- This makes use of specialized analytic tools and calibrated phantoms. To prevent CT reconstruction, the patient rests supine over the phantom with a cushion filled with gel or water between them. The HU measurements are converted into BMD values with the aid of these calibrated phantoms. Simultaneous calibration is the procedure of simultaneously assessing the patient and phantom. Image analysis was used to create a solid state cann-genant phantom using five-phase solid state calcium hydroxyapatite phantoms. Siemens primarily uses the phantom with two calcium hydroxyapatite phantoms for commercial QCT.

Single slice QCT- This was the first QCT technique used to measure lumbar spine Bone Mineral Densitometry. To ensure that the mid-vertebral section is parallel to the vertebral end plates, the T11-L4 vertebral area was scanned using a gantry tilt and a slice thickness of 10 mm. In order to reduce the radiation exposure, 80 kVp and 120 mAs were utilized.

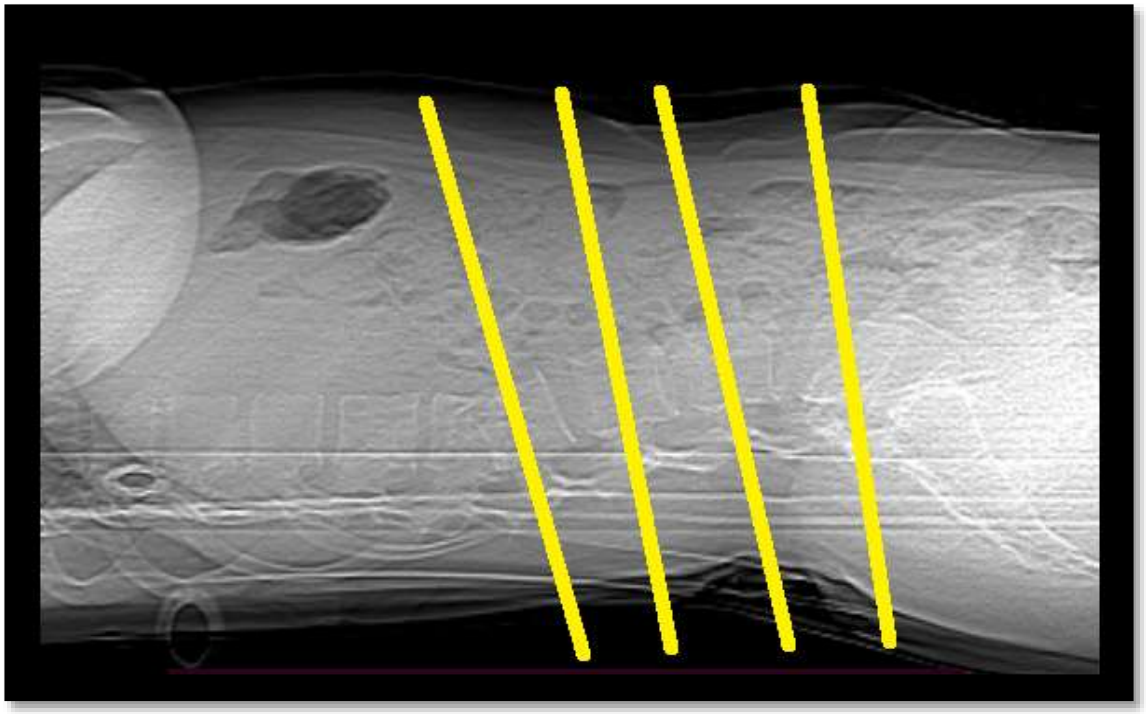

Figure 1.6: Representation of single-slice quantitative CT, using a series of three to four mm slice angled parallel to the vertebral end plates.

Volumetric QCT - With the benefits of slice thickness of 1-3 mm and no gantry tilt, this is easier to execute and has excellent accuracy. To reduce the radiation dosage, 80 kVp and 50–200 mAs were applied to the T11–L4 area. According to the American College of Radiology's 2008 and 2013 QCT standards, BMD levels between 120 and 80 mg/cm3 are considered to be indicative of osteoporosis, whereas BMD values below 80 mg/cm3 are considered to be indicative of osteoporosis. There was a strong link found between these set values and the DXA scan's t-score. This suggests that QCT may be applied to BMD assessment.

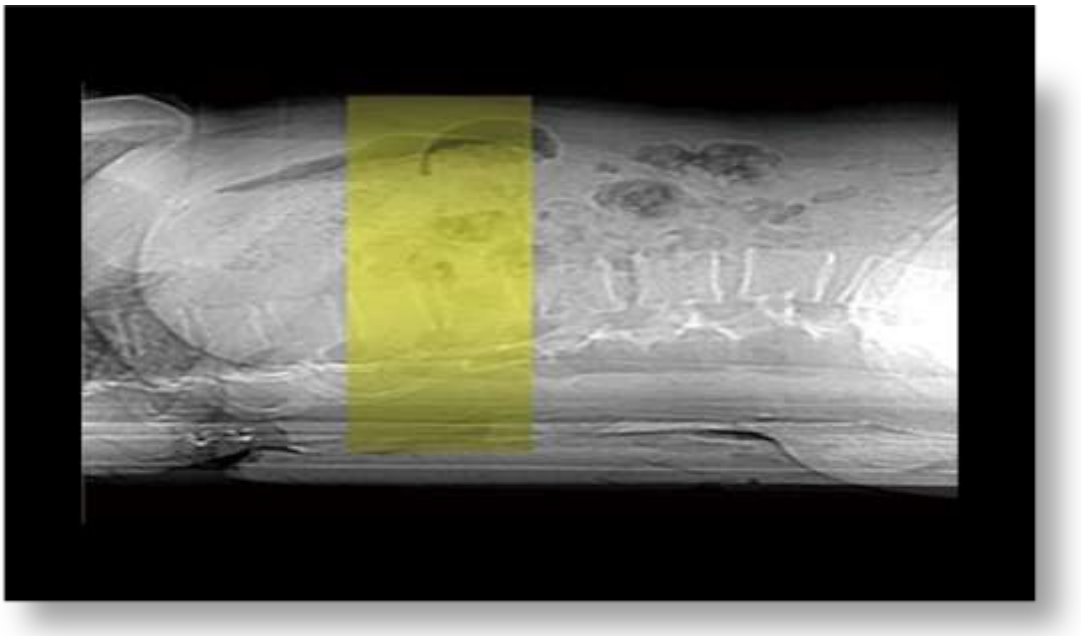

Figure 1.7: 3D volumetric quantitative CT

Benefits of QCT over DEXA- whereas QCT employs a CT scanner, volumetric data is used for BMD, which is more sensitive and size independent, whereas DEXA scans are size dependant. Additionally, it makes it possible to assess certain regions independently, such as the cortical and trabecular, which aids in determining the extent of the afflicted area. Skeletal strength may be checked in CT using various geometric perspectives. [8]

1.7: DEXA- A tool for measuring bone mineral density. DXA is the best method currently available for evaluating bone mineral density (BMD) and assisting in the diagnosis of osteoporosis and osteoopenia, according to the WHO. Two modest doses of X-rays are emitted in this modality, and soft tissue and bone absorb them differently. The BMD is computed using the difference in attenuation. DXAs have extremely low radiation doses—as little as 10% of a typical chest radiograph. T-score and Z-score are the results of the DXA, which typically takes 5–10 minutes and involves the hip and lumbar spine. [9]

Figure 1.8: DEXA modality

1.8: T-score- The figure that compares to a young adult of the same sex with peak bone mass

Figure 1.9: Representation of T-score. [10]

Z-score – This number shows a comparison with the value of other individuals of the same age, gender and size.

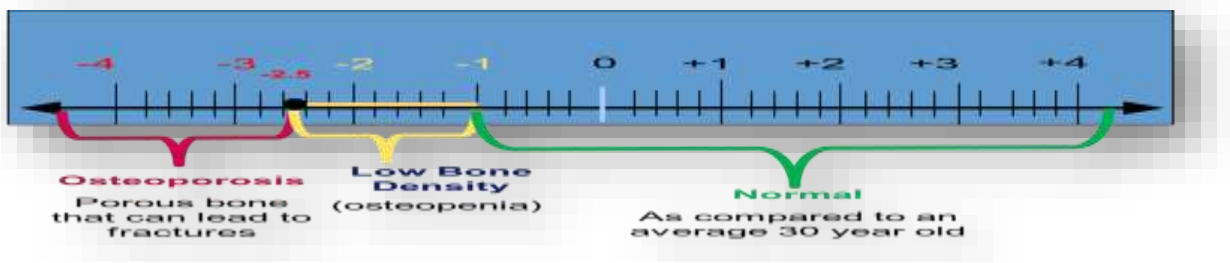

Figure 1.10: Representation of Z-score

1.8: FRAX - In order to assist in screening and treatment for the general public, a fracture risk assessment tool uses an algorithm based on demographic specifications to predict the risk of fracture. Since its debut in 2008, 71 models for 66 nations—representing over 80% of the global population—have been created.

1.9: HOUNSFIELD UNITS - X-rays operate on the attenuation principle, which states that radiation attenuates more when a substance is denser. The linear attenuation coefficient (u), which is used in CT to assess X-ray attenuation, is translated into the CT number using mathematical formulas. The CT numbers, which stand for the various shades of gray for various organs, are termed HU in honor of Sir G.N. Hounsfield.

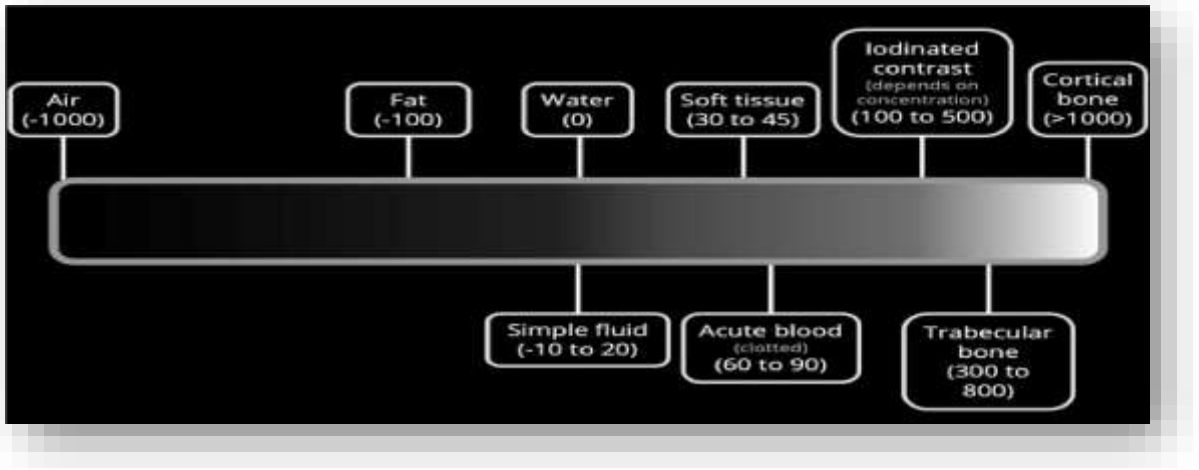

Figure 1.11: Hounsfield Unit Scale.

MRI INTRODUCTION

MRI is a medical imaging technique that uses radio frequency (RF) pulses and a magnetic field to produce images of anatomical structures, the presence of disease, and the variety of biological processes that take place in the human body. (5) The magnetic resonance image (MR picture) shows the radiofrequency (RF) signals that the tissue generates during the image acquisition process. Signals originate from a state of magnetization that is produced in the tissue when the patient is exposed to a high magnetic field. Tissue magnetization requires the presence of magnetic nuclei. The exact physical characteristic of the tissue or fluid that is seen in the image depends on how the magnetic field is changed throughout the acquisition process. The process of acquiring a picture is a repetitive cycle, similar to a heartbeat. Tissue magnetization must undergo a number of alterations during each cycle. [13]

1.10 HISTORY OF MRI

The work of mathematician Jean Baptiste Joseph Fourier (1768-1830) is where NMR (today known as MRI) got its start. One of Fourier's contributions to the discipline was the creation of a mathematical method for examining heat transmission between solid things. Phase and frequency signal processing in NMR gradually advanced as a result of this discovery, allowing for quick analysis in the field.

In honour of Nikola Tesla, a Serbian inventor who made important contributions to the area of electromagnetism and lived from 1856 to 1943, the Tesla is the unit of measurement for magnetic field strength. The revolving magnetic field was one of his most significant findings. Tesla's contributions transformed our knowledge of and use of magnetic fields. The advancement of Magnetic Resonance Imaging (MRI) technology is one of the many businesses that continue to benefit from his efforts.

The renowned Irish scientist Sir Joseph Larmor (1857–1942) made important advances in the science of physics. Larmor is famous for developing the "Larmor equation," which had a significant influence on the field of nuclear magnetic resonance (NMR). According to this equation, which can be written as $\omega = \gamma B0$, the frequency of precession of the nuclear magnetic moment (ω) is exactly proportional to the product of the gyromagnetic ratio (γ) and the magnetic field intensity (B0).

Based on the magnetic characteristics of specific periodic system nuclei, Felix Bloch Edward Purcell reported a physicochemical phenomena in the 1940s. In a magnetic field, it was found that some nuclei absorbed electromagnetic spectrum energy and then released it when they reverted to their initial forms. The Larmor connection showed that the radiofrequency and the magnetic field intensity matched.

A pioneering work on the measurement of T1 and T2 relaxation durations in rat tissues was carried out in 1971 by Raymond

Damadian. He discovered an important finding when comparing cancerous and normal tissue in his studies. Damadian discovered that the relaxation durations of normal tissue were shorter than those of malignant tissue. This discovery established the groundwork for the advancement of Magnetic Resonance Imaging (MRI) as a diagnostic technique and was a significant turning point in the area of medical imaging.

BASIC PRINCIPLE OF MRI

Principle of MRI primarily involves 4 steps: Longitudinal magnetisation, Transverse magnetisation, MR signal and Localisation of MR signal.

- Placing the patient in a magnet
- Sending radiofrequency pulse by coil
- Receiving signals from the patient by coil
- Transforming a signal into an image by complex processing in the computer

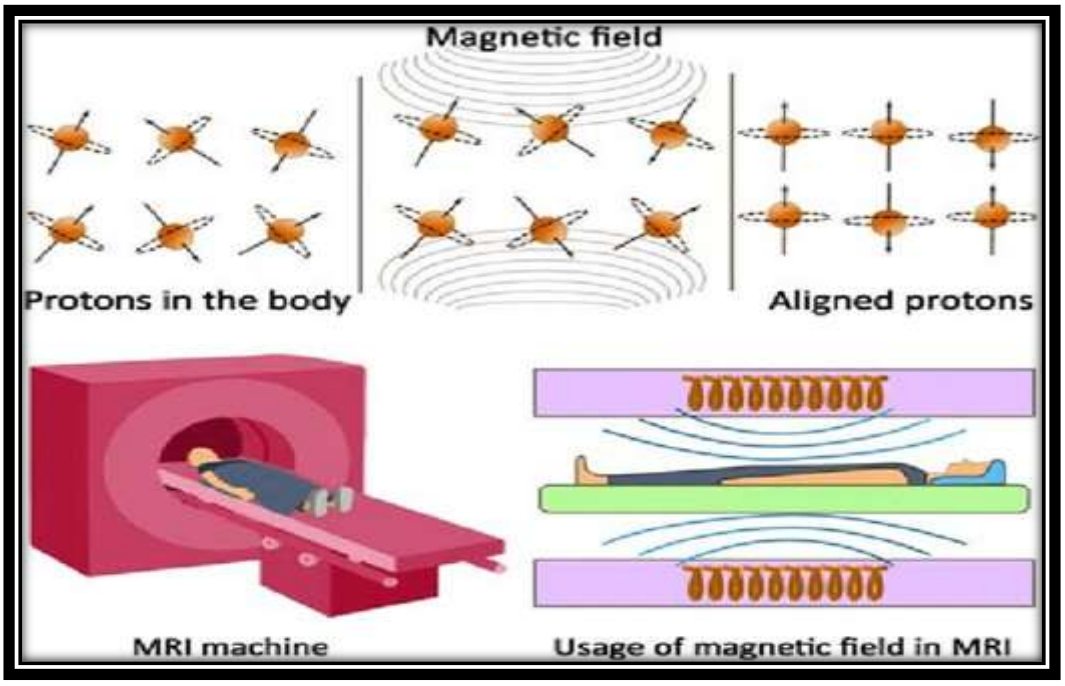

Figure 1.12: Representation of MRI working principle.

HOW DOES PROTONS HELPS IN MR IMAGING

Since H+ ions only contain one particle, the proton, the positively charged particle found in every atom's nucleus, provides the basis for MR imaging. Positively charged protons move in a rotatory motion known as spin. Any charge that travels produces current, and each current has a tiny magnetic field surrounding it known as the Magnetic dipole moment.

Protons move randomly throughout the body in any direction when there is no external magnetic field present. When an external magnetic field applied (the patient is placed in the magnetic field), these protons align and spin in the direction of the external magnetic field, some align parallel to the external magnetic field, while others align antiparallel.

● Protons that align not only revolve around one another but also travel in a cone-like pattern along their axis of spin. Precession is the term for this proton movement and the cone-like structure it produces.

● Precessional frequency is the number of protons that precess in a certain amount of time, and it is expressed in Hertz (Hz).

● The external magnetic field has a direct relationship with the precessional frequency. Consequently, the higher the precession frequency, the stronger the magnetic field.

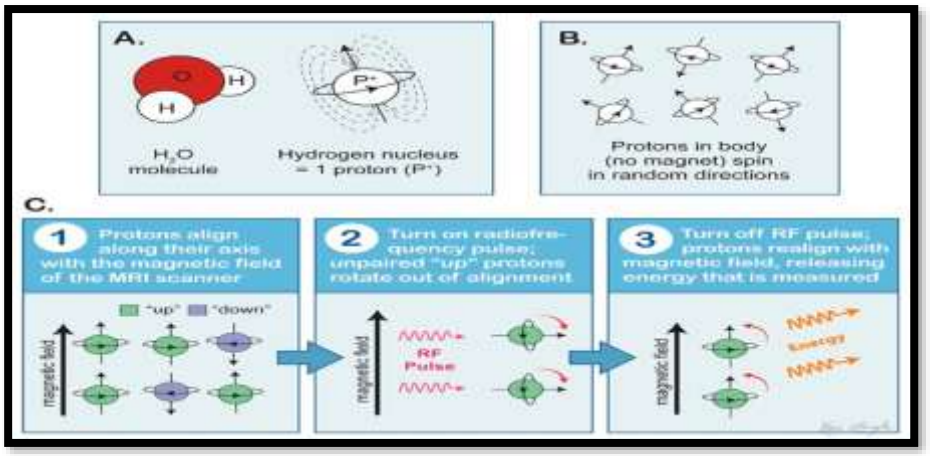

Figure 1.13: Representation of Proton helping in imaging.

MR PULSE SEQUENCE: The set of radiofrequency pulses administered to the tissues to create the pictures is known as an MR pulse sequence.

RADIOFREQUENCY PULSE: This type of energy pocket is what gives MRIs their ability to create images of things. MRI uses two different kinds of radiofrequency pulses. The first is known as a 90° or excitation pulse, and it excites the NMV (protons) from the longitudinal to the transverse phase.

The second is a refocusing or 180° rephasing pulse that recovers the excited protons from longitudinal to transverse magnetization.

Multiple sequences are combined into an MRI protocol, and an MRI pulse sequence is made up of several parameters. Time of Echo (TE), Time of Repetition (TR), and Flip angle are some of these characteristics.

(a)TIME OF ECHO: It is the amount of time that passes between the beginning of an RF pulse and the echo or signal being received.

(b)TIME OF REPETITION: It is the amount of time that passes between the beginning of one RF pulse and the beginning of the subsequent one.

(c) FLIP ANGLE: An RF pulse rotates a longitudinal magnetization vector away from the z-axis at this angle. The scanning time will decrease when the flip angle is reduced.

T1 Weighted Imaging

T1 weighted The spin lattice picture is another name for imaging. It illustrates the variation in tissue's T1 relaxation period and is one of the fundamental radiofrequency pulse sequences in MRI. T1 weighting depends on a tissue net magnetization vector's longitudinal relaxation.

When an RF pulse puts spin aligned in an external magnetic field into the transverse plane, they glide back towards the external magnetic field's initial equilibrium, however not all tissue returns to the equilibrium in the same period of time.

The TE and TR of T1 weighted imaging are short.

Fat looks bright in T1 images because it rapidly realigns its longitudinal magnetization with the external magnetic field. Water has less transverse magnetization following an RF pulse because its longitudinal magnetization realignment is far slower.
Water hence appears black and has a poor signal.

On the T1 weighted picture, fluid looks black and fat appears bright. [14]

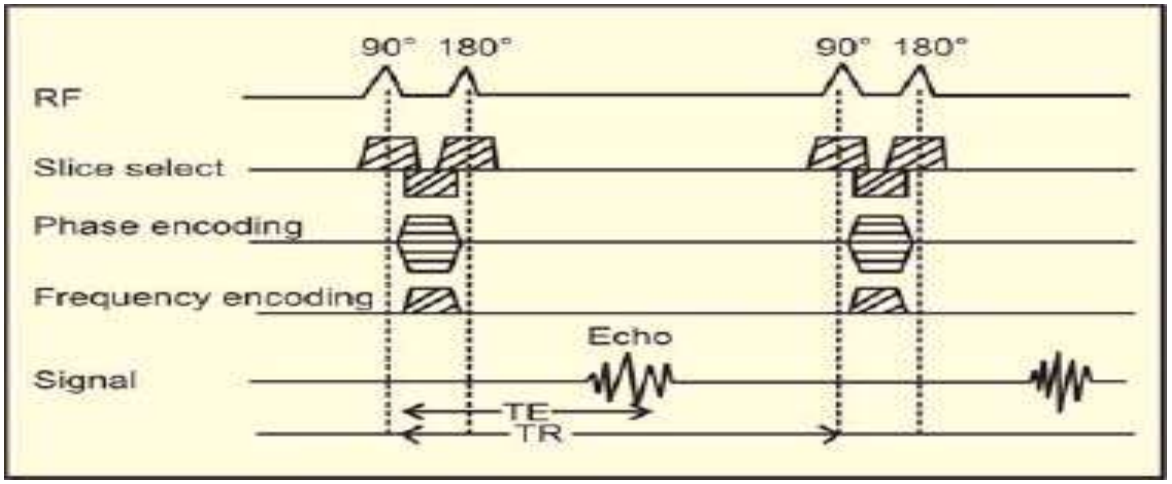

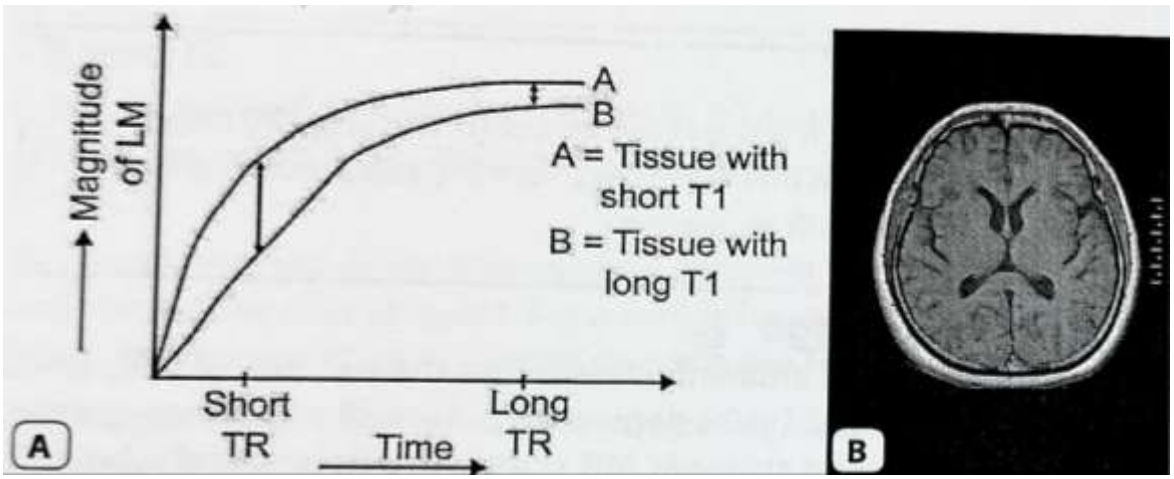

Figure 1.14: A & B: REPRESENTING T1 WEIGHTED IMAGE

T1 WEIGHTED IMAGE CHARACTERISTIC TABLE

MUSCLE	Intermediate
CSF	Dark
BONE	Dark
BONE MARROW	Bright
BLOOD VESSELS	Generally dark, it can be either bright or dark according on the flow characteristics.
SPINAL CORD	Intermediate signal

FAT	Bright
INTERVERTEBRAL DISC	Nucleus pulposus and annulus intermediate
LIGAMENTS	Intermediate
NERVE ROOTS	Intermediate signal

T2 WEIGHTED IMAGING

The transverse relaxation of the net magnetization vector is necessary for T2 weighted imaging. Long TE and TR are necessary for T2 weighted imaging.

T1 weighting is the result of spin relaxation from the transverse plane towards the main magnetic field following an excitation pulse.

On the other hand, the difference of the spin decay from the aligned precession in the transverse plane is seen as a T2 weighted picture.

On the T2 weighted picture, fat looks black and fluid appears bright. [14]

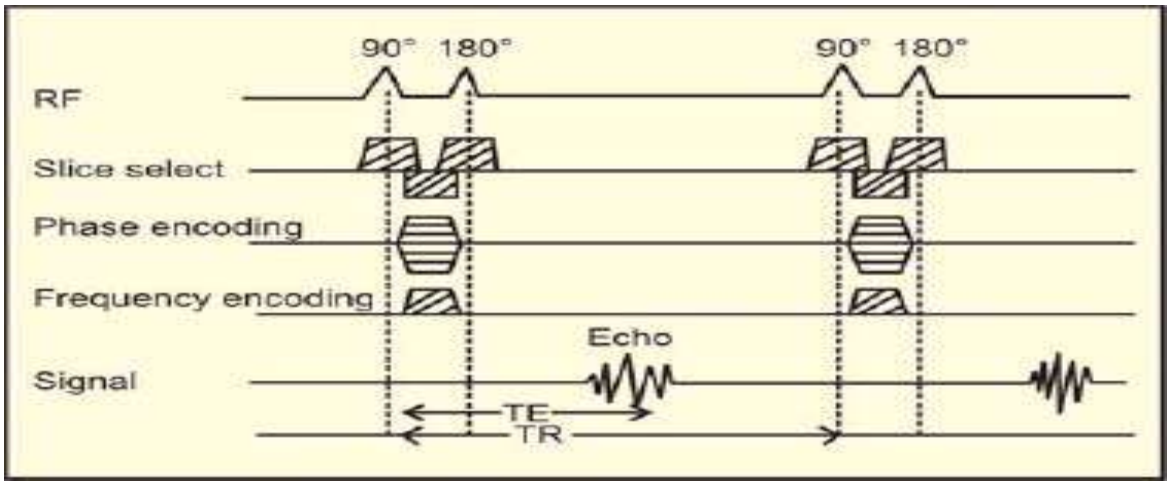

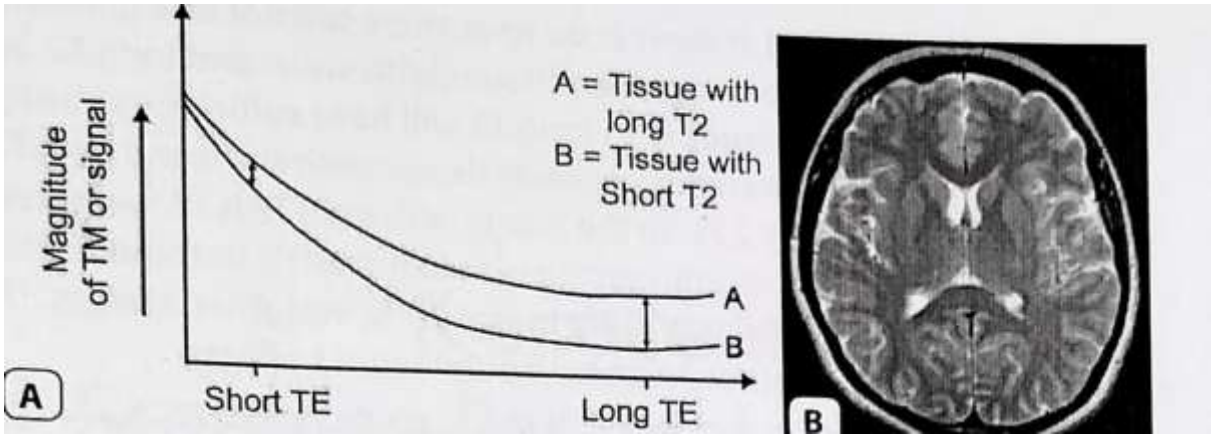

Figure 1.15: A & B: REPRESENTING T2 WEIGHTED IMAGE

T2 WEIGHTED IMAGE CHARACTERISTIC TABLE

MUSCLE	Intermediate to dark
CSF	Bright
BONE	Dark (low signal)
BONE MARROW	Intermediate to Bright
BLOOD VESSELS	Mostly dark, depending upon flow characteristic, can be bright or can be dark
SPINAL CORD	Intermediate signal
FAT	Bright but darker than T1
INTERVERTEBRAL DISC	Nucleus pulposus and annulus intermediate
LIGAMENTS	Intermediate to dark
NERVE ROOTS	Intermediate signal

GRADIENT ECHO PULSE SEQUENCE

An alternate method to spin echo sequence that differs from it in its operation is gradient echo pulse sequence. The gradients are used to rephrase the magnetic moment of the hydrogen nuclei, which usually flip angles lower than 90 degrees, in a gradient echo pulse sequence.

Both of these methods enable shorter TE and TR when compared to the spin echo sequence pulse sequence. Weighting imaging approaches use gradient echo pulse sequences, which are quite complex. The following are the elements that influence weighting imaging:

(a) Residual transverse magnetization; (b) parameters (TR, TE, and flip angle). (c) The stable condition [14]

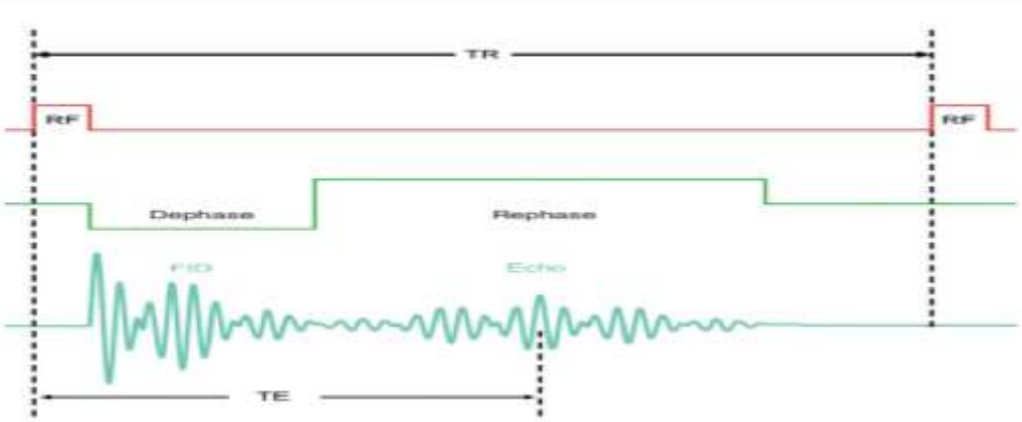

Figure 1.16: Representation of GRE Pulse Sequenece.

2. AIM & OBJECTIVE

2.1 AIM

Quantitative estimation of bone mineral density in lumbar spine by comparing CT and 1.5 Tesla MRI.

2.2 OBJECTIVES

• To assess Lumbar spine on the Basis of Gender in the northern up population by using CT and MRI.

• To compare the MRI T1, T2 and GRE signal intensity values with the QCT, Hounsfield unit and BMD values of CT in order to diagnose osteoporosis.

2.3 NEED OF STUDY

• To evaluate how MRIs contribute to the calculation of bone mineral density Since it does not use ionizing radiation and thus has advantages over CT & DEXA in assessment of Bone Mineral Density.

3. MATERIAL AND METHODOLOGY

3.1 STUDY SITE

• Department of Radio-Diagnosis and Imaging, Teerthanker Mahaveer Hospital and Research Centre, Moradabad, Uttar Pradesh, India.

3.2 TYPE OF STUDY

• Prospective Study clinical based.

3.3 DESIGN OF STUDY

• Cross - sectional study and prospective observational

3.4 STUDY POPULATION

• Western UP population.

3.5 STUDY DURATION

• The duration of One year.

3.6 PARTICIPANTS

• Sources of Data are patients referred to the Radiology Department for the prescribed examination of CT Whole Abdomen, Lumbar spine.

• Both the IPD and OPD patients are included into the study.

3.7 SAMPLE SIZE

• 44 Patients

• Calculated by slovin's formula $n = N/(1+Ne^2)$.

3.8 CRITERIA

• Convenient Sampling

3.9 INCLUSION CRITERIA

• Patients from IPD and OPD.

• Patients that has been referred for the CT Abdomen.

• Patients that has been referred for the CT Lumbar.

• Patient with back pain.

• Both sexes above 18 years.

3.10 EXCLUSION CRITERIA

• Patient undergone Recent Surgery.

• Patient with the spine surgery.

• Paediatric Patient.

• Patient with Lumbar deformities.

• Metal Fragments, Bullets, or shrapnel anywhere in the body.

• Claustrophobic patients.

3.11 MATERIAL METHOD

• Our study is based upon Computed Tomography (United Imaging 160 slices, UCT) and MRI (Siemens Magnetom 1.5 Tesla).

• We are going to measure the following parameters: Hounsfield Unit, T1 weighted signal intensity, T2 weighted signal intensity, GRE signal intensity.

• All measurements done by using workstation.

•All the measured data are recorded on MS – excel sheet.

3.12 ARMAMENTARIUM

Figure 4.1: 1.5 TESLA MRI, SIEMENS MAGNETOM AVANTO

Figure 4.2: Computed Tomography (United Imaging 160 slices, UCT)

3.13 DATA ANALYSIS

• The collected data were summarized by using the Descriptive Statistics: frequency, percentage; mean and S.D.

• The Independent sample "t" test was used to compare the imaging parameters across lumbar levels as well as quantitative computed tomography (QCT) assessment; between males and female.

• The One-way ANOVA was used to compare the imaging parameters across lumbar levels as well as QCT; according to age groups.

• The Binary logistic regression model was used to determine gender according to imaging parameters across lumbar levels and QCT assessment.

• To find the relation of imaging parameters across lumbar levels with QCT; The Pearson correlation coefficient ("r") was used. The p value < 0.05 was considered as significant. Data were analyzed by using the SPSS software (SPSS Inc.; Chicago, IL) version 29.0.10.

TABLE 4.1: PULSE SEQUENCES AND THEIR PARAMETER USED FOR IMAGING.

Sequence	TE (ms)	TR (ms)	Slice Thickness (mm)	Slice Increment (mm)	FOV Read (mm)	Phase Encoding Direction
T1-Weighted (Spin Echo)	10–20	400–600	3–4	0.3–0.4	280–320	Anterior-Posterior (AP)
T2-Weighted (Fast Spin Echo)	80–120	3000–6000	3–4	0.3–0.4	280–320	Anterior-Posterior (AP)
GRE (Gradient Echo)	4–10	20–50	3–4	0.3–0.4	280–320	Anterior-Posterior (AP)

TABLE 4.2: PROTOCOL FOR ROUTINE SPINE CT

Patient Positioning	Supine position with head first and arms elevated.
Topogram Position	Is decided by radiographer to include area of interest.
Mode of Scanning	Helical
Scan Orientation	Cranio-caudal
FOV	Must include area of interest
Milliampere	60
Voltage	110 – 120 KV
Slice Thickness	2-4 mm
Slice Interval	1.0 – 2.0 mm
Reconstruction Algorithm	Sharp for the bone and smooth for the soft tissues
3 D Reconstruction	SSD, MIP and MPR

TABLE 4.3: PROTOCOL FOR ROUTINE ABDOMEN CT

Patient Positioning	Supine position with head first and arms extended above the level of head.
Topopgram/Landmark	Level of nipples to 3cm below the inferior border of pubic symphysis.
Scan Mode	Helical (single breath hold)
Scan orientation	Cranio-caudal
Field of view	Must include Area of Interest with soft tissue.

Milliampere	60-70
Kilovoltage	120
Slice Thickness	3-5mm
Slice Interval	1.5-2.5mm
Kernel	Smooth(medium)
3-D Reconstruction	MIP, MPR

TABLE 4.4: PROTOCOL FOR MR LUMBAR SPINE IMAGING

Patient Positioning	Supine position with head first, arms kept besides the body.
Coil	Body coil
Mode of scan	2-D
Topogram/Landmark	Mandible
Scout	T1 (Sagittal)
Pulse sequence	T1 SE (Axial and Sagittal Plane) T2 FSE (Axial and Sagittal Plane) STIR (Axial and Sagittal Plane) PD, FLAIR (Axial and Sagittal Plane) GRE (Sagittal and Coronal Plane) T1 Sequence Postcontrast
Slice Thickness	3-4 mm
Slice Interval	0-2 mm

CHAPTER -5

RESULT

In this study there were 44 patients (22 male & 22female) were included whose mean age is 46.02 year (range 28 to 66).

Table 5.1: Descriptive Statistics for age

(n = 44)	Range	Mean	S.D.
Age (Years)	28.0 to 66.0	46.02	11.14

The table explains the mean according to age such as 46.02 respectively and standard deviation 11.14 respectively.

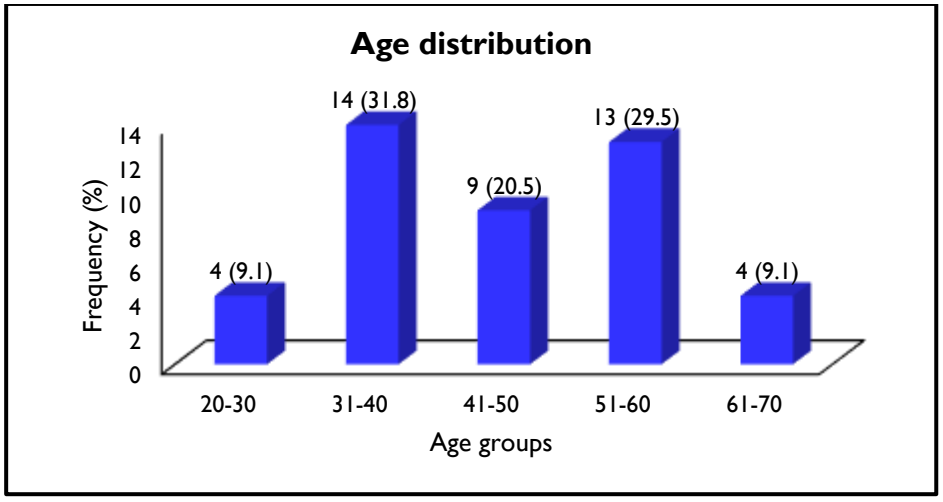

Graph 5.1: Bar graph represents maximum % of frequency of age found in between 31 to 40 age groups.

Table 5.2: Age and gender distribution

		Frequency	%
Age groups	20-30	4	9.1
	31-40	14	31.8
	41-50	9	20.5
	51-60	13	29.5
	61-70	4	9.1
Gender	Male	22	50
	Female	22	50

The table represents age and gender distribution & their frequency distribution.
Maximum frequency shows with age group 31-40 is 14 and percentage is 31.8%.
According to gender male shows equal percentage of frequency than female.

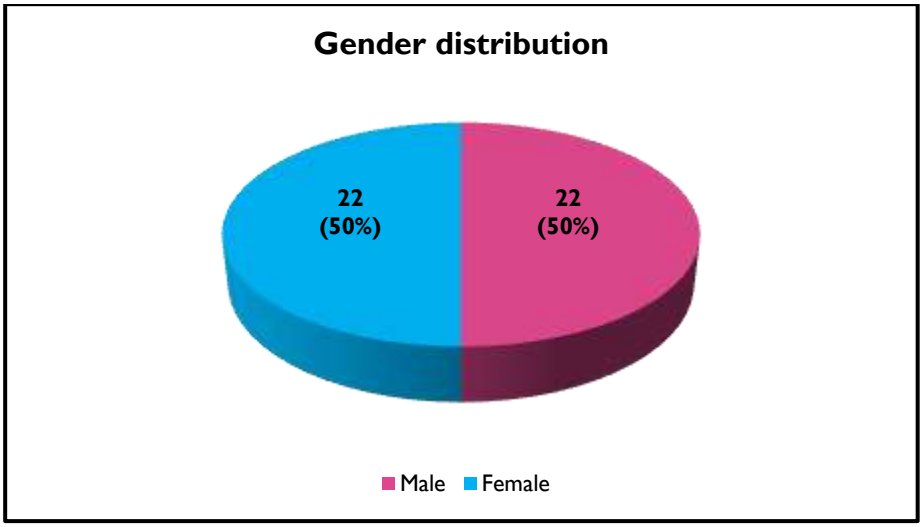

Graph 5.2 Pie chart shows the gender distribution which represents 50% male and 50% female.

Table 5.3: Age according to gender

		Gender			
		Male		Female	
		n	%	n	%
Age groups	20-30	1	4.5	3	13.6
	31-40	9	40.9	5	22.7
	41-50	3	13.6	6	27.3
	51-60	8	36.4	5	22.7
	61-70	1	4.5	3	13.6

The table explains age groups according to gender and sample in between age groups with their percentage of male and female in different age groups.

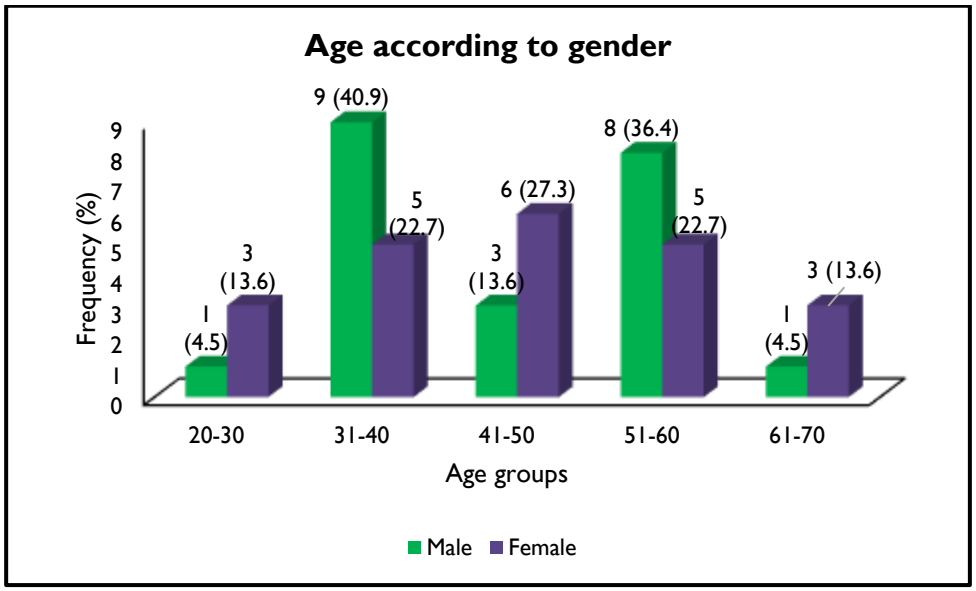

Graph 5.3 The bar graph represents the frequency of age according to gender as the male and female. Maximum frequency percentage found in age group of 31-40 years.

Table 5.4: Assessment of imaging parameters across lumbar levels

		Range	Mean	S.D.
L1	T1	160.1 to 363.2	252.44	45.07
	T2	50.0 to 270.2	176.35	48.06
	GRE	54.8 to 270.2	83.59	31.11
	CT	97.2 to 345.0	173.94	52.34
L2	T1	157.8 to 387.1	260.15	52.99
	T2	52.4 to 327.1	179.37	54.66
	GRE	49.6 to 243.6	84.72	27.88
	CT	67.3 to 350.0	169.92	55.65
L3	T1	149.2 to 352.6	257.24	51.34
	T2	55.4 to 283.1	170.64	53.56
	GRE	54.0 to 229.4	80.51	26.39
	CT	82.2 to 252.2	172.97	39.71
L4	T1	123.7 to 356.1	253.06	54.27
	T2	75.4 to 266.9	168.39	48.91
	GRE	39.4 to 191.8	77.82	23.14
	CT	100.9 to 416.4	180.02	56.02
L5	T1	134.9 to 884.7	280.96	113.70

	T2	20.1 to 331.3	184.10	71.97
	GRE	34.1 to 306.7	80.31	38.26
	CT	99.8 to 371.6	185.13	62.83

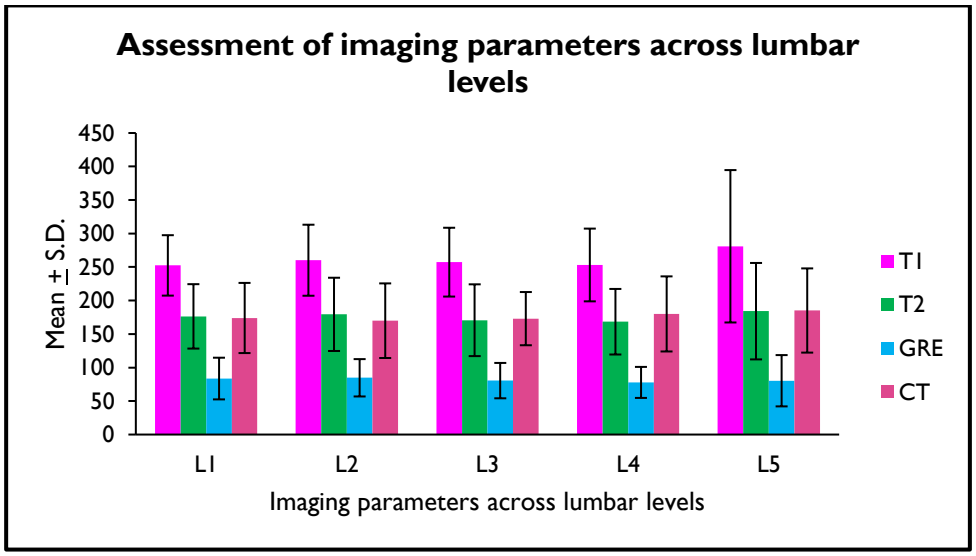

Graph 5.4: The Bar Graph represents imaging parameters across lumbar levels

Table 5.5: Assessment bone mineral density using quantitative computed tomography

		Range	Mean	S.D.
QCT	L1	85.8 to 259.3	139.56	36.64
	L2	64.9 to 262.8	136.74	38.96
	L3	75.3 to 194.3	138.88	27.80
	L4	88.4 to 309.3	143.81	39.21
	L5	87.7 to 277.9	147.39	43.98

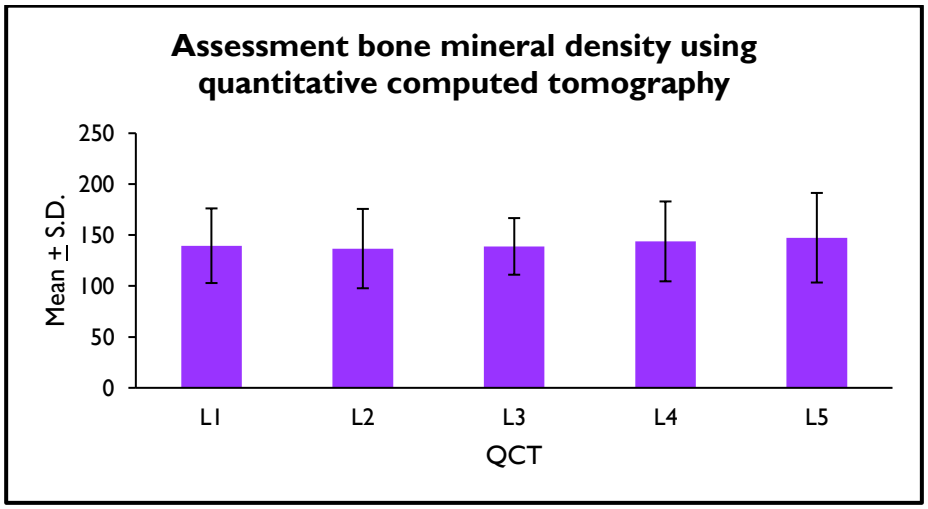

Graph 5.5 The bar graph represents assessment of bone mineral density using QCT across the lumbar levels according to their mean value with standard deviation

Table 5.6: Comparison of imaging parameters across lumbar levels according to gender

		Male		Female		"t"	p value
		Mean	S.D.	Mean	S.D.		
L1	T1	251.95	50.60	252.92	39.98	-0.07	0.945
	T2	183.63	49.55	169.06	46.51	1.01	0.320
	GRE	89.82	41.45	77.35	13.50	1.34	0.187
	CT	175.17	47.12	172.71	58.20	0.15	0.878
L2	T1	259.62	59.75	260.68	46.68	-0.07	0.948
	T2	186.14	51.56	172.60	58.00	0.82	0.417
	GRE	92.47	35.73	76.97	13.72	1.90	0.064
	CT	167.88	54.83	171.96	57.67	-0.24	0.811
L3	T1	262.67	48.79	251.82	54.37	0.70	0.490
	T2	179.77	55.44	161.50	51.25	1.14	0.263
	GRE	85.32	34.73	75.70	13.08	1.22	0.231
	CT	173.34	36.00	172.59	43.96	0.06	0.951
L4	T1	242.19	49.41	263.93	57.81	-1.34	0.187
	T2	168.60	52.87	168.18	45.87	0.03	0.978
	GRE	81.27	30.20	74.37	12.63	0.99	0.328
	CT	176.87	44.96	183.16	66.21	-0.37	0.714
L5	T1	263.87	71.42	298.05	144.08	-1.00	0.324
	T2	187.19	83.70	181.02	59.83	0.28	0.780
	GRE	86.82	52.05	73.81	14.11	1.13	0.264
	CT	189.13	59.62	181.12	67.05	0.42	0.677

("t" = Independent sample "t" test)

The table shows "The Independent sample "t" test was used to compare the imaging parameters across lumbar levels; according to gender. There was no difference ($p > 0.05$) in the entire parameters of imaging parameters across lumbar levels; between males and females"

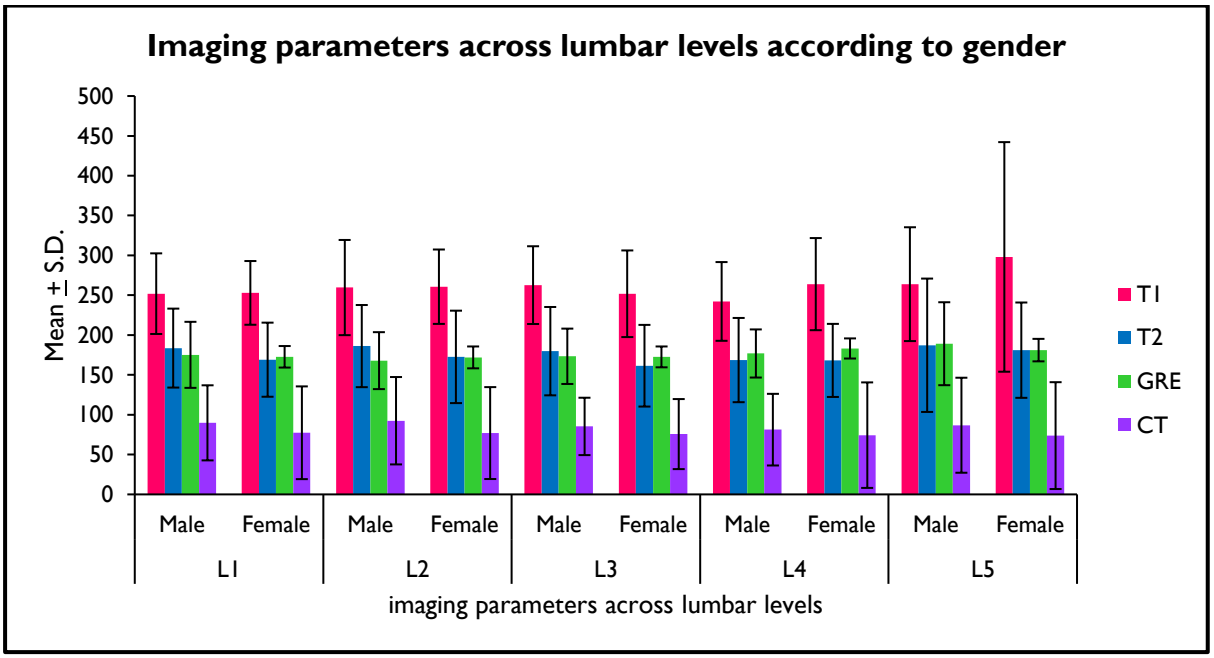

Graph 5.6: The bar graph represents Imaging parameters across lumbar levels according to gender according to gender distribution and their mean value with standard deviation.

Table 5.7: Comparison of bone mineral density using quantitative computed tomography according to gender

		Male		Female		"t"	p value
		Mean	S.D.	Mean	S.D.		
QCT	L1	140.42	32.98	138.70	40.74	0.15	0.878
	L2	135.31	38.38	138.17	40.37	-0.24	0.811
	L3	139.14	25.20	138.61	30.77	0.06	0.951
	L4	141.61	31.47	146.01	46.35	-0.37	0.714
	L5	150.19	41.73	144.58	46.94	0.42	0.677

("t" = Independent sample "t" test)

The table shows "The Independent sample "t" test was used to compare the bone mineral density using quantitative computed tomography; according to gender. There was no difference (p > 0.05) in the entire parameters of bone mineral density using quantitative computed tomography; between males and females"

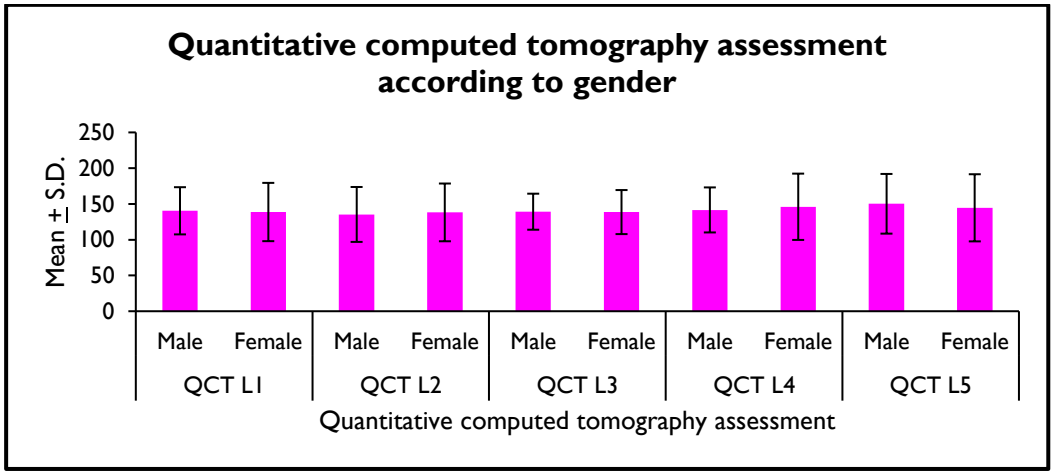

Graph 5.7: The Bar graph represents the Imaging parameters across lumbar levels according to gender.

Table 5.8: Comparison of imaging parameters across lumbar levels according to age groups

		20-30		31-40		41-50		51-60		61-70		"F"	p value
		Mean	S.D	Mean	S.D	Mean	S.D	Mean	S.D	Mean	S.D		
L1	T1	255.81	56.62	232.71	29.44	224.53	25.62	285.90	49.20	272.12	34.41	4.75	0.003*
	T2	165.94	66.43	167.55	30.18	144.30	41.17	219.49	35.54	149.44	50.49	6.01	0.001*
	GRE	81.65	14.69	81.72	13.44	74.12	12.70	93.42	53.96	81.46	9.15	0.53	0.715
	CT	215.00	69.91	203.95	58.63	164.49	33.79	149.94	26.17	127.16	39.66	4.36	0.005*
L2	T1	255.86	65.15	233.83	34.81	238.79	34.92	302.99	56.62	265.39	45.42	4.45	0.005*
	T2	150.52	68.41	171.54	35.95	149.07	44.65	229.14	45.69	142.04	46.25	6.26	0.001*
	GRE	71.17	14.29	86.42	12.54	76.36	13.88	92.60	46.26	85.53	20.98	0.69	0.602
	CT	243.37	82.43	186.16	43.43	161.18	26.68	138.89	31.09	160.15	103.47	4.02	0.008*
L3	T1	251.85	50.90	243.11	35.74	247.95	53.23	272.27	64.58	284.17	47.40	0.89	0.476
	T2	154.17	53.29	168.25	46.01	152.42	43.23	200.05	61.79	140.85	50.32	1.77	0.155

	GRE	76.28	21.75	75.98	10.95	72.80	14.95	92.04	43.27	80.49	5.57	0.94	0.453
	CT	227.18	35.08	186.34	29.43	173.28	33.31	151.71	30.97	140.31	51.87	5.48	0.001*
L4	T1	260.76	78.46	236.08	36.70	244.68	74.81	266.41	49.38	280.28	46.41	0.85	0.501
	T2	137.32	43.94	166.05	44.92	150.49	36.50	201.03	41.35	141.86	73.43	2.89	0.035*
	GRE	80.66	18.33	72.92	11.19	72.09	23.28	86.12	34.73	78.08	3.12	0.71	0.591
	CT	191.25	48.74	177.28	38.07	207.46	86.75	157.17	40.10	190.85	70.32	1.19	0.332
L5	T1	267.28	87.42	241.35	38.96	310.55	224.98	304.38	70.47	290.63	59.50	0.72	0.585
	T2	164.41	98.00	172.69	48.87	138.01	54.78	238.78	62.29	169.76	100.22	3.78	0.011*
	GRE	81.82	20.44	71.92	9.10	68.52	21.95	97.39	64.97	79.21	4.70	1.04	0.401
	CT	181.08	54.69	191.10	50.71	217.91	88.14	160.13	38.77	175.75	97.39	1.21	0.323

("F" = One-way ANOVA; * Significant)

The table shows "The One-way ANOVA was used to compare the imaging parameters across lumbar levels; according to age groups. There was a difference ($p < 0.05$) in the L1-T1; L1-T2; L1-CT, L2-T1; L2-T2; L2-CT, L3-CT; L4-T2; and L5-T2; according to the age groups"

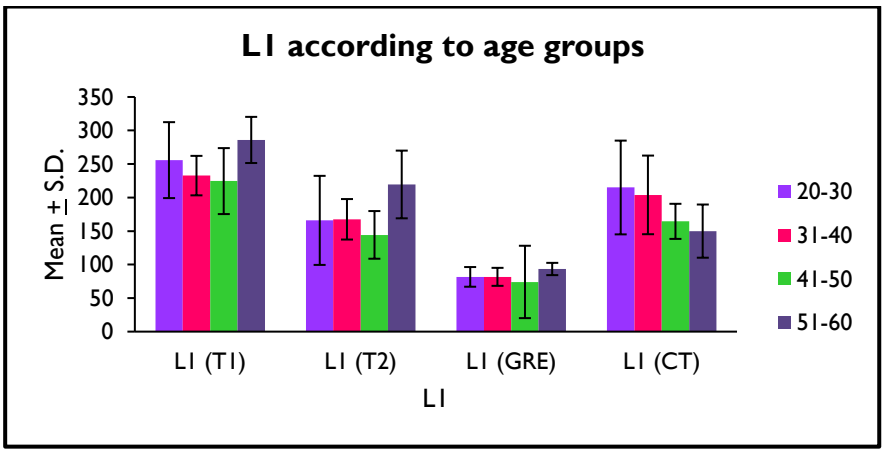

Graph 5.8: The Bar graph represents the L1 lumbar level according to the age groups and their mean value with standard deviation.

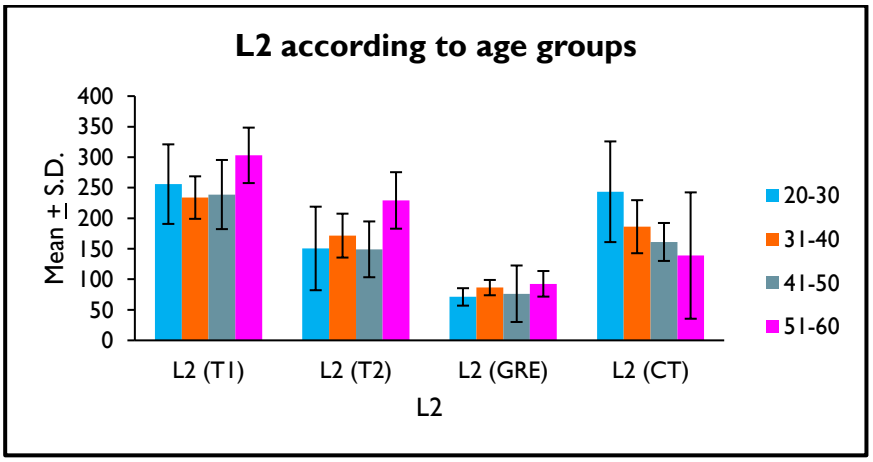

Graph 5.9: The Bar graph represents the L2 lumbar level according to the age groups and their mean value with standard deviation

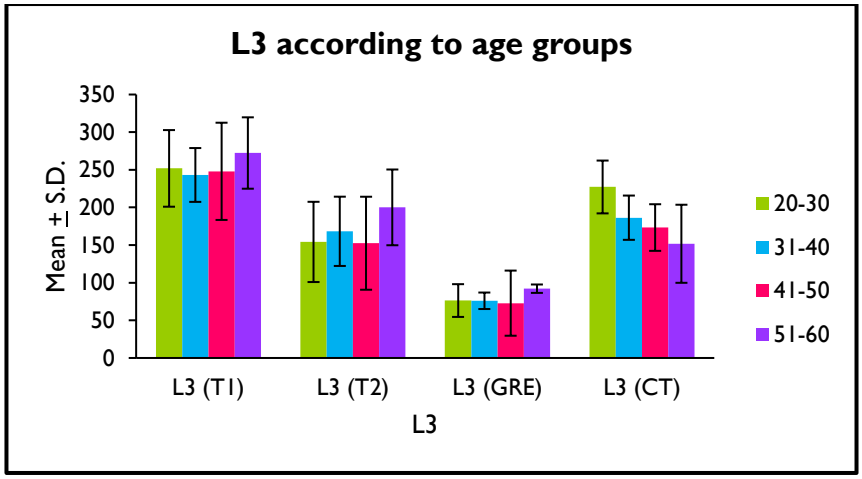

Graph 5.10: The Bar graph represents the L3 lumbar level according to the age groups and their mean value with standard deviation.

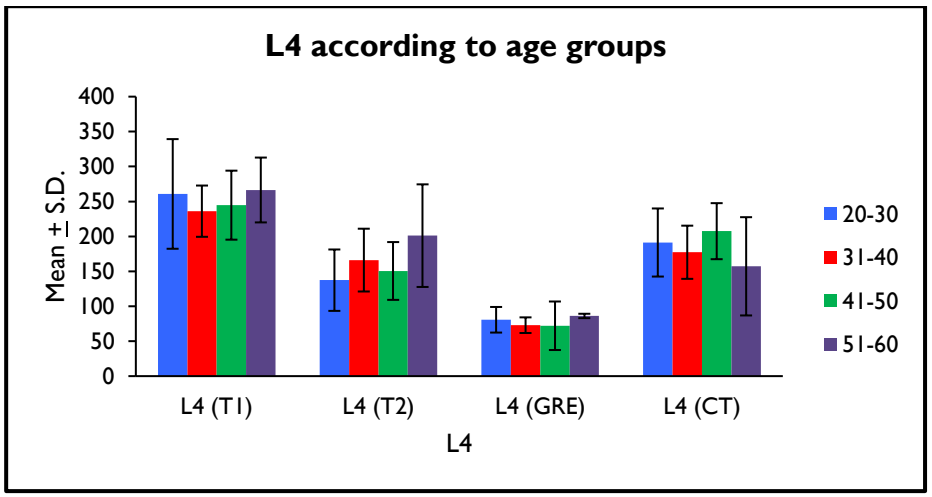

Graph 5.11: The Bar graph represents the L4 lumbar level according to the age groups and their mean value with standard deviation.

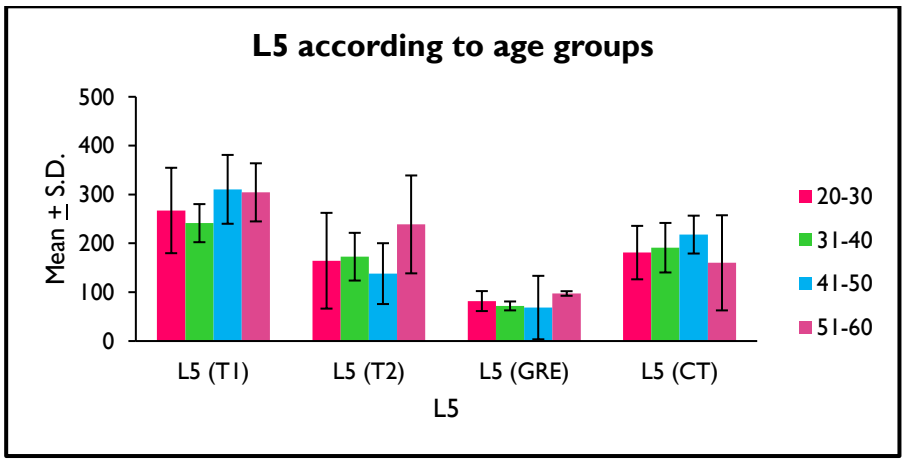

Graph 5.12: The Bar graph represents the L5 lumbar level according to the age groups and their mean value with standard deviation

Table 5.9: Comparison of bone mineral density using quantitative computed tomography according to age groups

		20-30		31-40		41-50		51-60		61-70		"F"	p value
		Mean	S.D.	Mean	S.D.	Mean	S.D.	Mean	S.D.	Mean	S.D.		
QCT	L1	168.30	48.94	160.56	41.04	132.94	23.65	122.76	18.32	106.81	27.76	4.36	0.005*
	L2	188.16	57.70	148.11	30.40	130.62	18.68	115.02	21.76	129.90	72.43	4.02	0.008*
	L3	176.82	24.55	148.24	20.60	139.10	23.32	124.00	21.68	116.02	36.31	5.48	0.001*
	L4	151.67	34.12	141.90	26.65	163.02	60.73	127.82	28.07	151.40	49.22	1.19	0.332
	L5	144.55	38.28	151.57	35.49	170.33	61.70	129.89	27.14	140.83	68.17	1.21	0.323

("F" = One-way ANOVA; * Significant)

The table shows "The One-way ANOVA was used to compare the bone mineral density using quantitative computed tomography; according to age groups. There was a difference ($p < 0.05$) in QCT-L1; QCT-L2; and QCT-L3; according to the age groups.

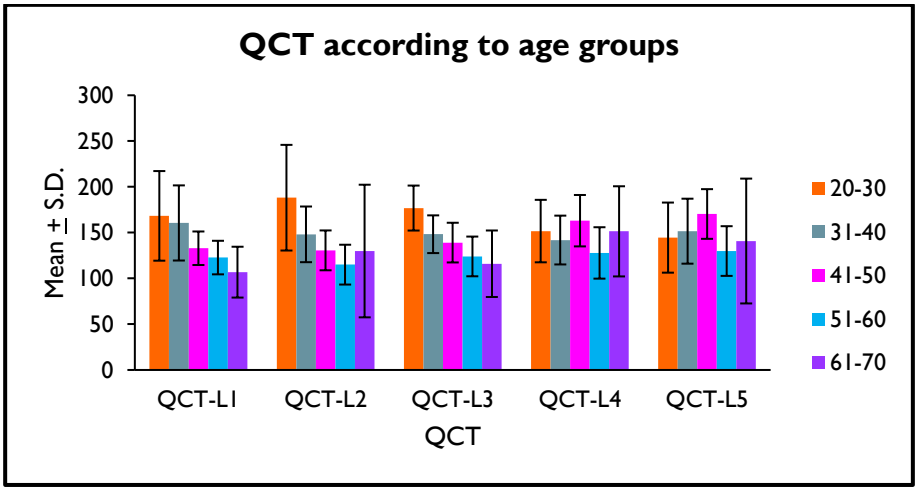

Graph 5.13: The Bar graph represents the QCT according to age groups across lumbar level according to the age groups and their mean value with standard deviation

Table 5.10: Classification table to determine gender according to imaging parameters across lumbar levels and QCT assessment

Observed		Predicted		
		Gender		Percentage Correct
		Male	Female	
Gender	Male	0	22	0
	Female	0	22	100
Overall Percentage				50

The table shows "The Binary logistic regression model was used to determine gender according to imaging parameters across lumbar levels and QCT assessment. The overall accuracy of the correct prediction was 50%; among males it was 0%, and for females the accuracy of correct prediction was 100%"

Table 5.11: Relation of imaging parameters across lumbar levels with QCT

			Imaging parameters				
			QCT-L1	QCT-L2	QCT-L3	QCT-L4	QCT-L5
L1	T1	"r"	-0.475	-0.224	-0.358	-0.298	-0.393
		p value	0.001*	0.144	0.017*	0.049*	0.008*
	T2	"r"	-0.112	-0.118	-0.099	-0.537	-0.445
		p value	0.468	0.445	0.524	< 0.001*	0.002*
	GRE	"r"	0.166	0.217	0.171	0.142	0.100
		p value	0.281	0.158	0.267	0.358	0.519
	CT	"r"	1.000	0.781	0.781	0.314	0.434
		p value	< 0.001*	< 0.001*	< 0.001*	0.038*	0.003*
L2	T1	"r"	-0.460	-0.306	-0.405	-0.300	-0.382
		p value	0.002*	0.043*	0.006*	0.048*	0.010*
	T2	"r"	-0.130	-0.209	-0.207	-0.562	-0.459
		p value	0.401	0.174	0.177	< 0.001*	0.002*
	GRE	"r"	0.139	0.176	0.130	0.130	0.094
		p value	0.367	0.254	0.402	0.401	0.543
	CT	"r"	0.781	1.000	0.813	0.396	0.478
		p value	< 0.001*	< 0.001*	< 0.001*	0.008*	0.001*
L3	T1	"r"	-0.425	-0.254	-0.462	-0.252	-0.393
		p value	0.004*	0.096	0.002*	0.099	0.008*
	T2	"r"	-0.209	-0.219	-0.230	-0.594	-0.487
		p value	0.174	0.153	0.133	< 0.001*	0.001*
	GRE	"r"	0.052	0.050	0.063	0.068	0.003
		p value	0.737	0.748	0.683	0.662	0.983
	CT	"r"	0.781	0.813	1.000	0.330	0.379
		p value	< 0.001*	< 0.001*	< 0.001*	0.029*	0.011*
L4	T1	"r"	-0.422	-0.244	-0.445	-0.227	-0.319
		p value	0.004*	0.111	0.002*	0.138	0.035*
	T2	"r"	-0.313	-0.375	-0.340	-0.613	-0.478
		p value	0.038*	0.012*	0.024*	< 0.001*	0.001*
	GRE	"r"	0.041	0.142	0.120	-0.034	-0.139
		p value	0.791	0.356	0.439	0.828	0.368
	CT	"r"	0.314	0.396	0.330	1.000	0.824
		p value	0.038*	0.008*	0.029*	< 0.001*	< 0.001*
L5	T1	"r"	-0.060	-0.042	0.019	-0.128	-0.121

		p value	0.698	0.786	0.904	0.408	0.433
	T2	"r"	-0.204	-0.236	-0.255	-0.425	-0.389
		p value	0.184	0.123	0.095	0.004*	0.009*
	GRE	"r"	0.038	0.086	0.082	-0.002	-0.107
		p value	0.806	0.580	0.595	0.991	0.489
	CT	"r"	0.434	0.478	0.379	0.824	1.000
		p value	0.003*	0.001*	0.011*	< 0.001*	< 0.001*

("r" = Pearson correlation coefficient; * Significant)

The table represents "The Pearson correlation coefficient ("r") was used to find the relation of imaging parameters across lumbar levels with QCT. The L1-T1 was negatively correlated (p < 0.05) with QCT- L1; QCT-L3; QCT-L4; and QCT-L5. The L1-T2 was negatively correlated (p < 0.05) with QCT-L4, as well as QCT-L5. The L1-CT was positively correlated (p < 0.05) with QCT-L1; QCT-L2; QCT-L3; QCT-L4; and QCT-L5. The L2-T1 was negatively correlated (p < 0.05) with QCT-L1; QCT-L2; QCT-L3; QCT-L4; and QCT-L5. The L2-T2 was negatively correlated (p < 0.05) with QCT-L4, as well as QCT-L5. The L2-CT was positively correlated (p < 0.05) with QCT-L1; QCT-L2; QCT-L3; QCT-L4; and QCT-L5. The L3-T1 was negatively correlated (p < 0.05) with QCT- L1; QCT-L3; and QCT-L5. The L3-T2 was negatively correlated (p < 0.05) with QCT-L4, as well as QCT-L5. The L3-CT was positively correlated (p < 0.05) with QCT-L1; QCT-L2; QCT-L3; QCT-L4; and QCT-L5. The L4-T1 was negatively correlated (p < 0.05) with QCT-L1; QCT-L3; and QCT-L5. The L4-T2 was negatively correlated (p < 0.05) with QCT-L1; QCT-L2; QCT-L3; QCT-L4; and QCT-L5. The L4-CT was positively correlated (p < 0.05) with QCT-L1; QCT-L2; QCT-L3; QCT-L4; and QCT-L5. The L5-T2 was negatively correlated (p < 0.05) with QCT-L4, as well as QCT-L5. Also, the L5-CT was positively correlated (p < 0.05) with QCT-L1; QCT-L2; QCT-L3; QCT-L4; and QCT-L5"

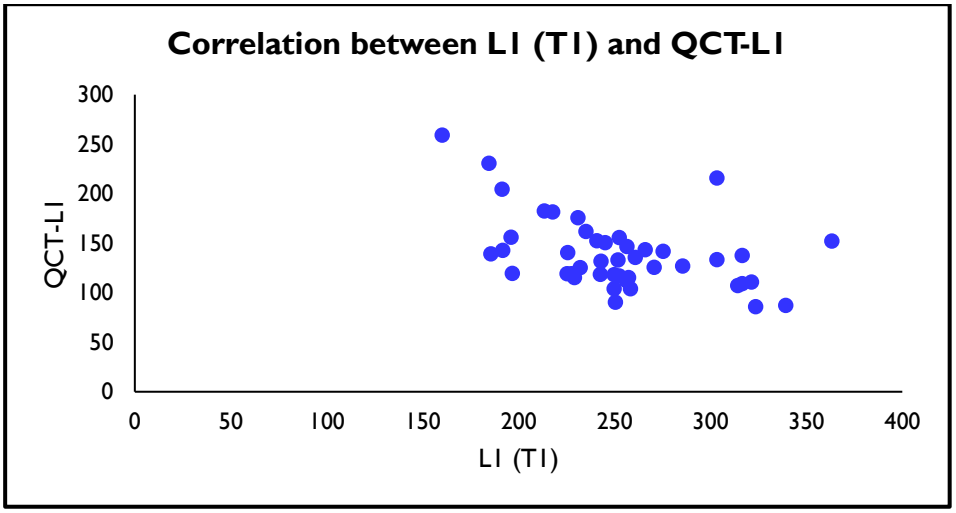

Graph 5.14: The Scatter graph shows correlation between L1 (T1) and QCT-L1

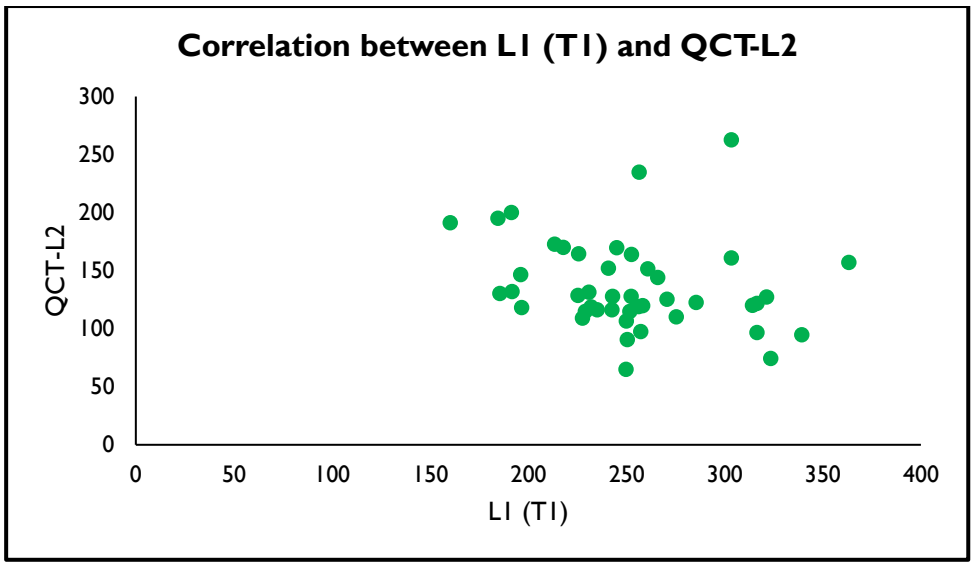

Graph 5.15: The Scatter graph shows correlation between L1 (T1) and QCT-L2

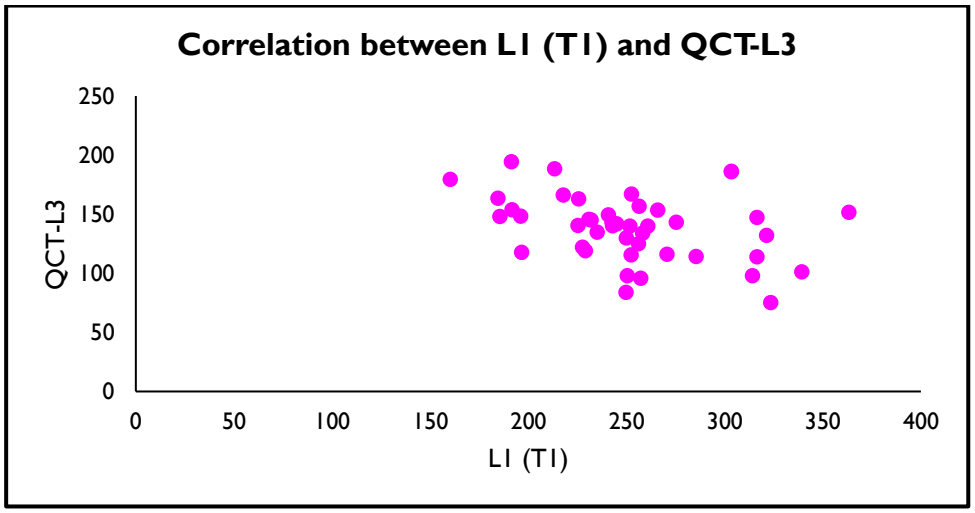

Graph 5.16: The Scatter graph shows correlation between L1 (T1) and QCT-L3

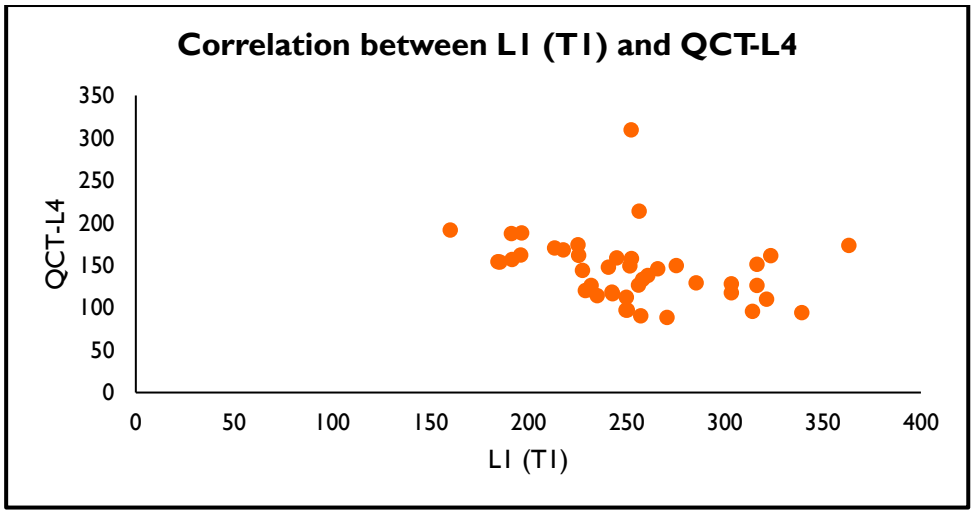

Graph 5.17: The Scatter graph shows correlation between L1 (T1) and QCT-L4

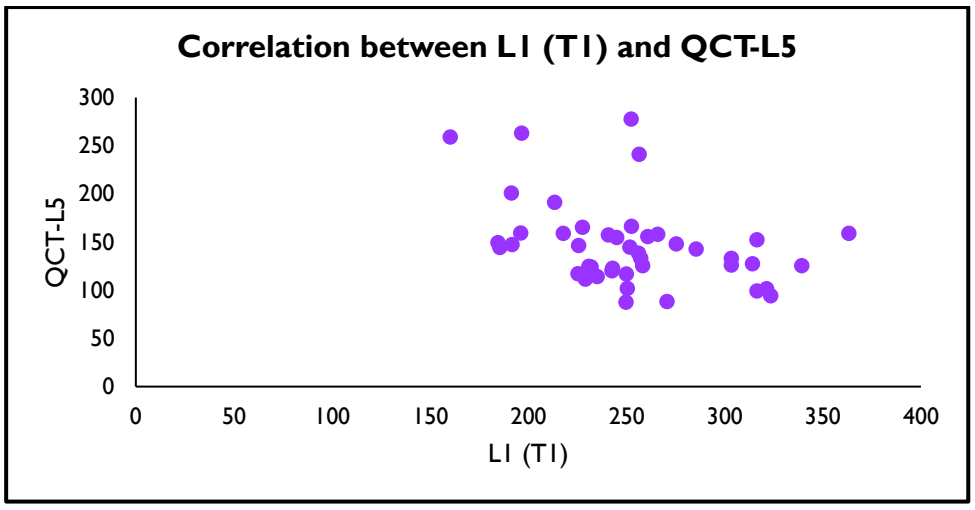

Graph 5.18: The Scatter graph shows correlation between L1 (T1) and QCT-L5

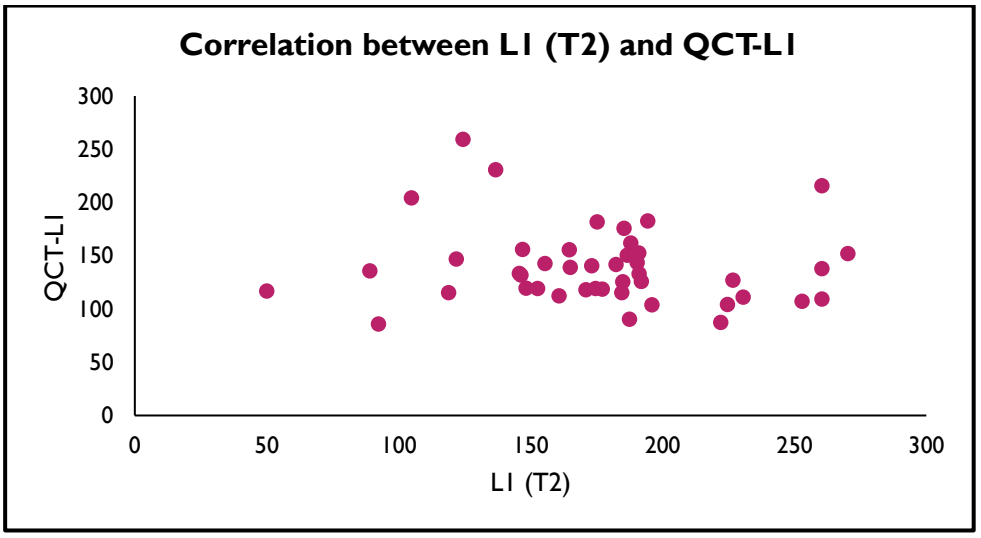

Graph 5.19: The Scatter graph shows correlation between L1 (T2) and QCT-L1

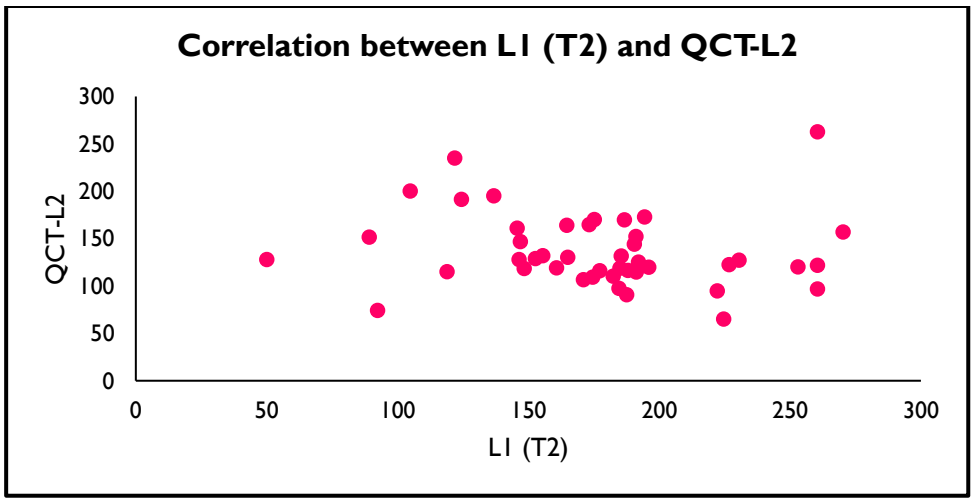

Graph 5.20: The Scatter graph shows correlation between L1 (T2) and QCT-L2

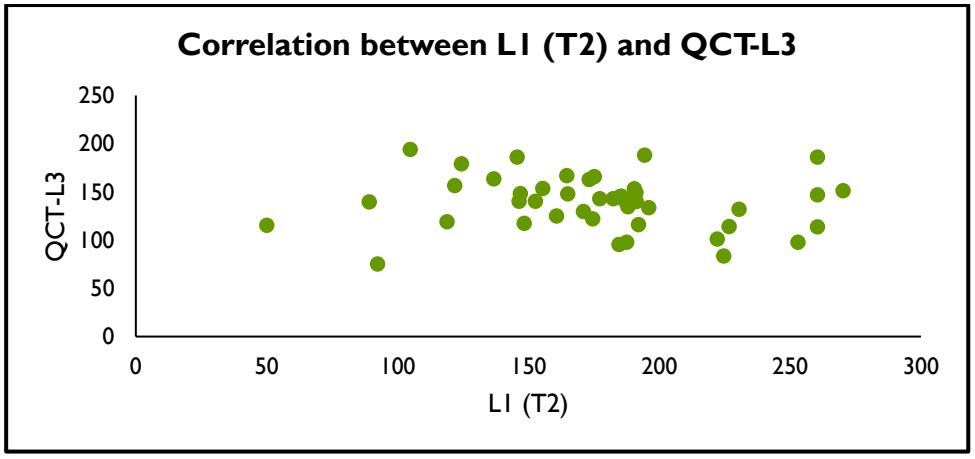

Graph 5.21: The Scatter graph shows correlation between L1 (T2) and QCT-L3

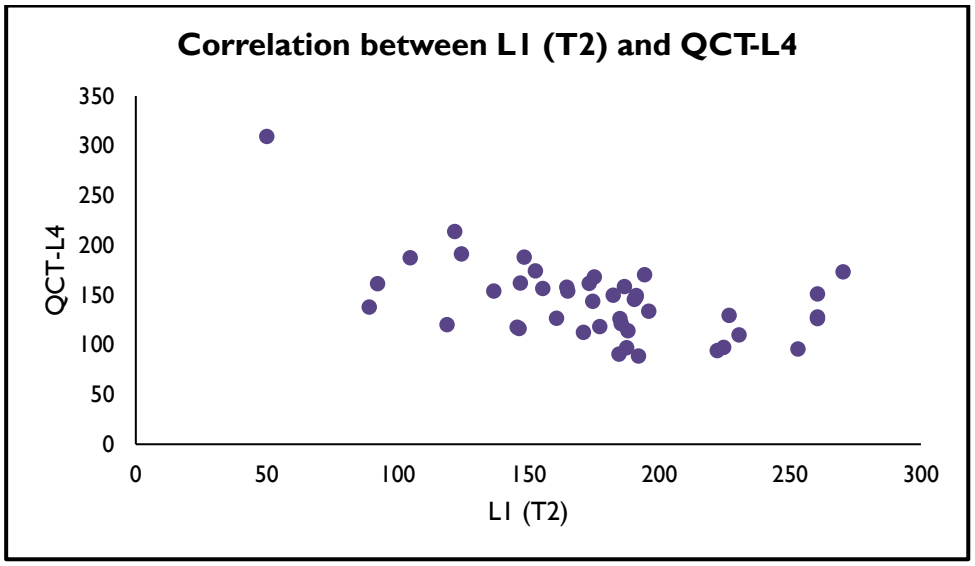

Graph 5.22: The Scatter graph shows correlation between L1 (T2) and QCT-L4

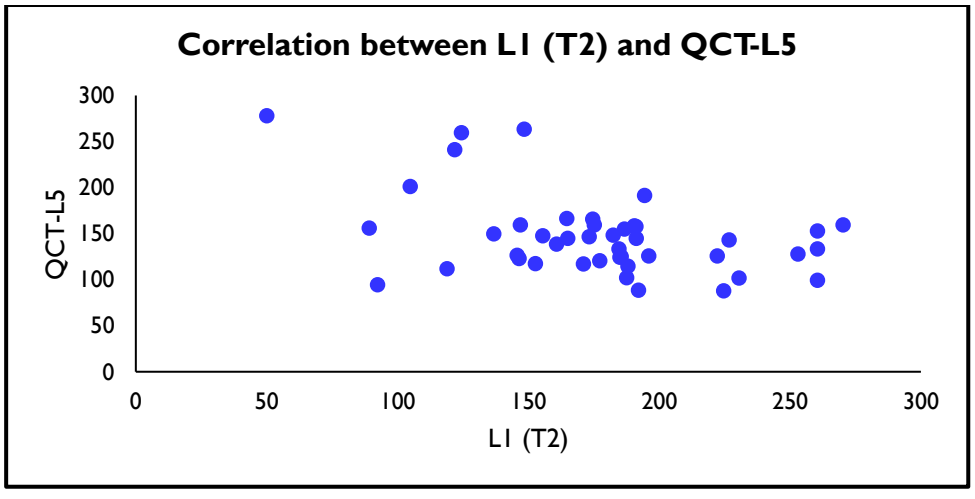

Graph 5.23: The Scatter graph shows correlation between L1 (T2) and QCT-L5

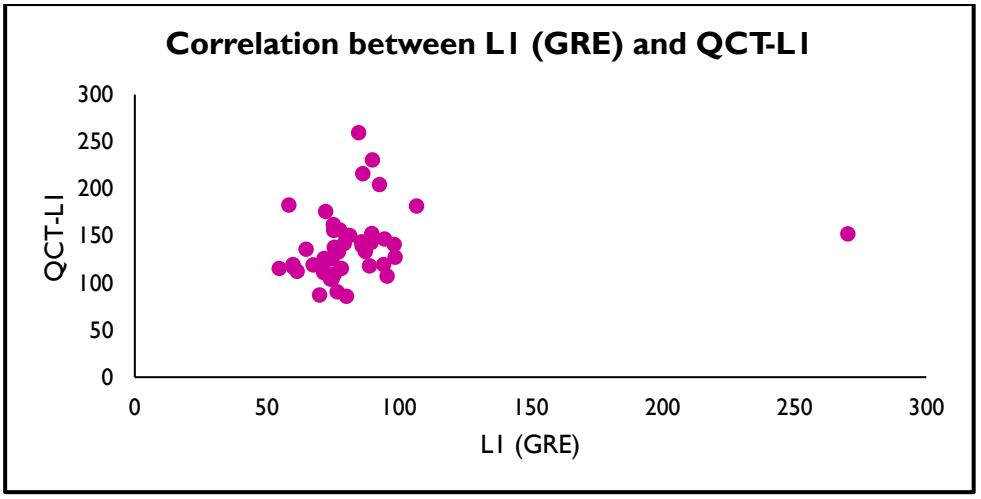

Graph 5.24: The Scatter graph shows correlation between L1 (GRE) and QCT-L1

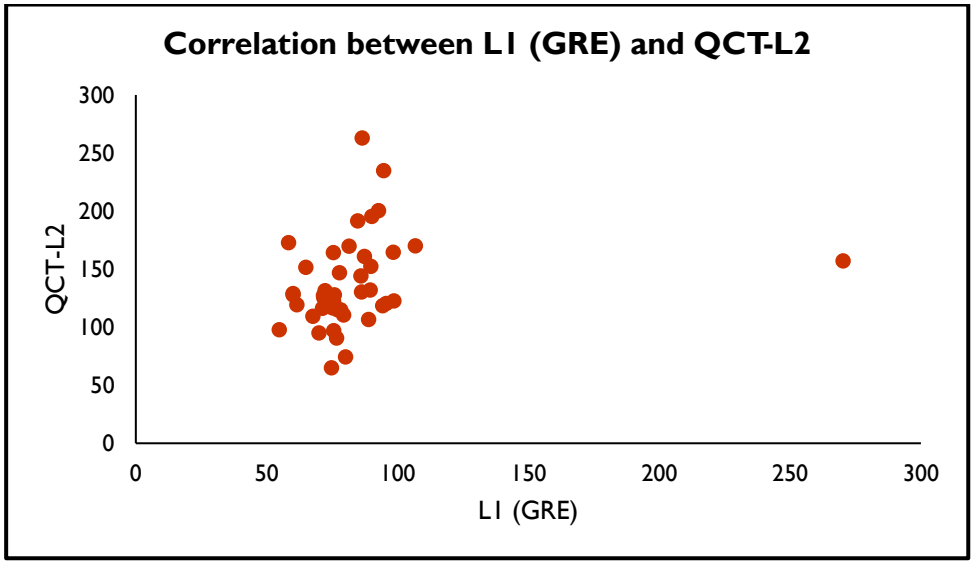

Graph 5.25: The Scatter graph shows correlation between L1 (GRE) and QCT-L2

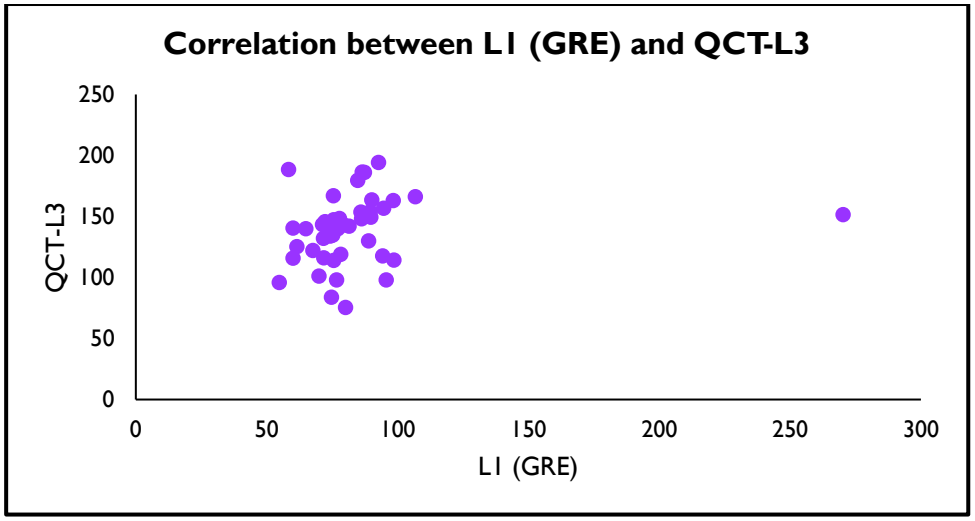

Graph 5.26: The Scatter graph shows correlation between L1 (GRE) and QCT-L3

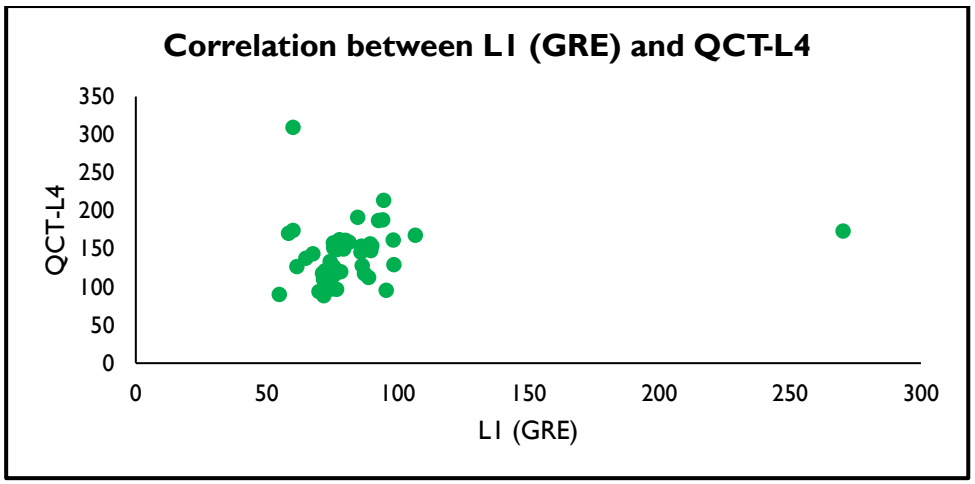

Graph 5.27: The Scatter graph shows correlation between L1 (GRE) and QCT-L4

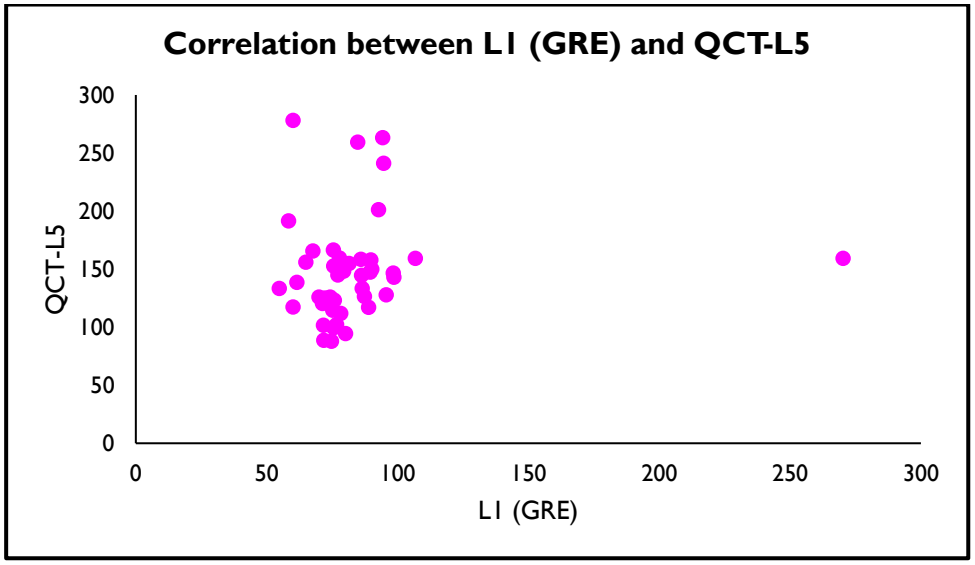

Graph 5.28: The Scatter graph shows correlation between L1 (GRE) and QCT-L5

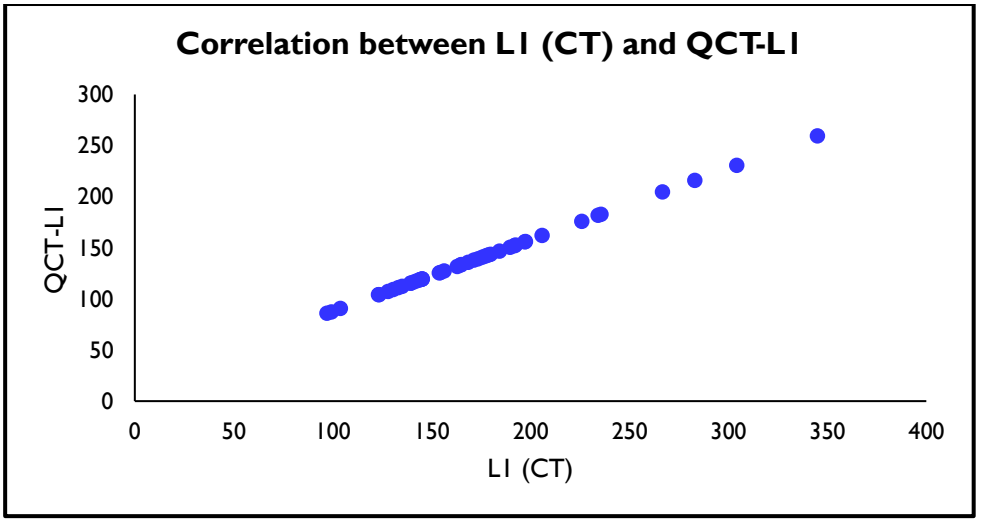

Graph 5.29: The Scatter graph shows correlation between L1 (CT) and QCT-L1

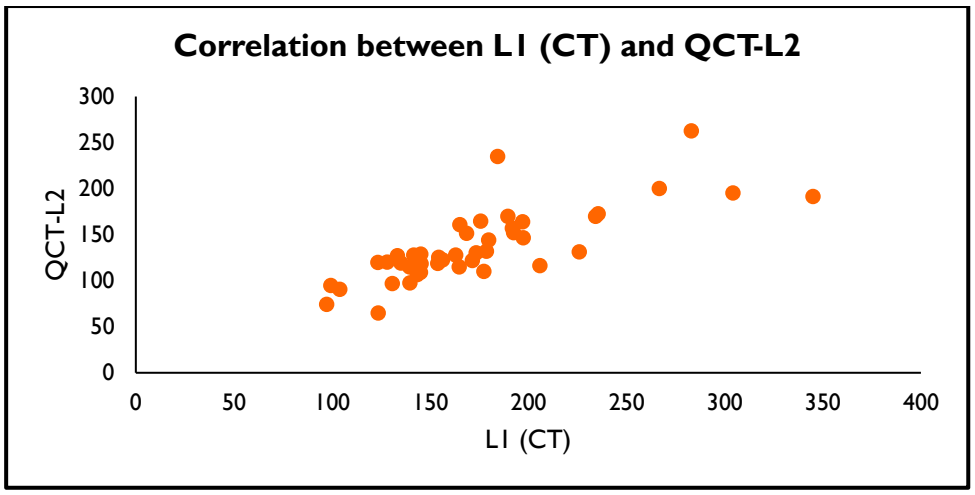

Graph 5.30: The Scatter graph shows correlation between L1 (CT) and QCT-L2

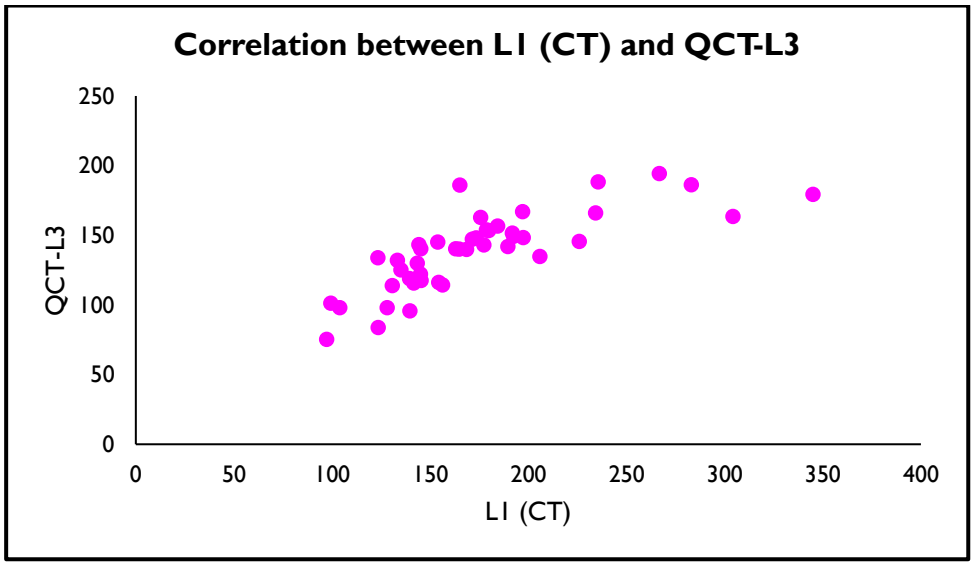

Graph 5.31: The Scatter graph shows correlation between L1 (CT) and QCT-L3

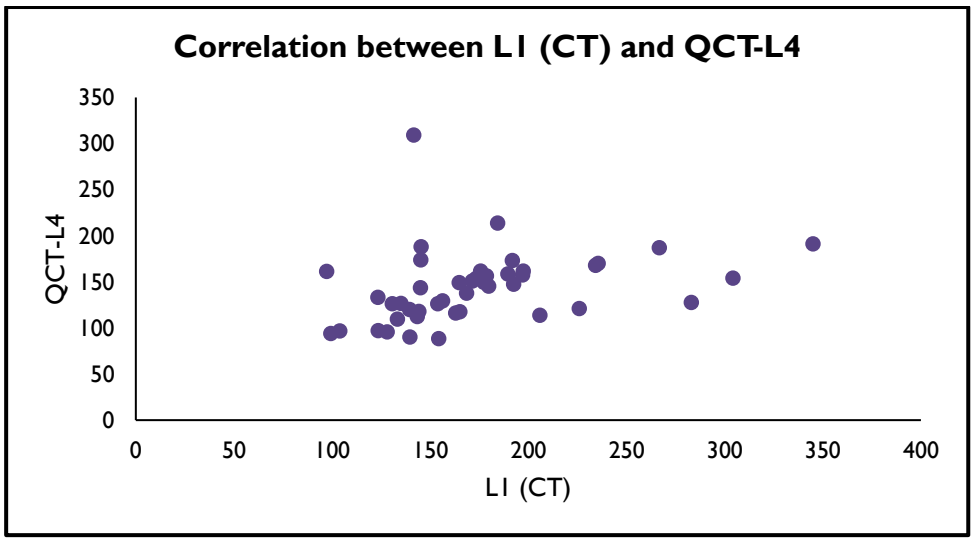

Graph 5.32: The Scatter graph shows correlation between L1 (CT) and QCT-L4

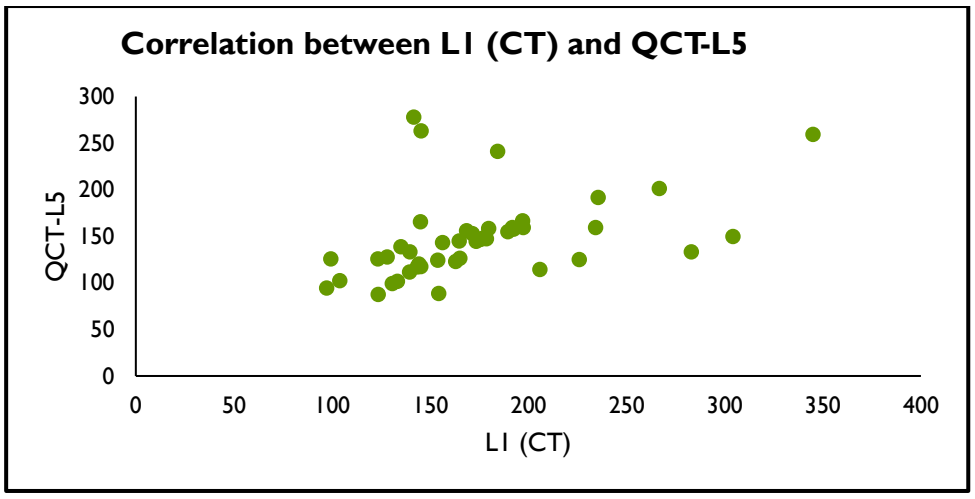

Graph 5.33: The Scatter graph shows correlation between L1 (CT) and QCT-L5

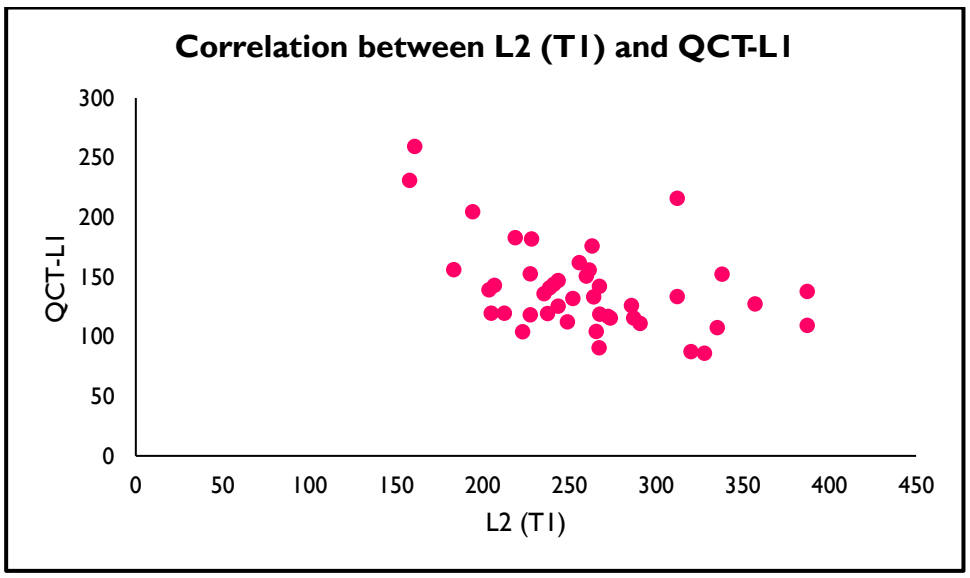

Graph 5.34: The Scatter graph shows correlation between L2 (T1) and QCT-L1

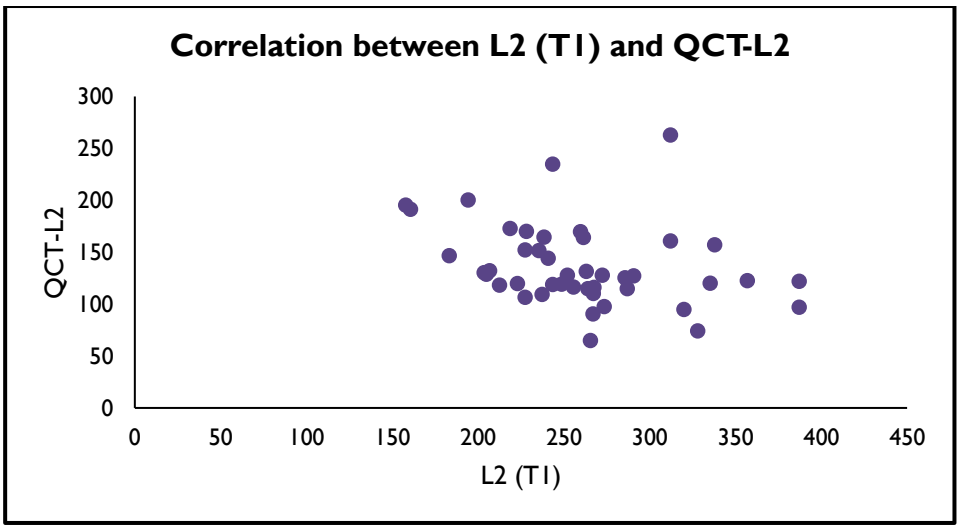

Graph 5.35: The Scatter graph shows correlation between L2 (T1) and QCT-L2

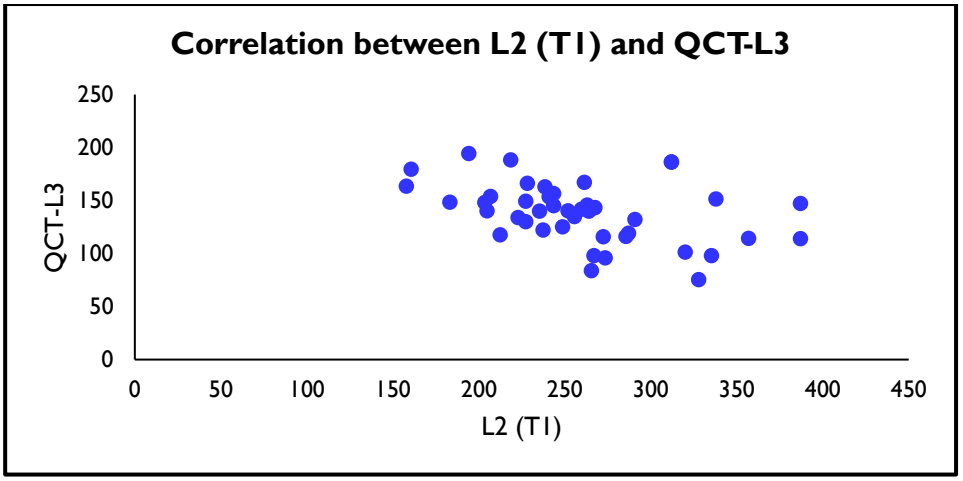

Graph 5.36: The Scatter graph shows correlation between L2 (T1) and QCT-L3

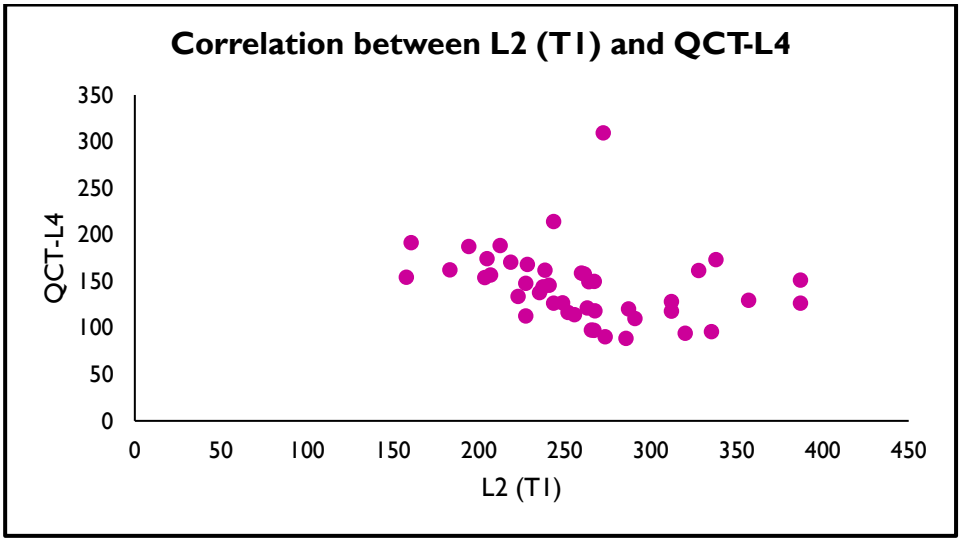

Graph 5.37: The Scatter graph shows correlation between L2 (T1) and QCT-L4

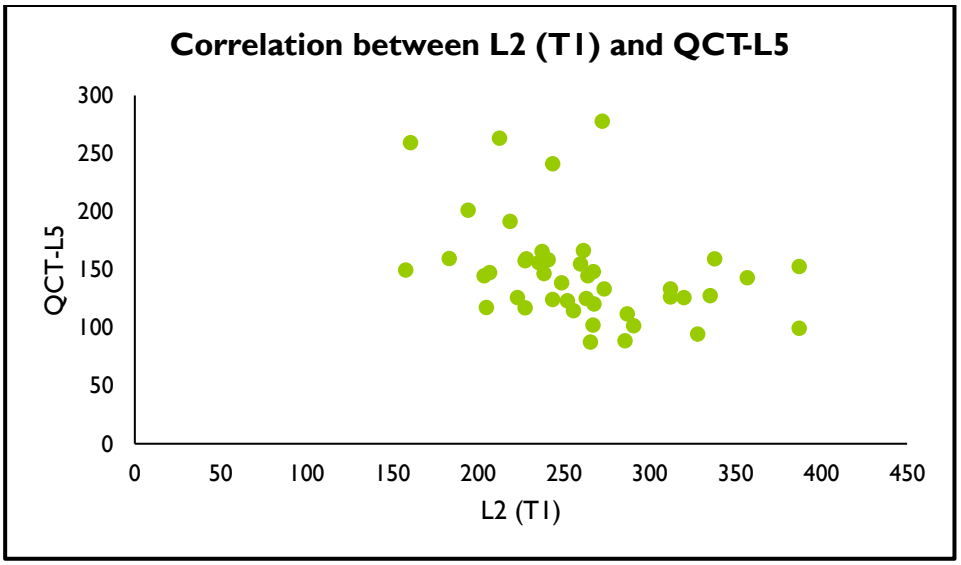

Graph 5.38: The Scatter graph shows correlation between L2 (T1) and QCT-L5

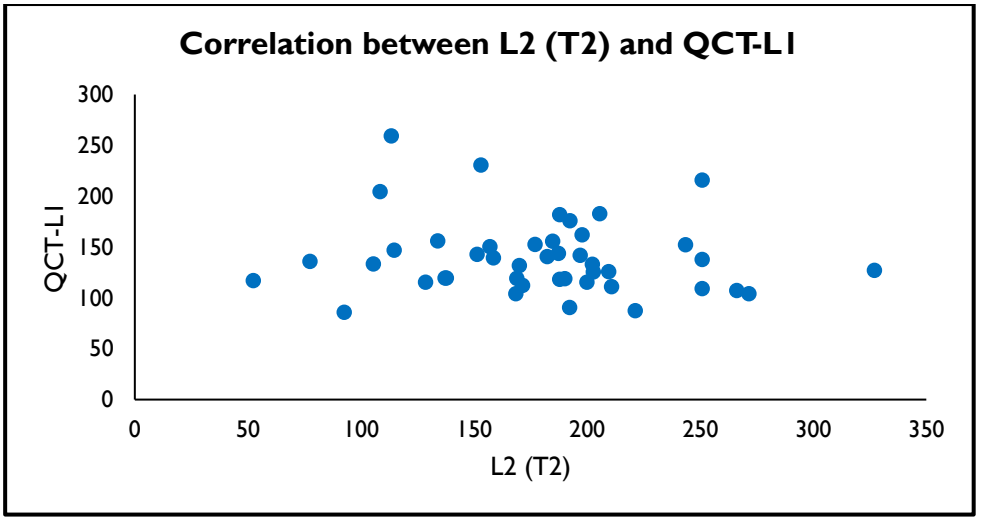

Graph 5.39: The Scatter graph shows correlation between L2 (T2) and QCT-L1

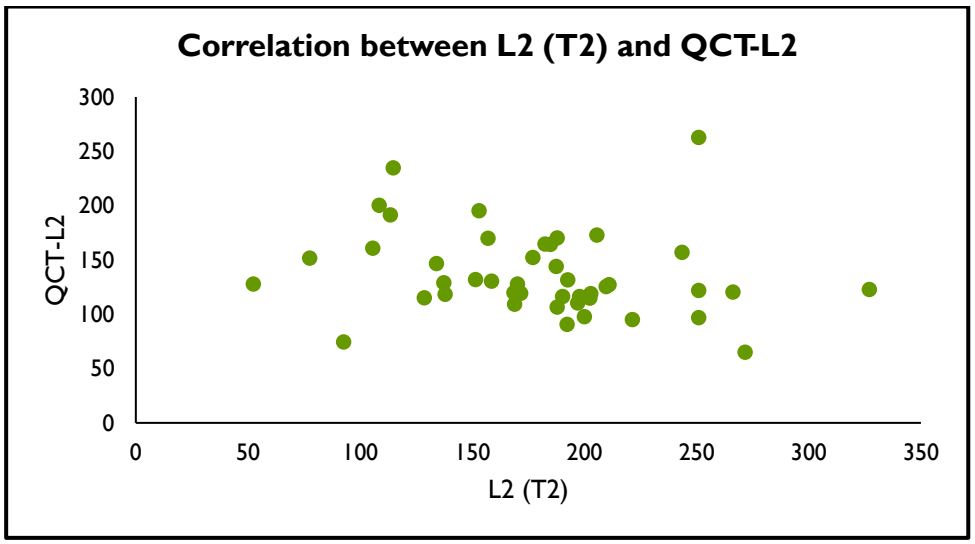

Graph 5.40: The Scatter graph shows correlation between L2 (T2) and QCT-L2

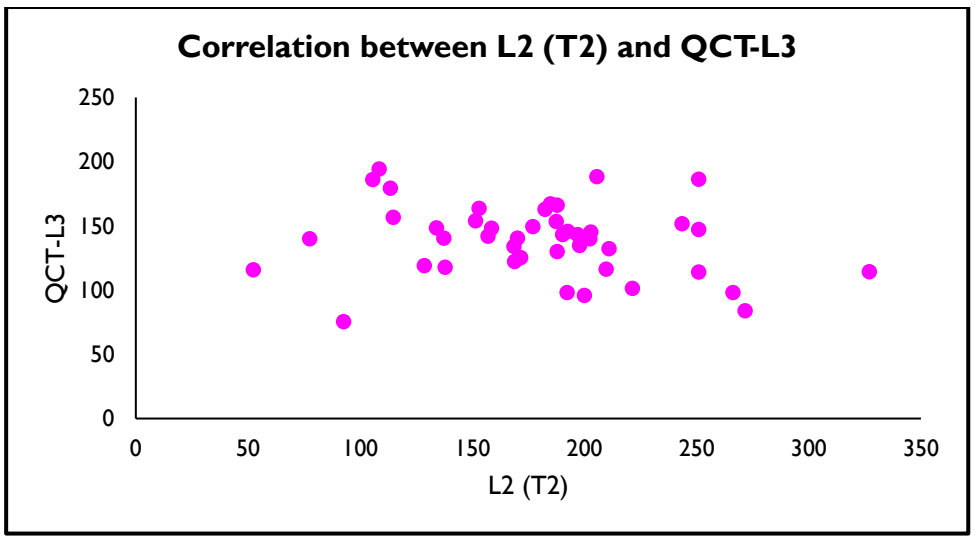

Graph 5.41: The Scatter graph shows correlation between L2 (T2) and QCT-L3

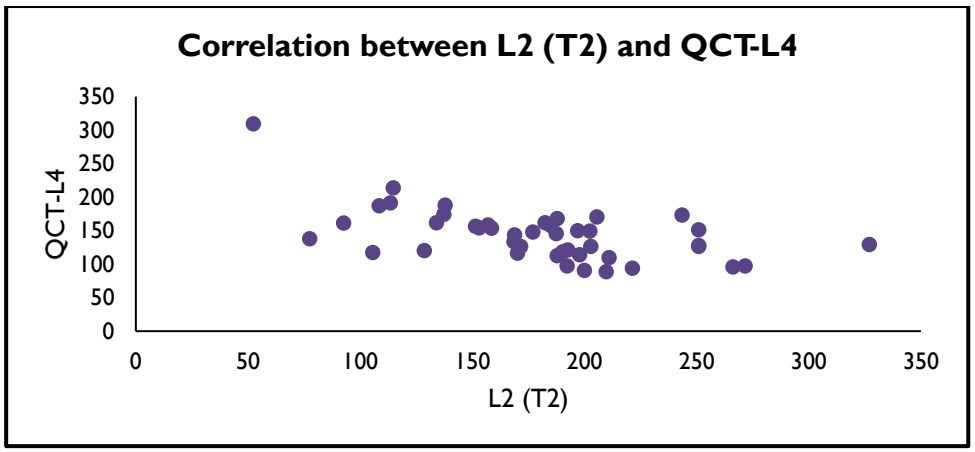

Graph 5.42: The Scatter graph shows correlation between L2 (T2) and QCT-L4

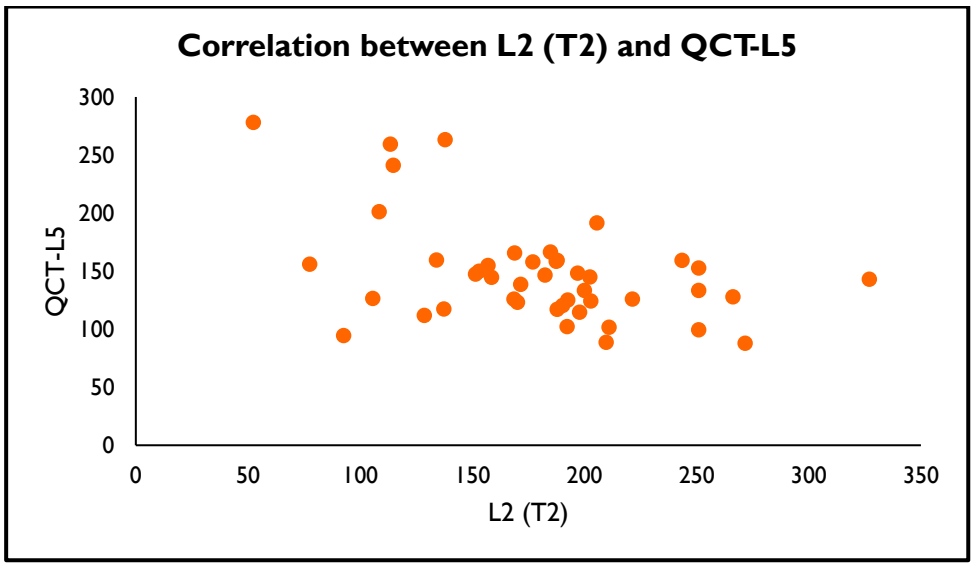

Graph 5.43: The Scatter graph shows correlation between L2 (T2) and QCT-L5

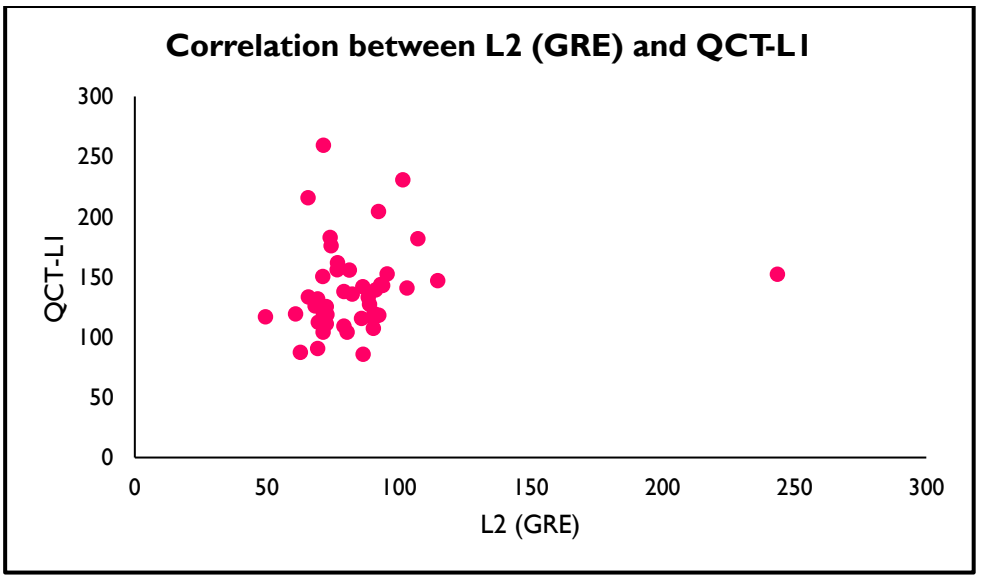

Graph 5.44: The Scatter graph shows correlation between L2 (GRE) and QCT-L1

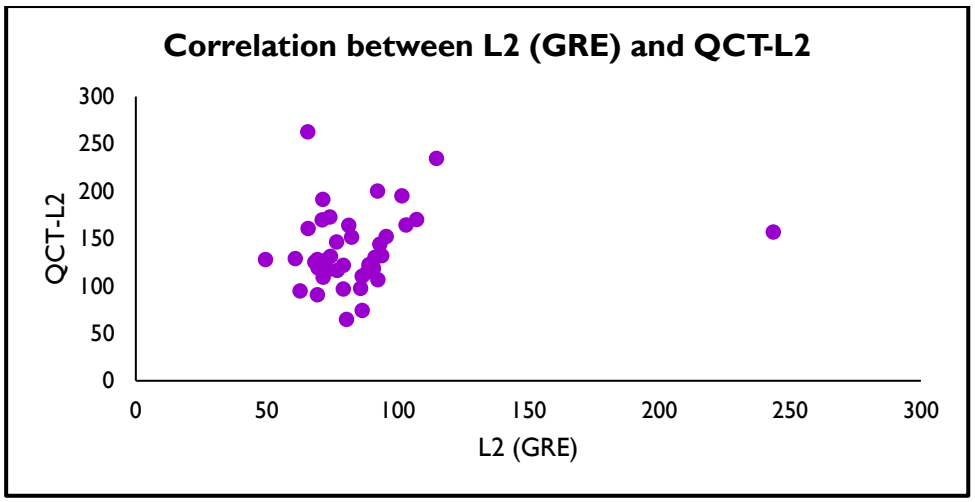

Graph 5.45: The Scatter graph shows correlation between L2 (GRE) and QCT-L2

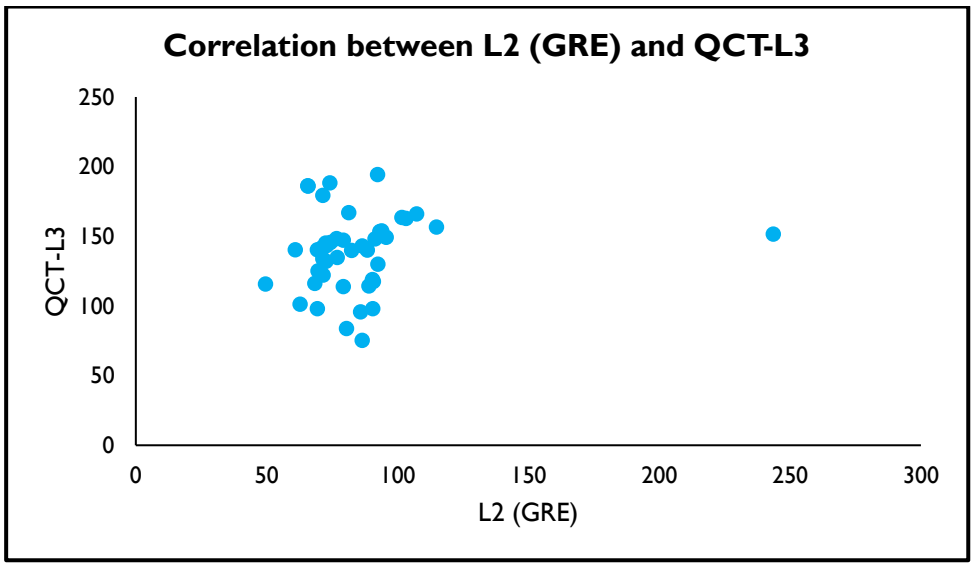

Graph 5.46: The Scatter graph shows correlation between L2 (GRE) and QCT-L3

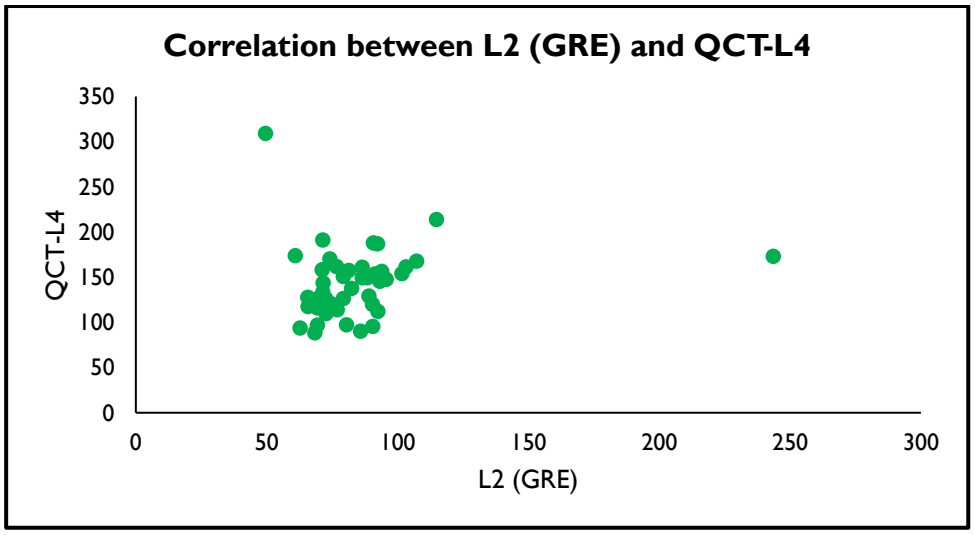

Graph 5.47: The Scatter graph shows correlation between L2 (GRE) and QCT-L4

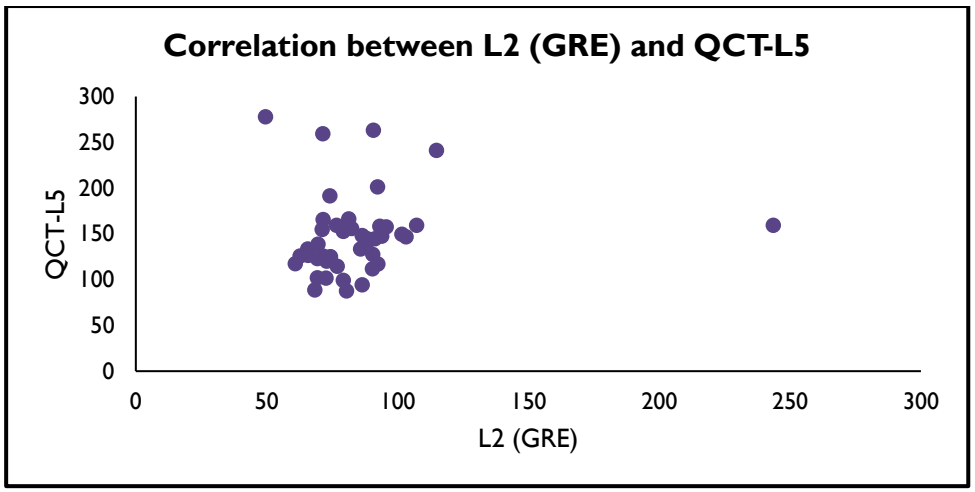

Graph 5.48: The Scatter graph shows correlation between L2 (GRE) and QCT-L5

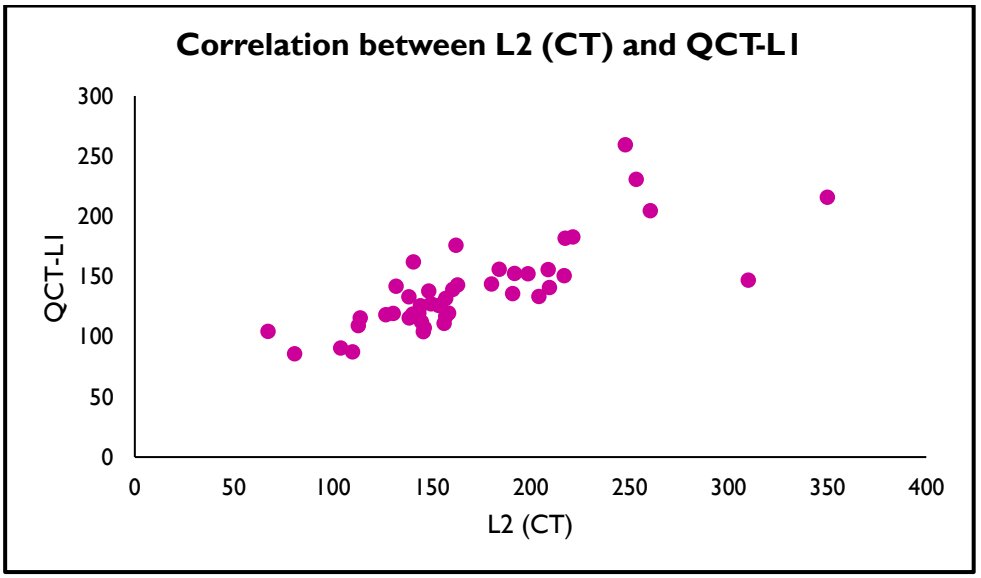

Graph 5.49: The Scatter graph shows correlation between L2 (CT) and QCT-L1

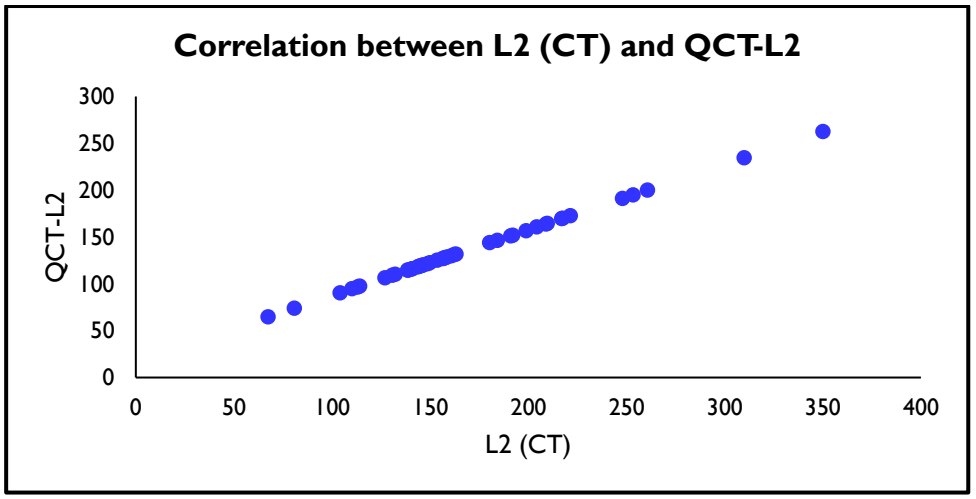

Graph 5.50: The Scatter graph shows correlation between L2 (CT) and QCT-L2

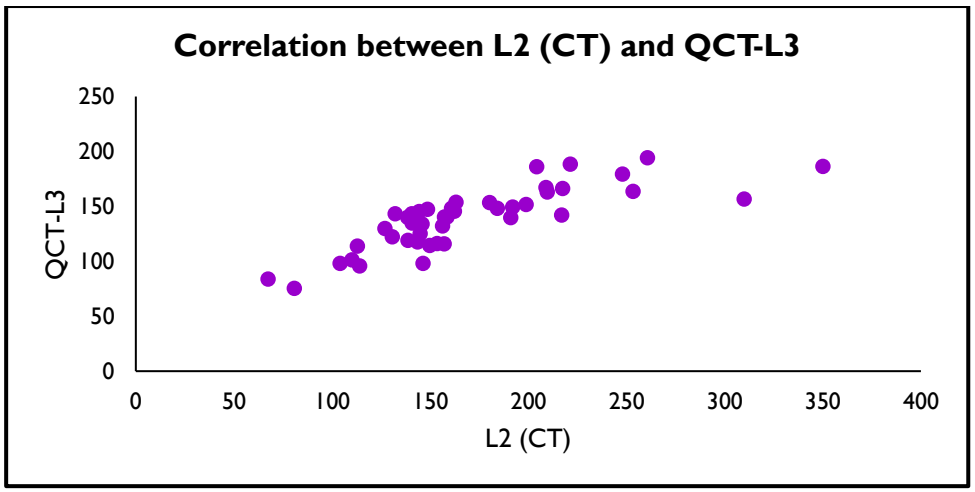

Graph 5.51: The Scatter graph shows correlation between L2 (CT) and QCT-L3

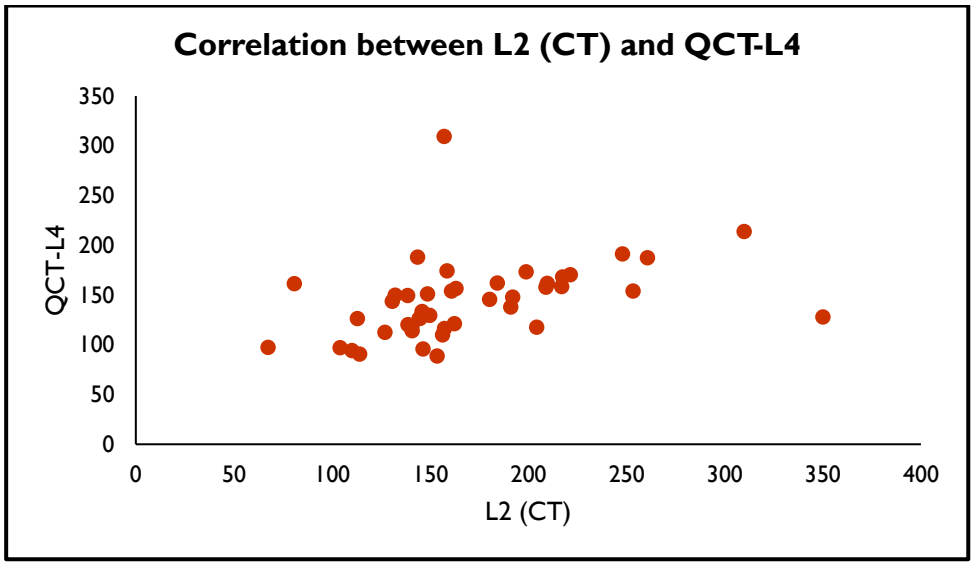

Graph 5.52: The Scatter graph shows correlation between L2 (CT) and QCT-L4

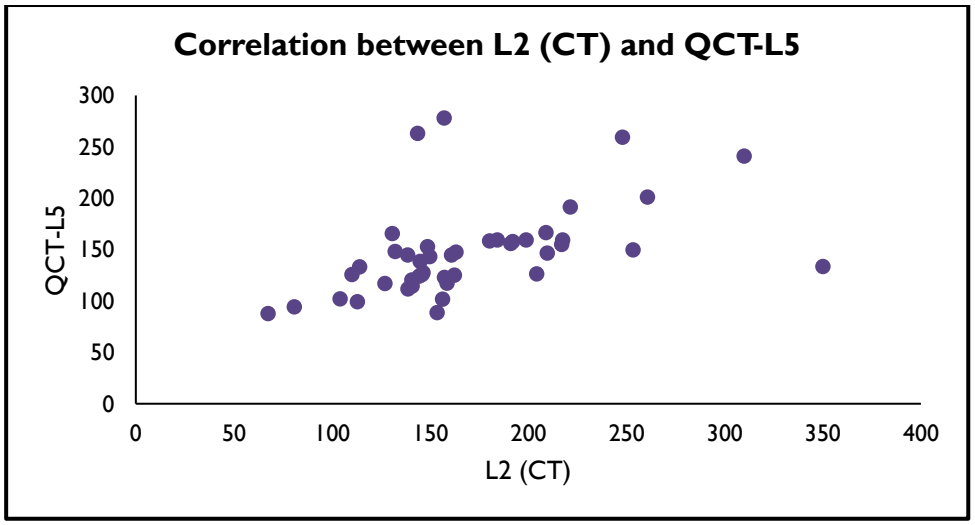

Graph 5.53: The Scatter graph shows correlation between L2 (CT) and QCT-L5

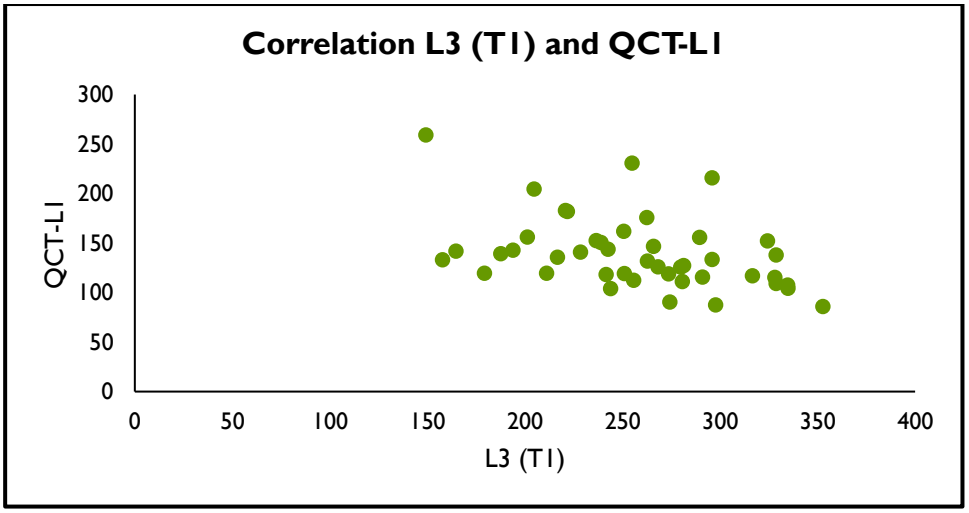

Graph 5.54: The Scatter graph shows correlation L3 (T1) and QCT-L1

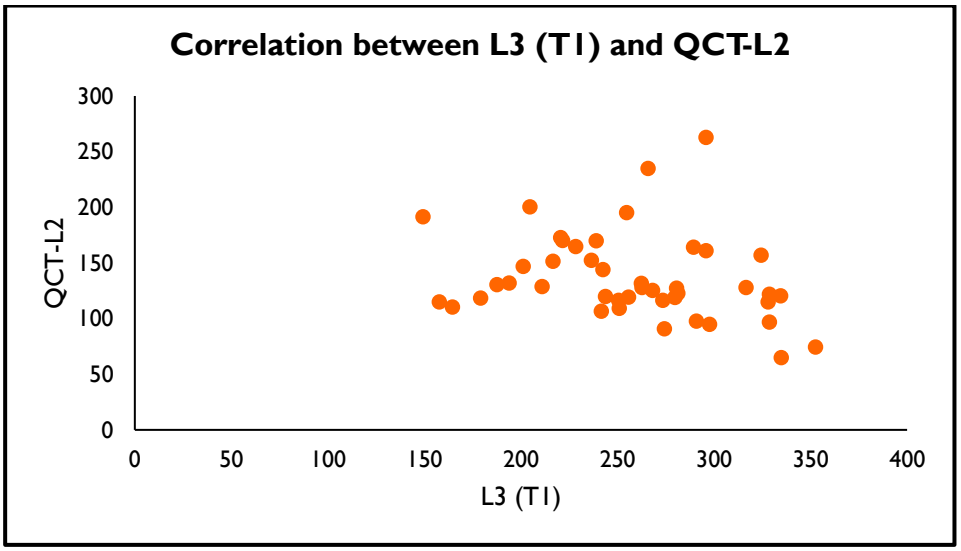

Graph 5.55: The Scatter graph shows correlation between L3 (T1) and QCT-L2

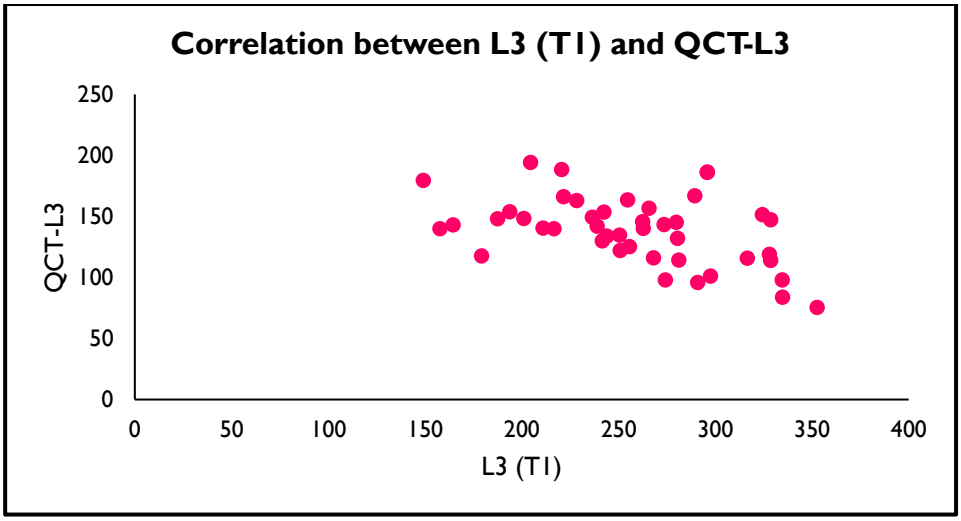

Graph 5.56: The Scatter graph shows correlation between L3 (T1) and QCT-L3

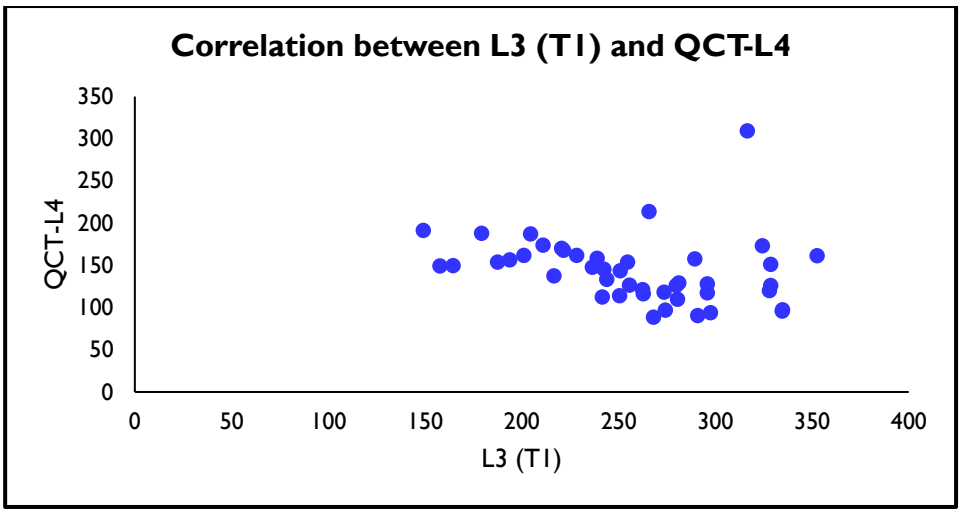

Graph 5.57: The Scatter graph shows correlation between L3 (T1) and QCT-L4

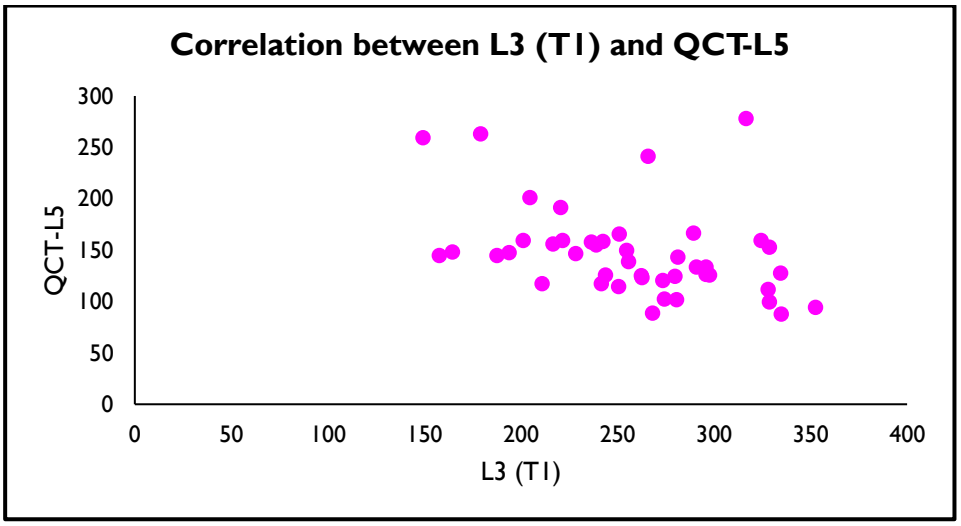

Graph 5.58: The Scatter graph shows correlation between L3 (T1) and QCT-L5

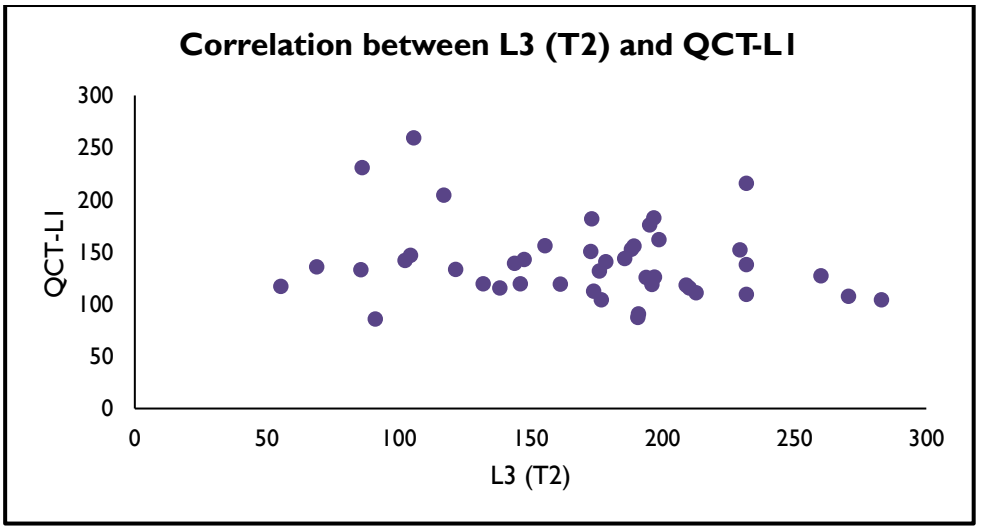

Graph 5.59: The Scatter graph shows correlation between L3 (T2) and QCT-L1

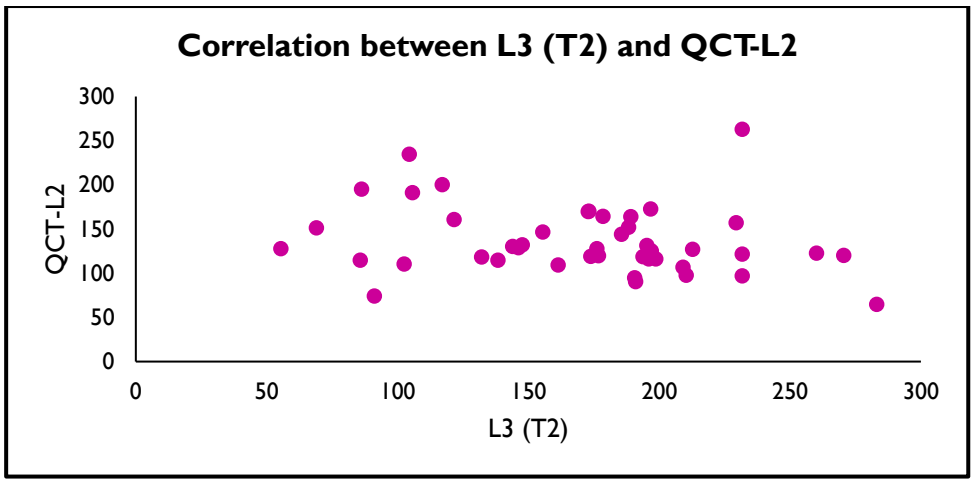

Graph 5.60: The Scatter graph shows correlation between L3 (T2) and QCT-L2

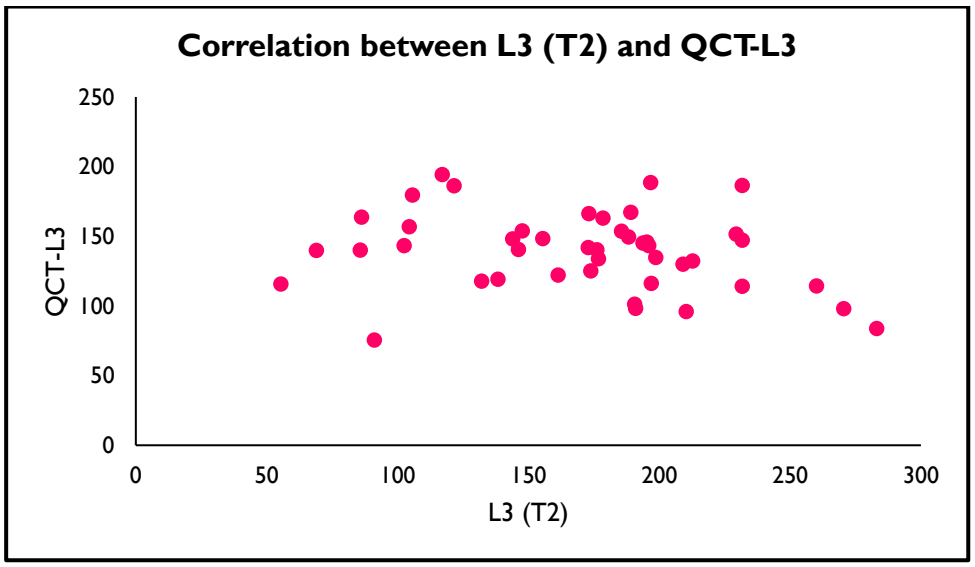

Graph 5.61: The Scatter graph shows correlation between L3 (T2) and QCT-L3

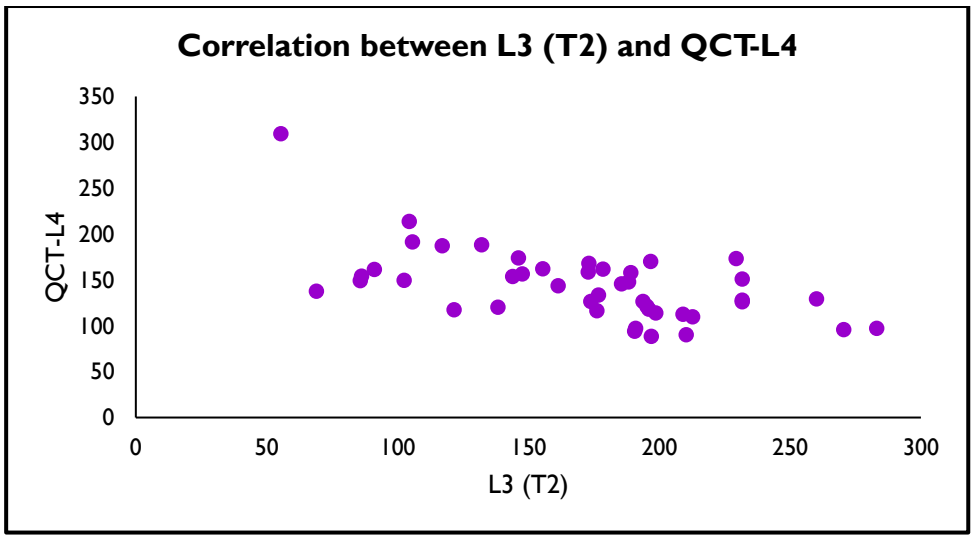

Graph 5.62: The Scatter graph shows correlation between L3 (T2) and QCT-L4

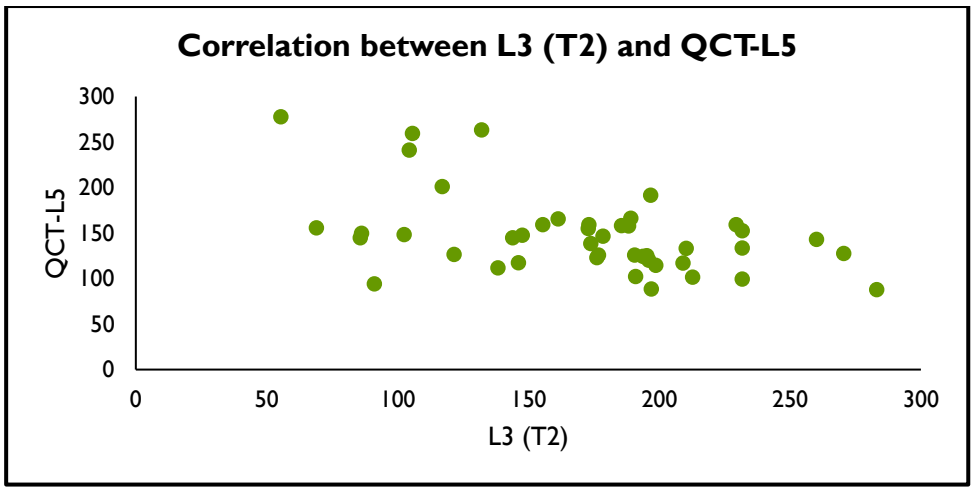

Graph 5.63: The Scatter graph shows correlation between L3 (T2) and QCT-L5

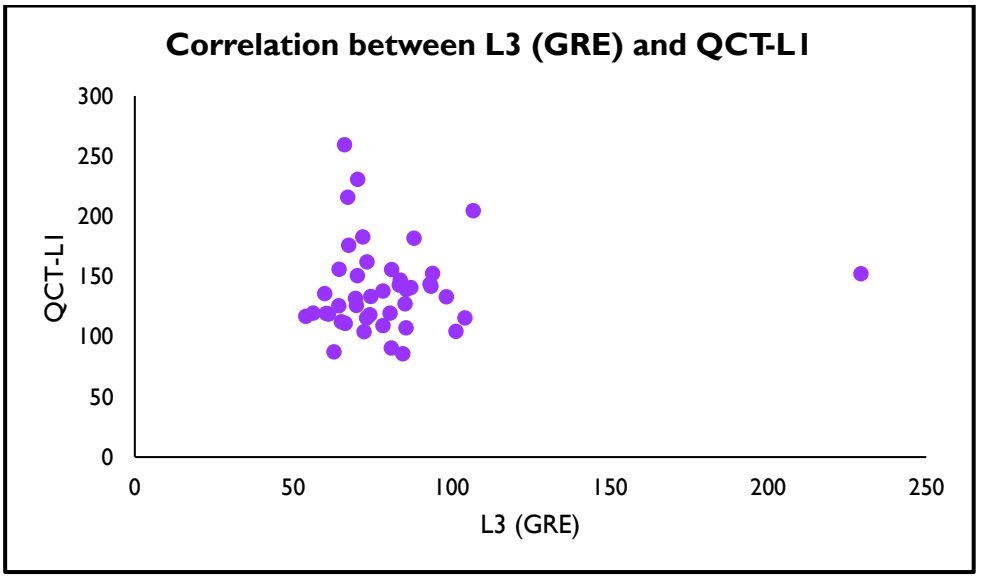

Graph 5.64: The Scatter graph shows correlation between L3 (GRE) and QCT-L1

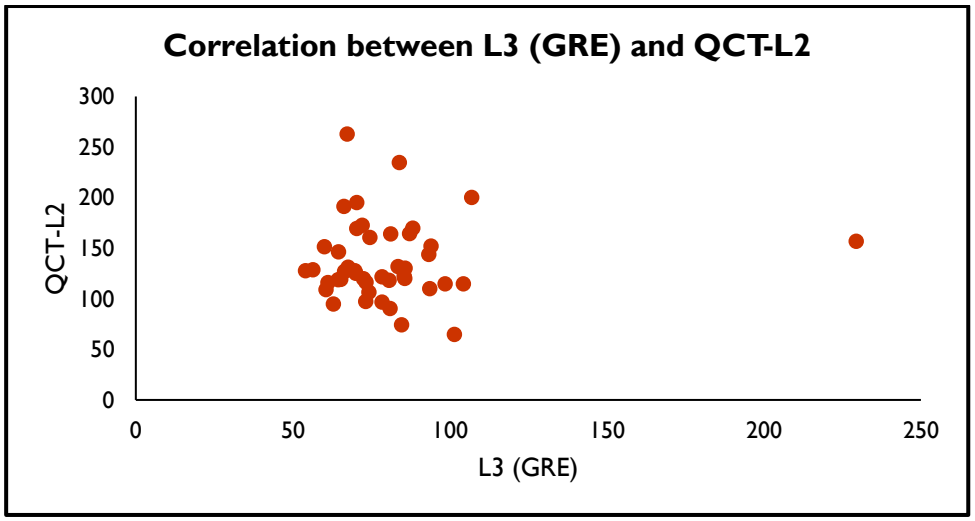

Graph 5.65: The Scatter graph shows correlation between L3 (GRE) and QCT-L2

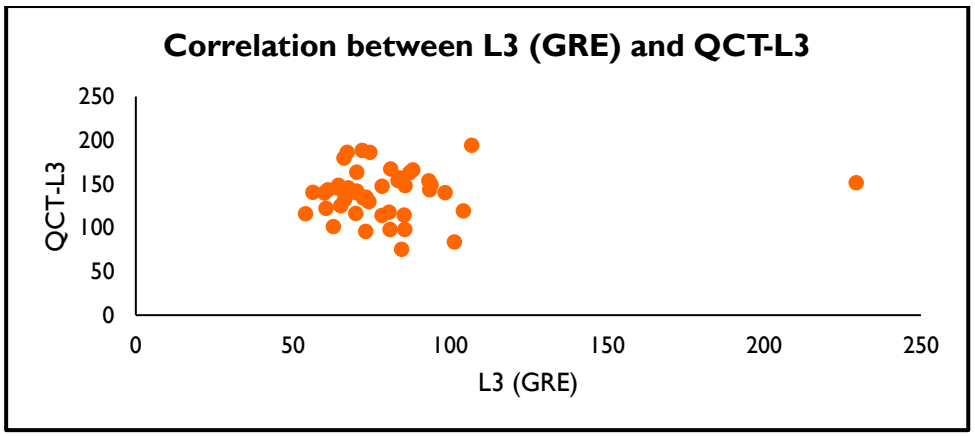

Graph 5.66: The Scatter graph shows correlation between L3 (GRE) and QCT-L3

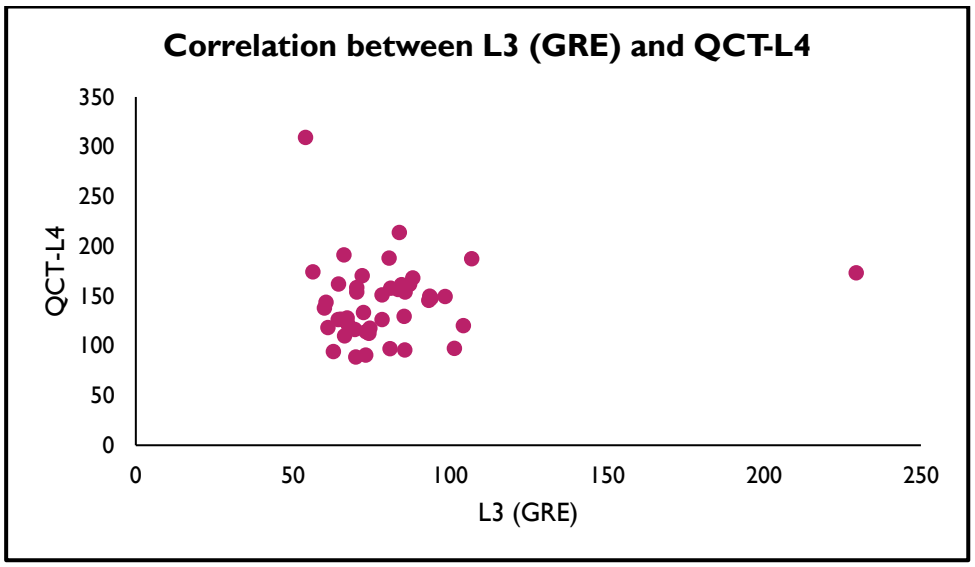

Graph 5.67: The Scatter graph shows correlation between L3 (GRE) and QCT-L4

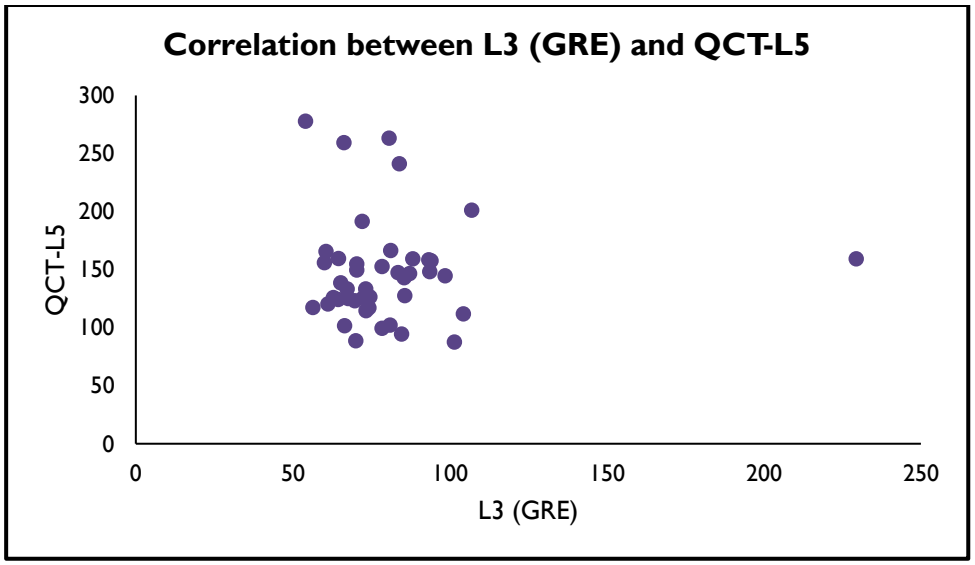

Graph 5.68: The Scatter graph shows correlation between L3 (GRE) and QCT-L5

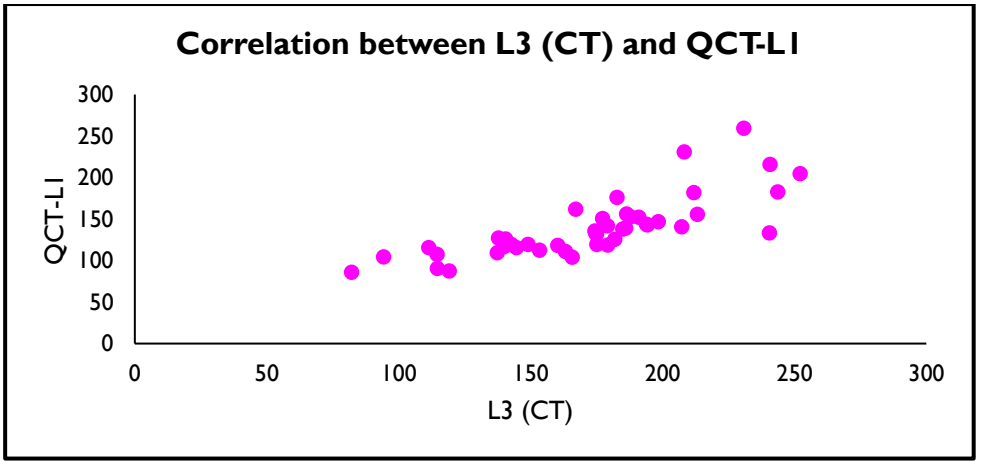

Graph 5.69: The Scatter graph shows correlation between L3 (CT) and QCT-L1

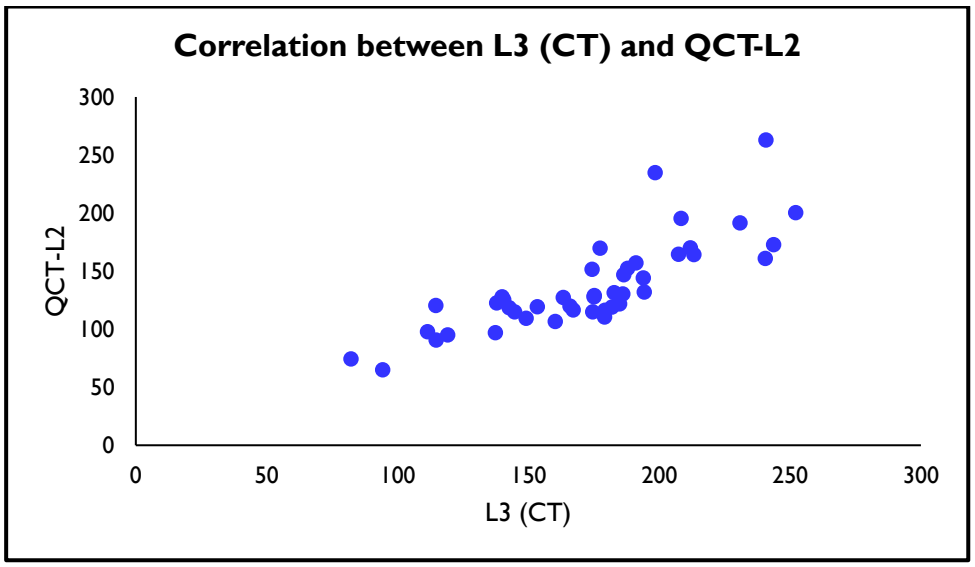

Graph 5.70: The Scatter graph shows correlation between L3 (CT) and QCT-L2

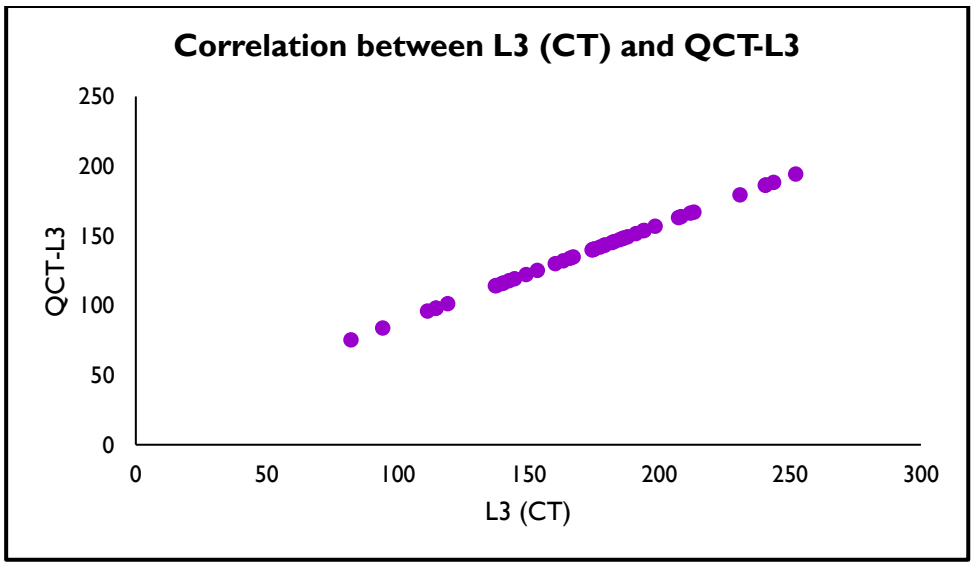

Graph 5.71: The Scatter graph shows correlation between L3 (CT) and QCT-L3

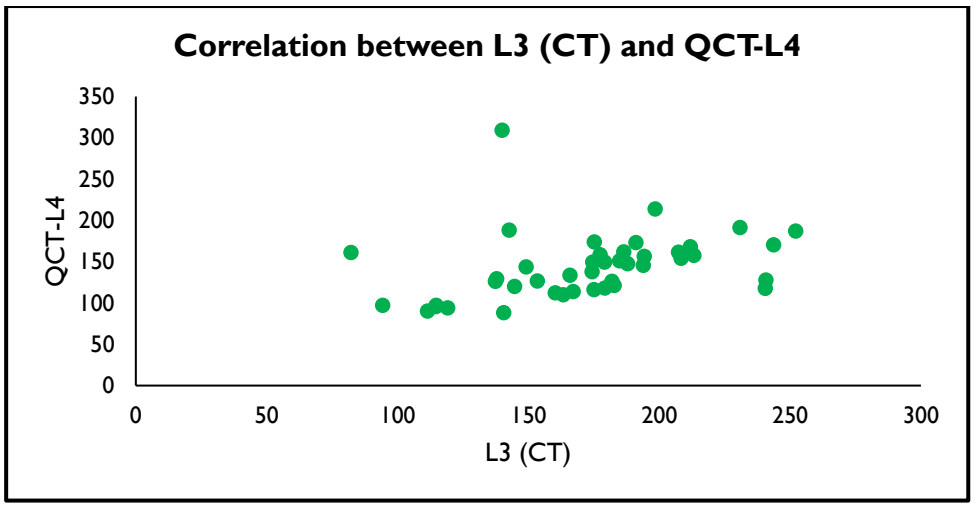

Graph 5.72: The Scatter graph shows correlation between L3 (CT) and QCT-L4

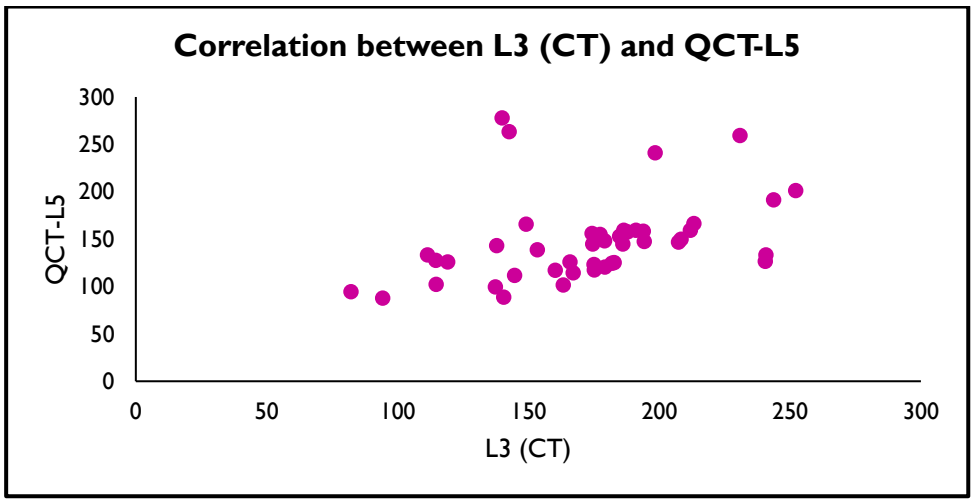

Graph 5.73: The Scatter graph shows correlation between L3 (CT) and QCT-L5

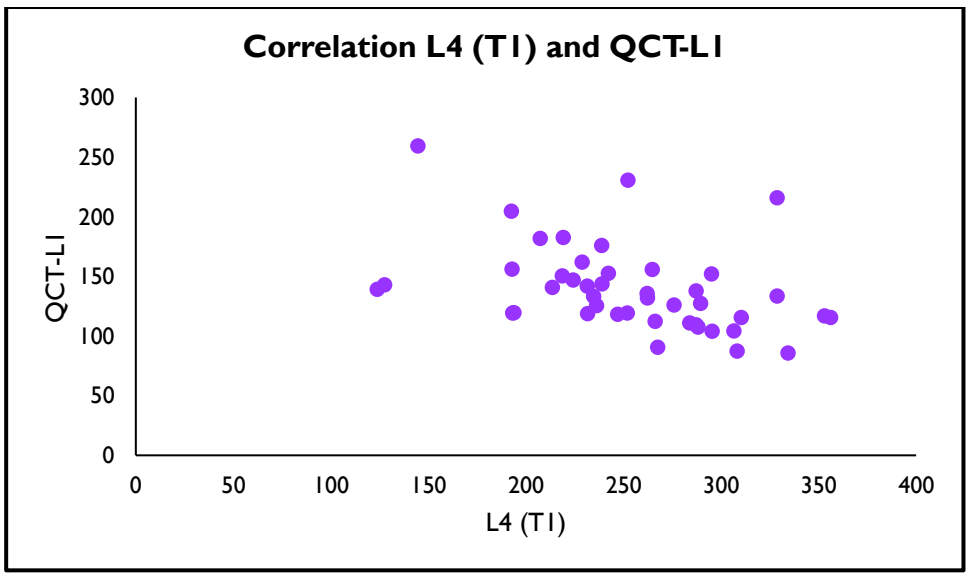

Graph 5.74: The Scatter graph shows correlation L4 (T1) and QCT-L1

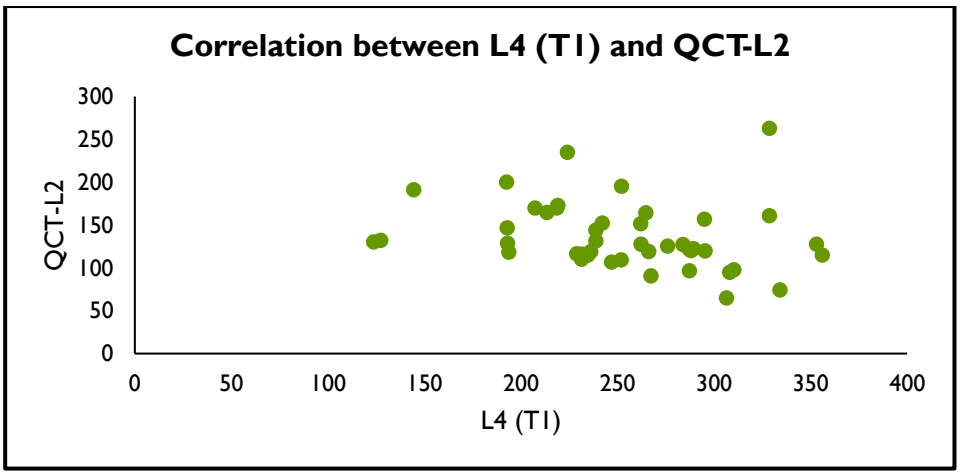

Graph 5.75: The Scatter graph shows correlation between L4 (T1) and QCT-L2

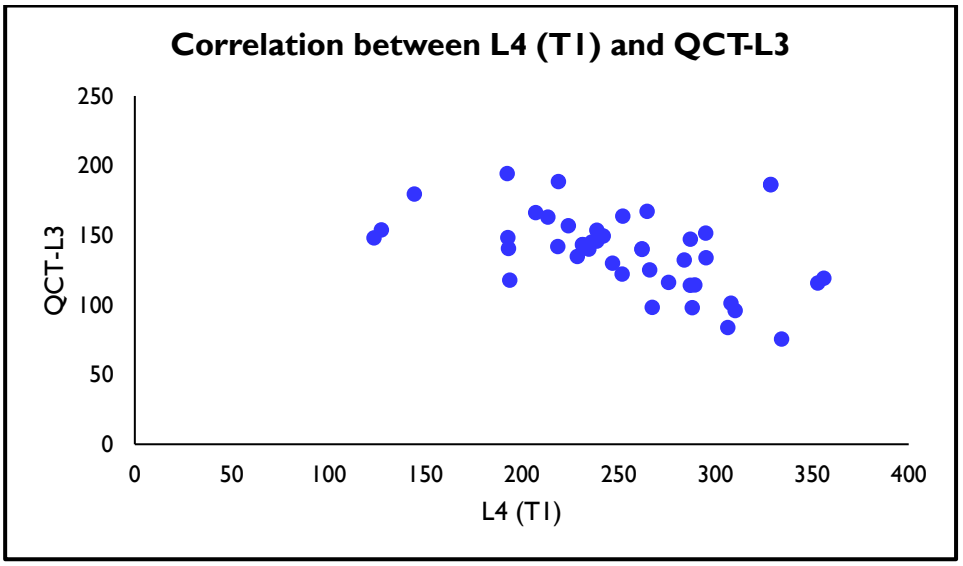

Graph 5.76: The Scatter graph shows correlation between L4 (T1) and QCT-L3

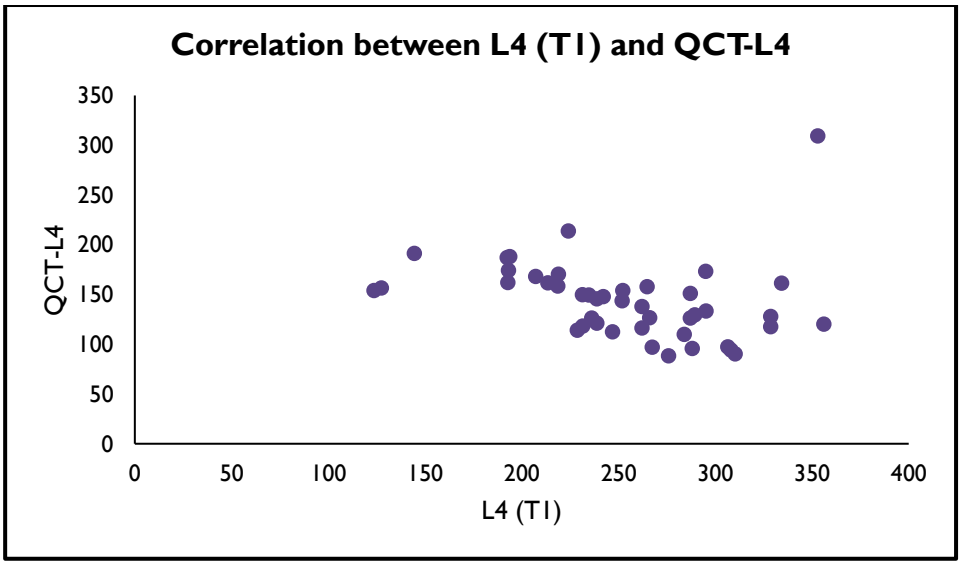

Graph 5.77: The Scatter graph shows correlation between L4 (T1) and QCT-L4

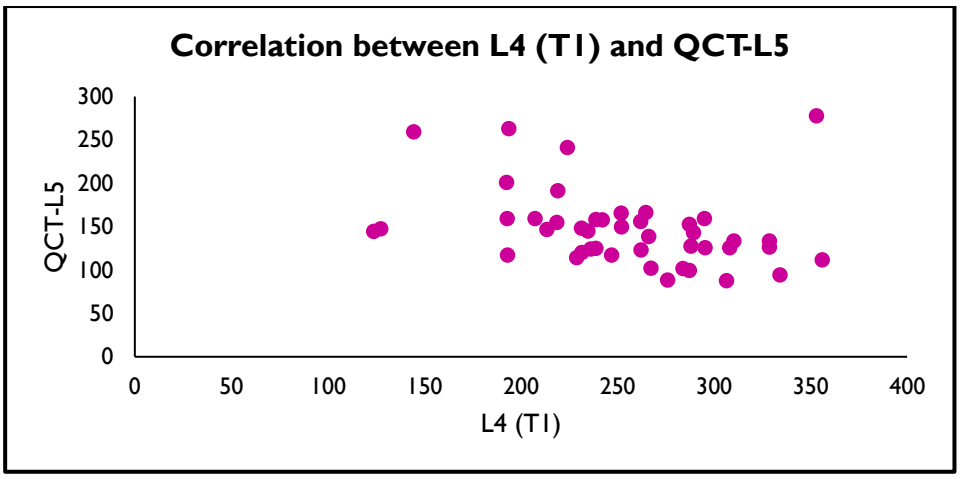

Graph 5.78: The Scatter graph shows correlation between L4 (T1) and QCT-L5

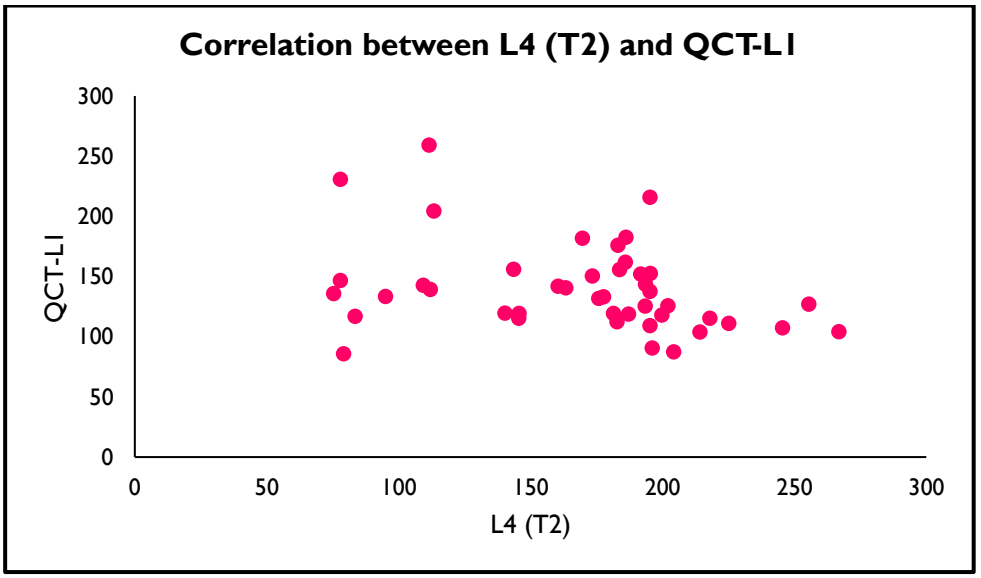

Graph 5.79: The Scatter graph shows correlation between L4 (T2) and QCT-L1

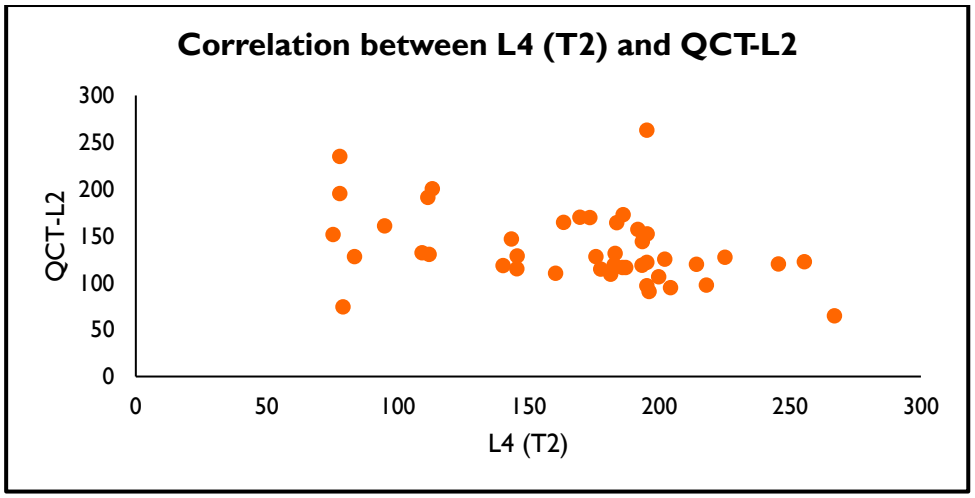

Graph 5.80: The Scatter graph shows correlation between L4 (T2) and QCT-L2

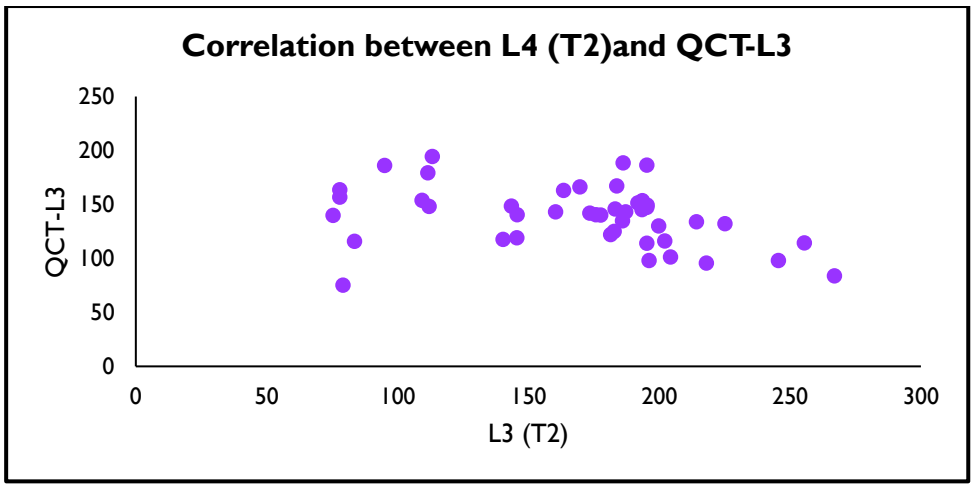

Graph 5.81: The Scatter graph shows correlation between L4 (T2) and QCT-L3

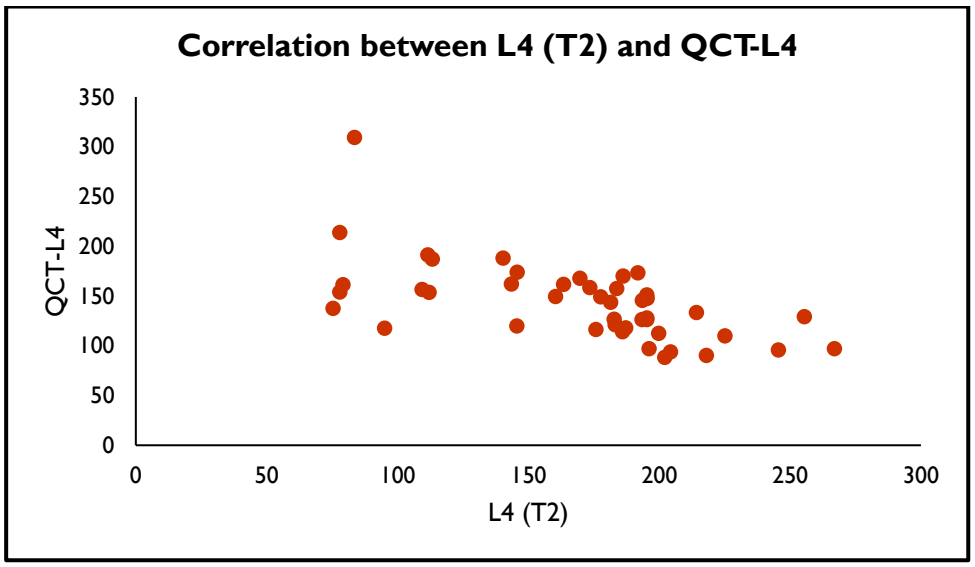

Graph 5.82: The Scatter graph shows correlation between L4 (T2) and QCT-L4

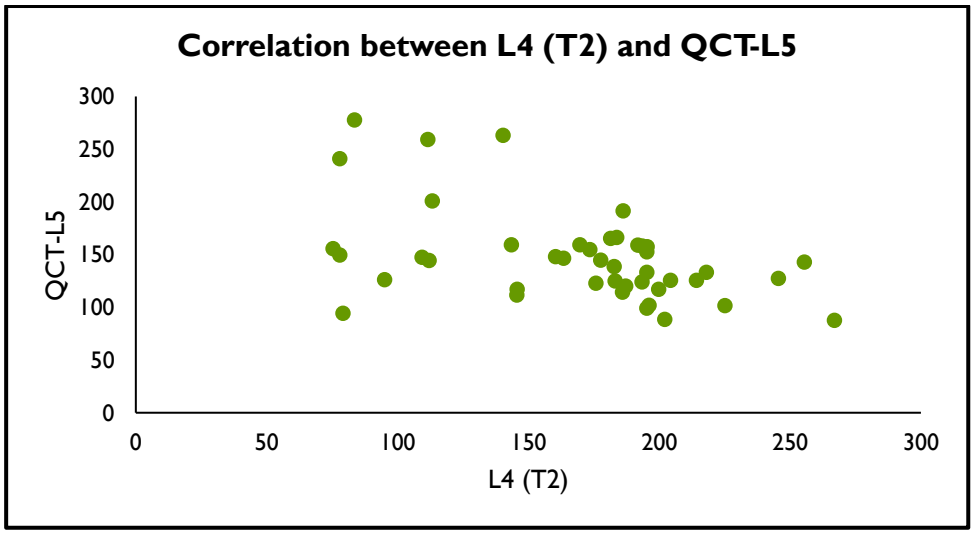

Graph 5.83: The Scatter graph shows correlation between L4 (T2) and QCT-L5

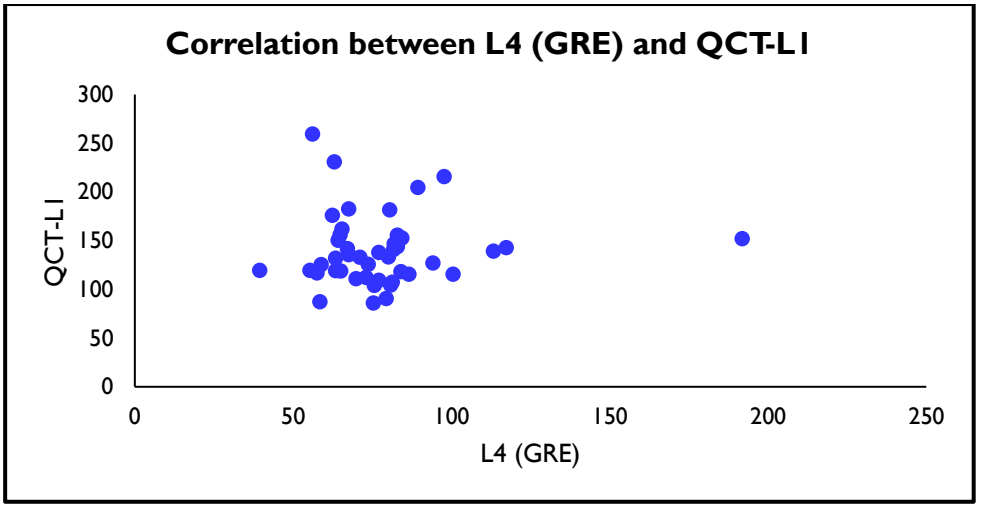

Graph 5.84: The Scatter graph shows correlation between L4 (GRE) and QCT-L1

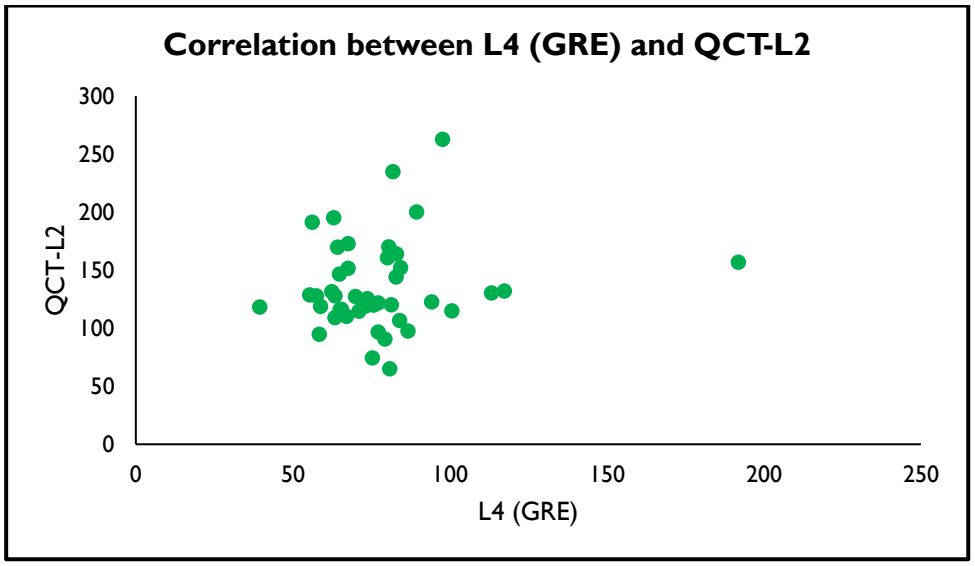

Graph 5.85: The Scatter graph shows correlation between L4 (GRE) and QCT-L2

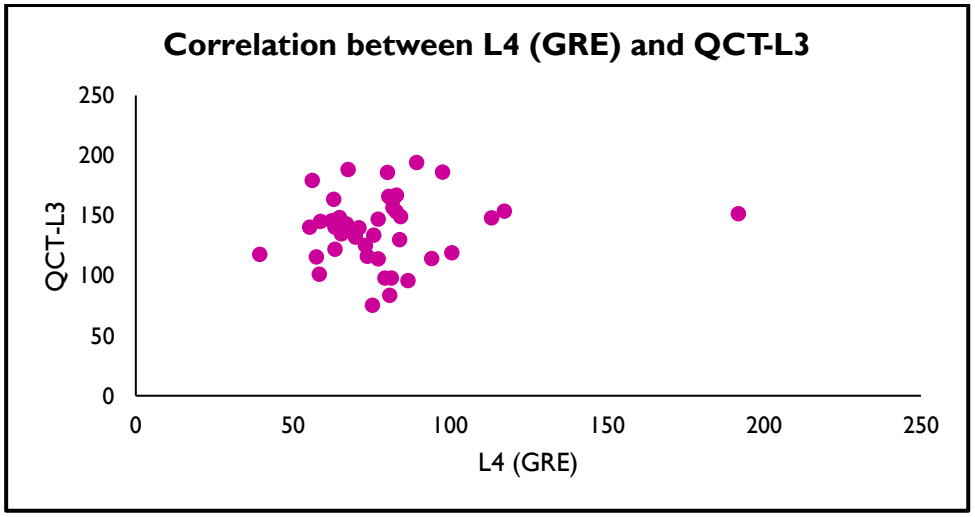

Graph 5.86: The Scatter graph shows correlation between L4 (GRE) and QCT-L3

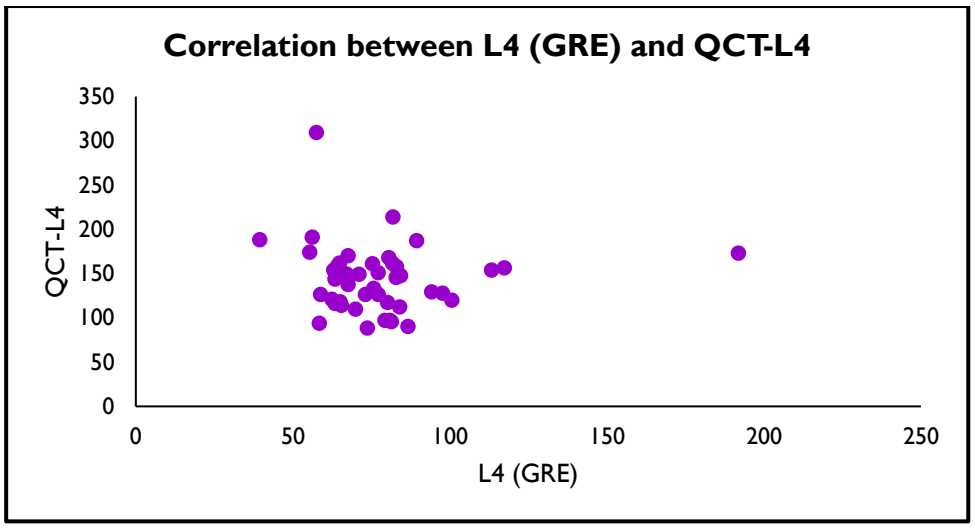

Graph 5.87: The Scatter graph shows correlation between L4 (GRE) and QCT-L4

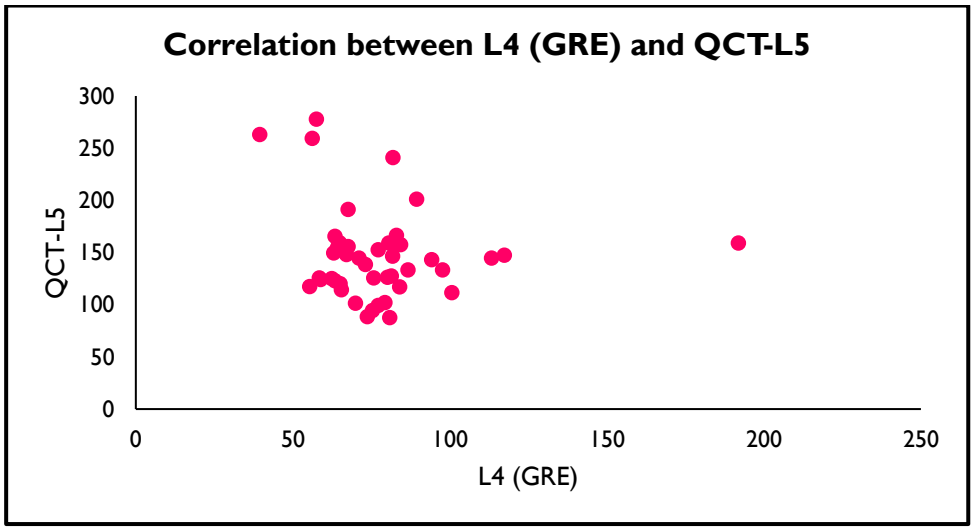

Graph 5.88: The Scatter graph shows correlation between L4 (GRE) and QCT-L5

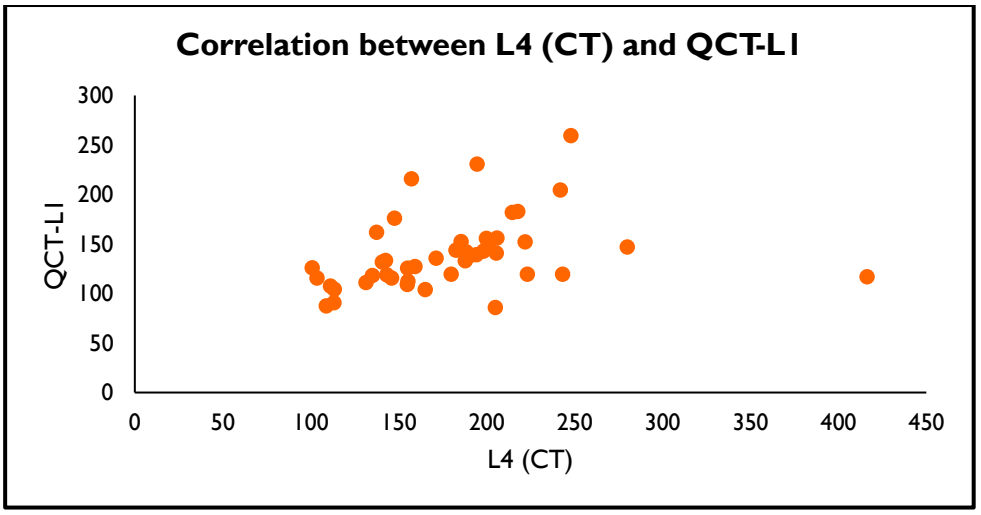

Graph 5.89: The Scatter graph shows correlation between L4 (CT) and QCT-L1

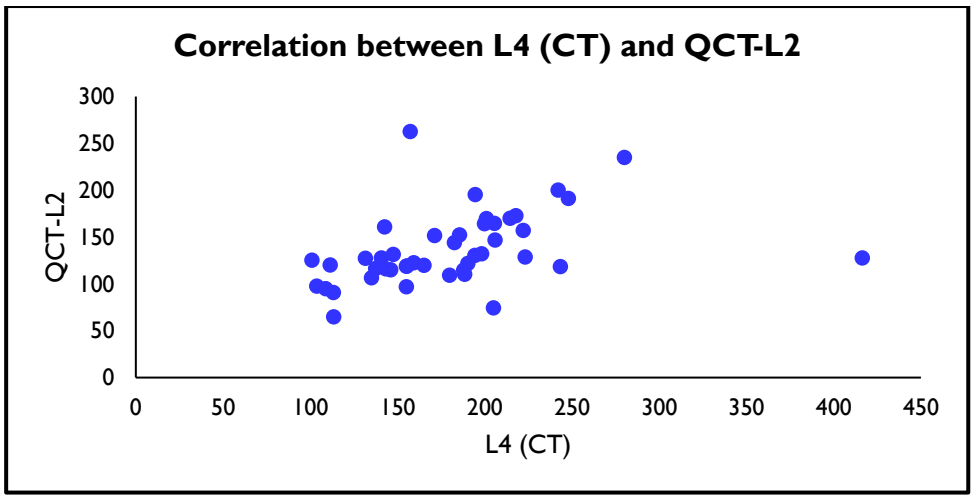

Graph 5.90: The Scatter graph shows correlation between L4 (CT) and QCT-L2

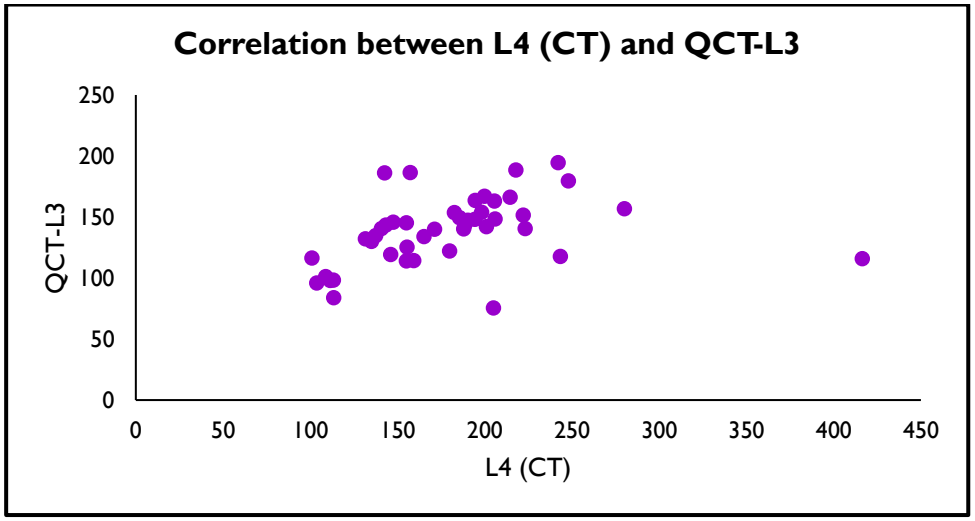

Graph 5.91: The Scatter graph shows correlation between L4 (CT) and QCT-L3

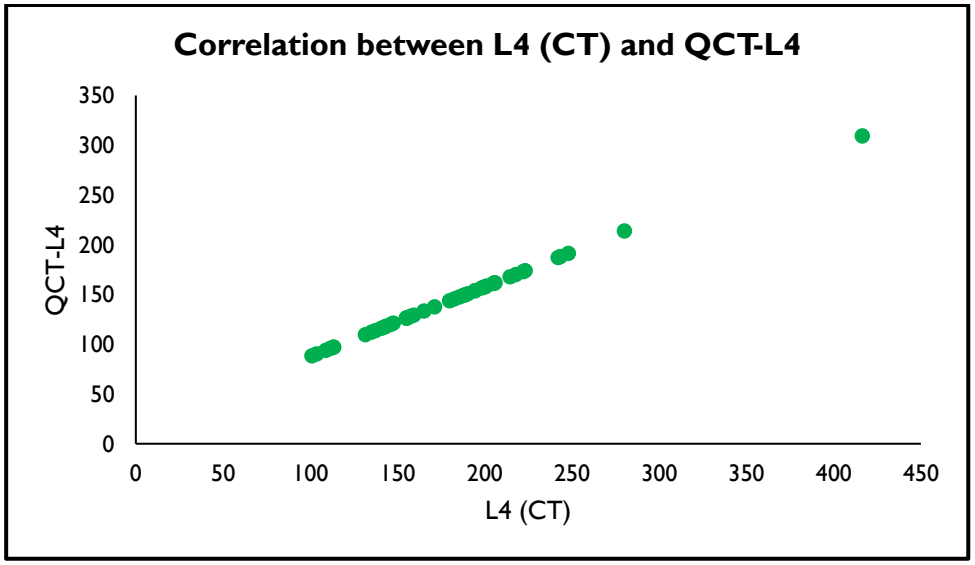

Graph 5.92: The Scatter graph shows correlation between L4 (CT) and QCT-L4

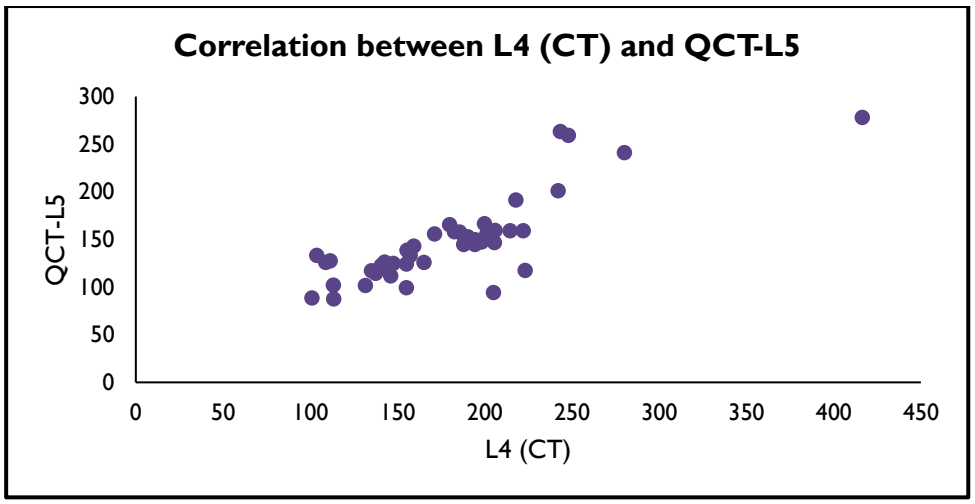

Graph 5.93: The Scatter graph shows correlation between L4 (CT) and QCT-L5

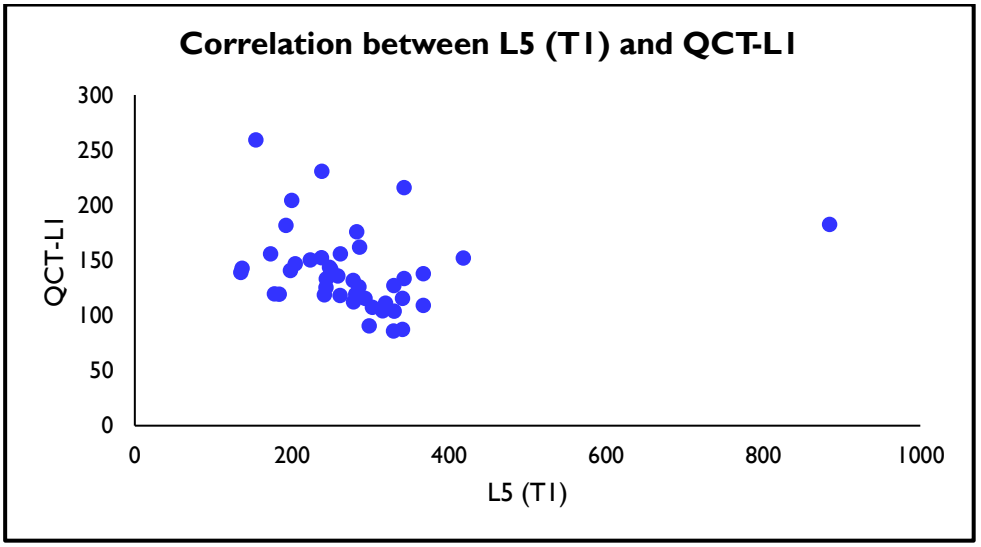

Graph 5.94: The Scatter graph shows correlation between L5 (T1) and QCT-L1

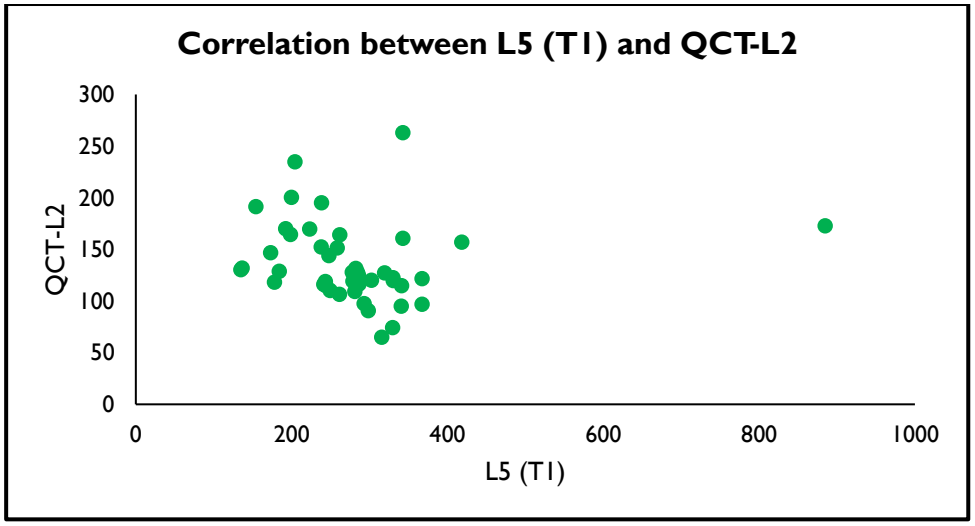

Graph 5.95: The Scatter graph shows correlation between L5 (T1) and QCT-L2

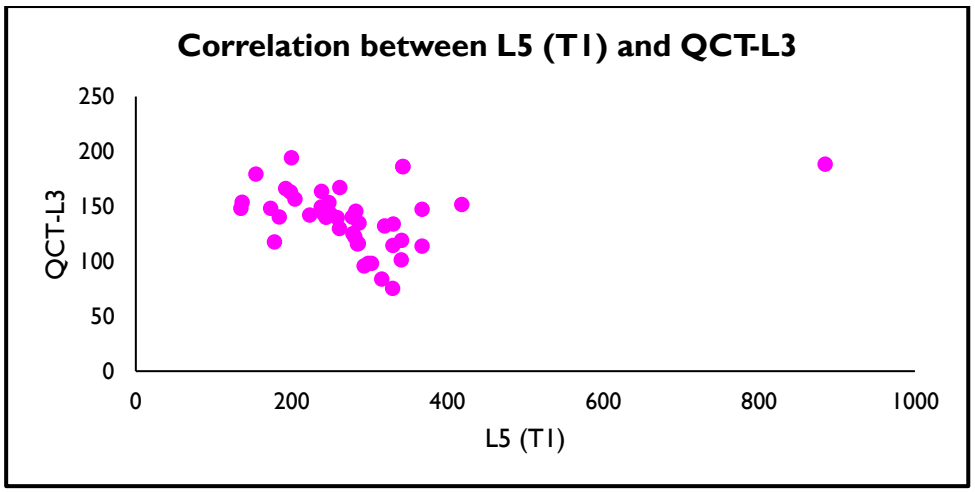

Graph 5.96: The Scatter graph shows correlation between L5 (T1) and QCT-L3

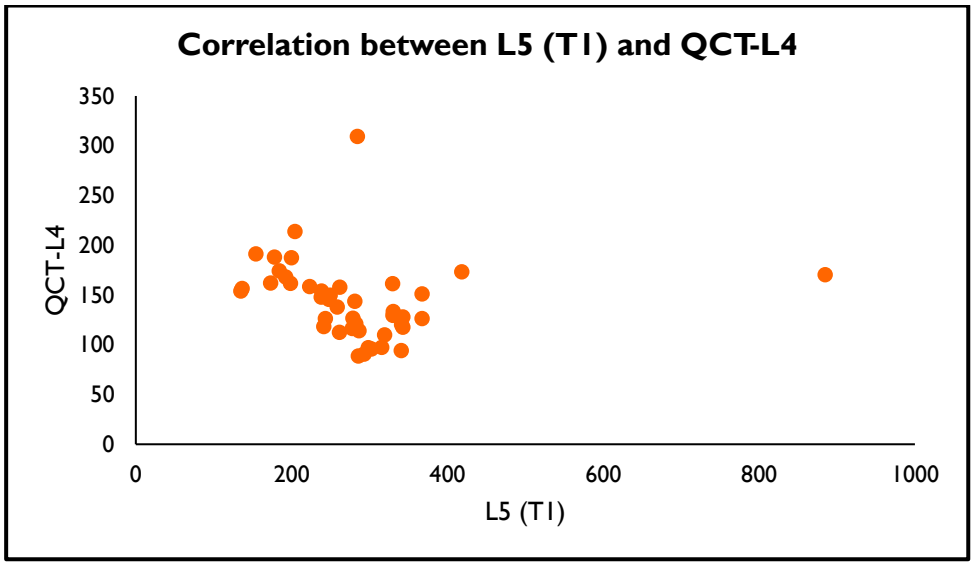

Graph 5.97: The Scatter graph shows correlation between L5 (T1) and QCT-L4

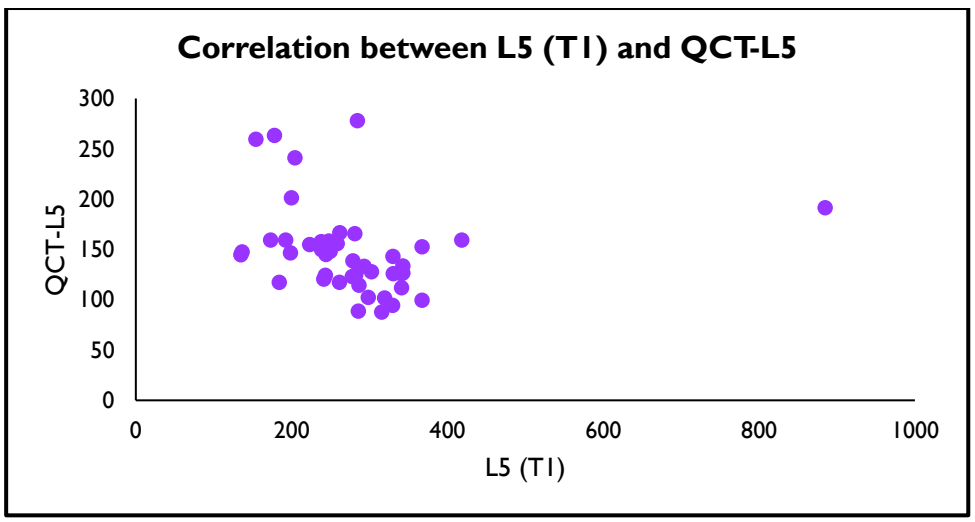

Graph 5.98: The Scatter graph shows correlation between L5 (T1) and QCT-L5

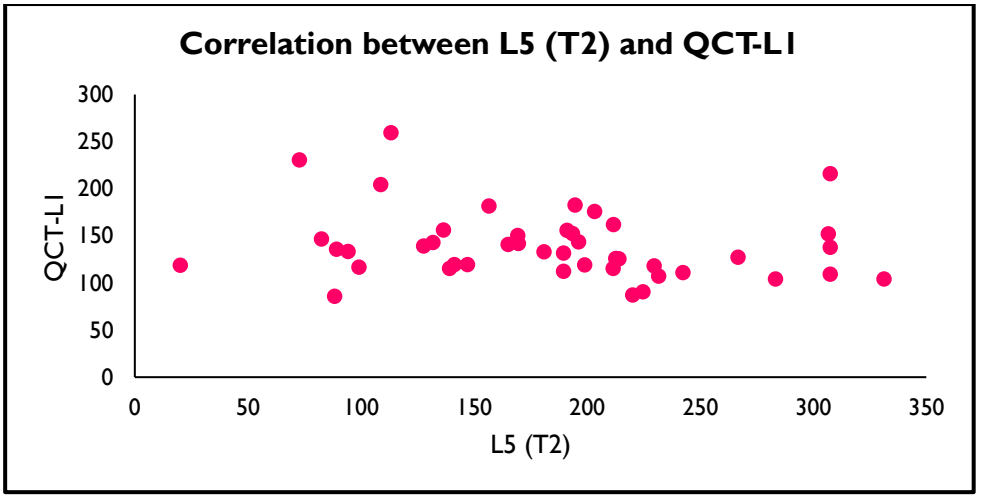

Graph 5.99: The Scatter graph shows correlation between L5 (T2) and QCT-L1

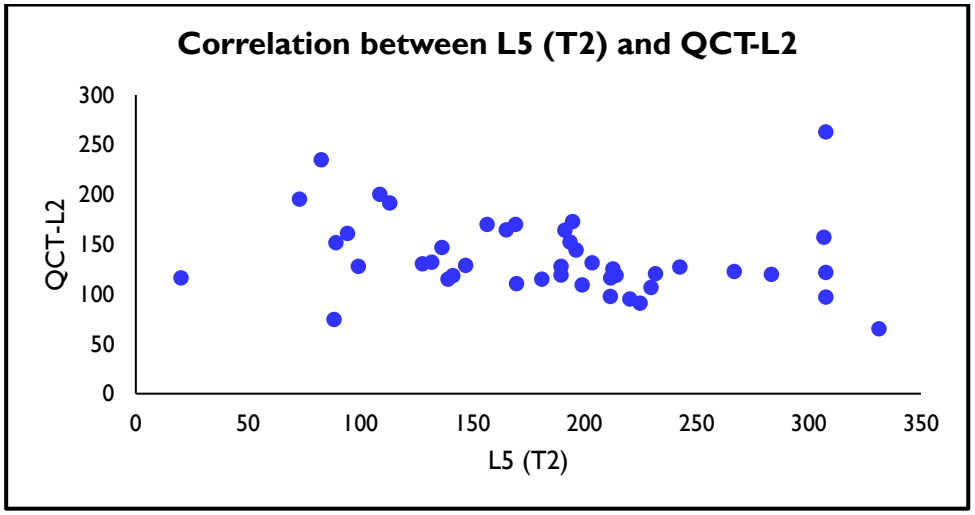

Graph 5.100: The Scatter graph shows correlation between L5 (T2) and QCT-L2

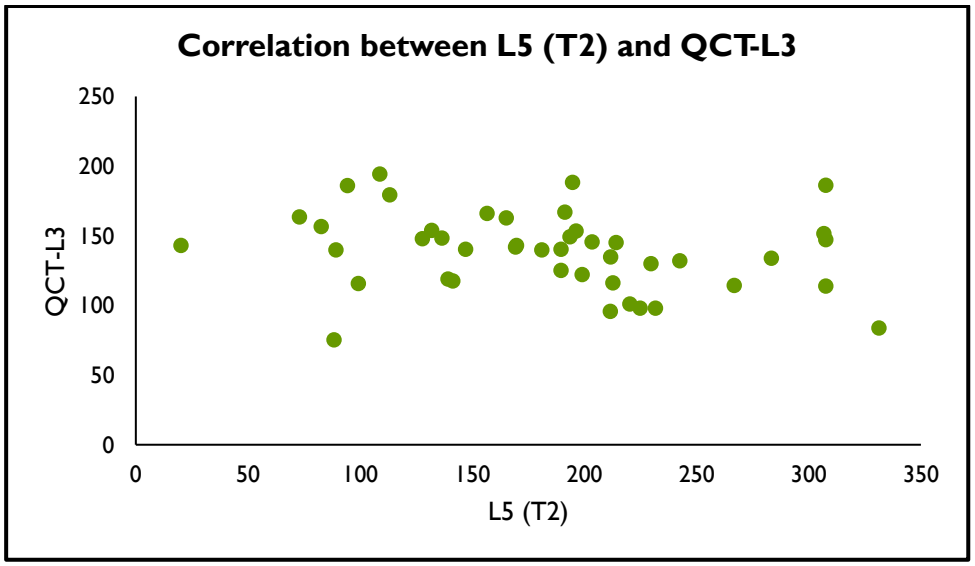

Graph 5.101: The Scatter graph shows correlation between L5 (T2) and QCT-L3

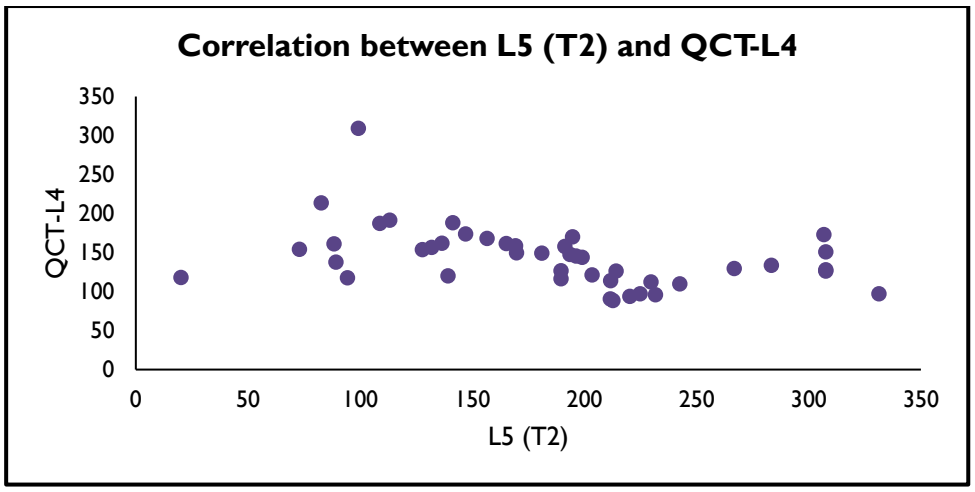

Graph 5.102: The Scatter graph shows correlation between L5 (T2) and QCT-L4

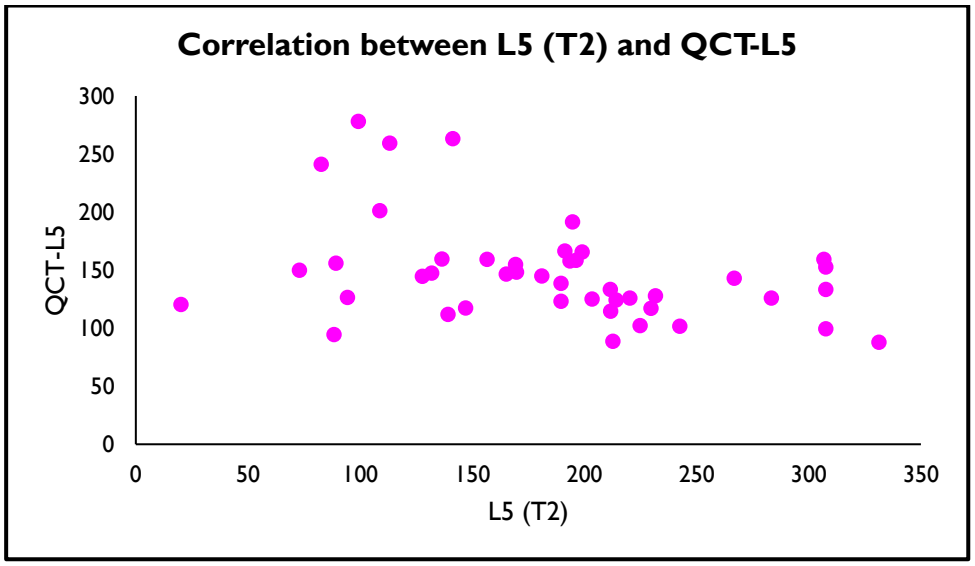

Graph 5.103: The Scatter graph shows correlation between L5 (T2) and QCT-L5

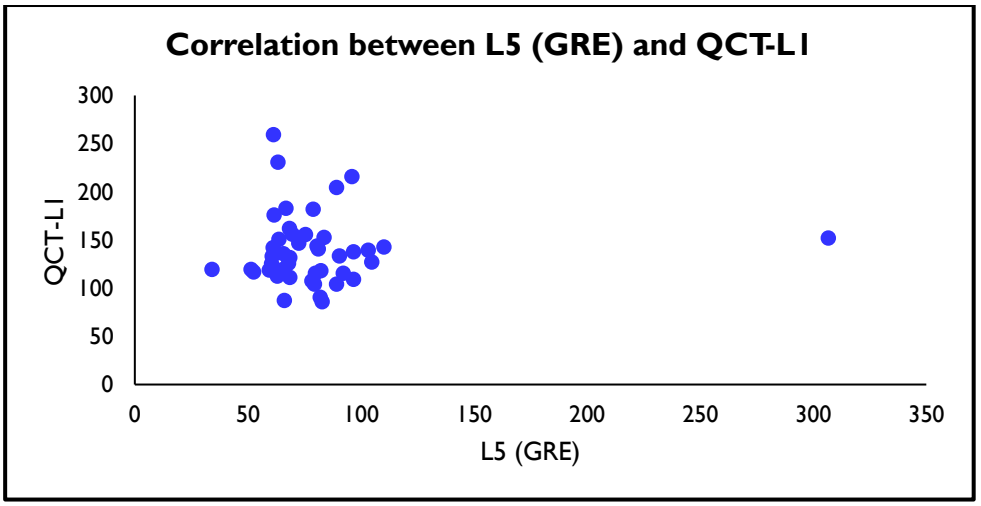

Graph 5.104: The Scatter graph shows correlation between L5 (GRE) and QCT-L1

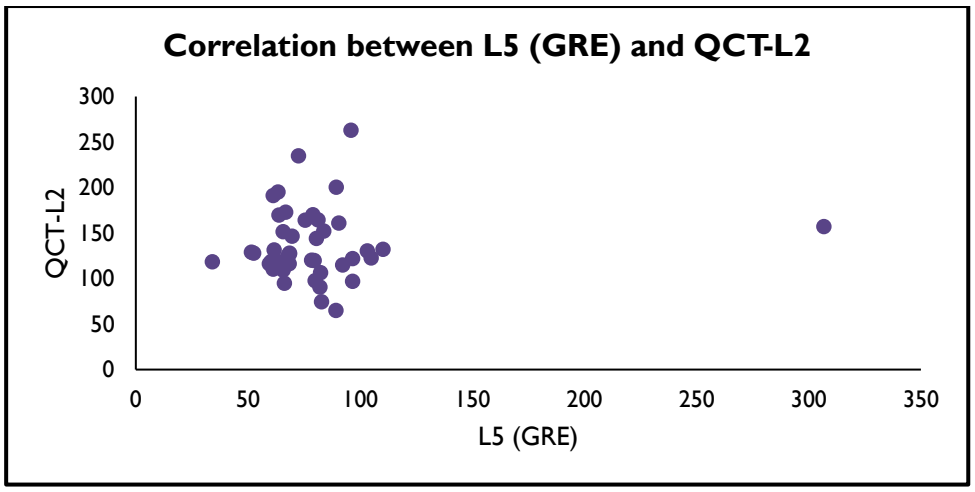

Graph 5.105: The Scatter graph shows correlation between L5 (GRE) and QCT-L2

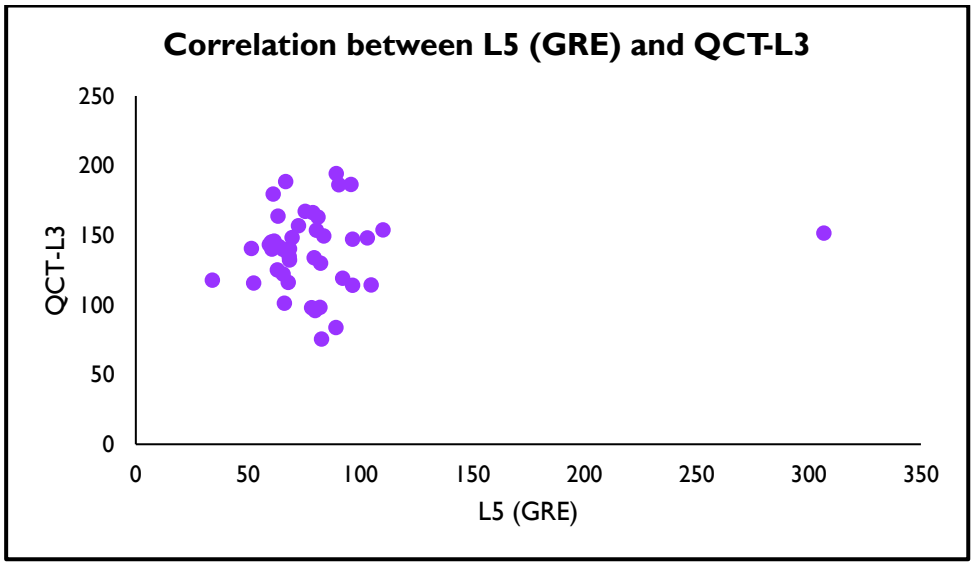

Graph 5.106: The Scatter graph shows correlation between L5 (GRE) and QCT-L3

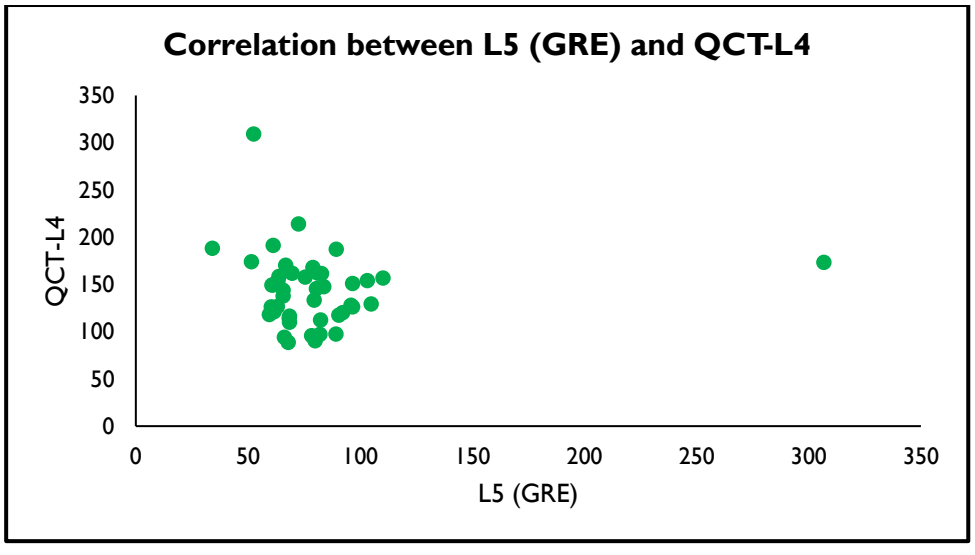

Graph 5.107: The Scatter graph shows correlation between L5 (GRE) and QCT-L4

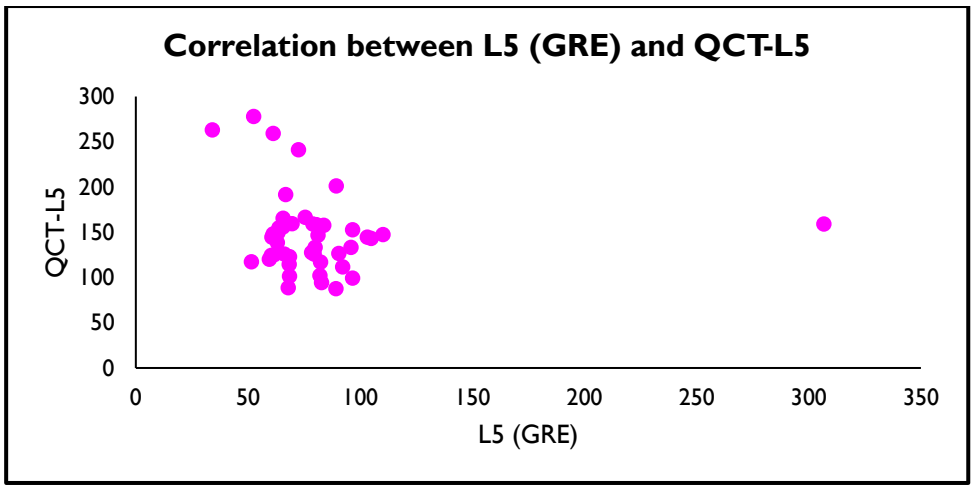

Graph 5.108: The Scatter graph shows correlation between L5 (GRE) and QCT-L5

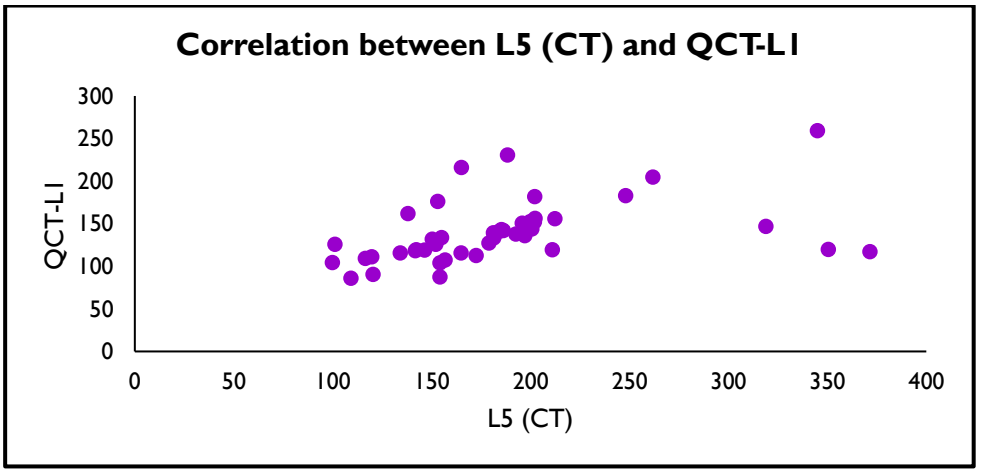

Graph 5.109: The Scatter graph shows correlation between L5 (CT) and QCT-L1

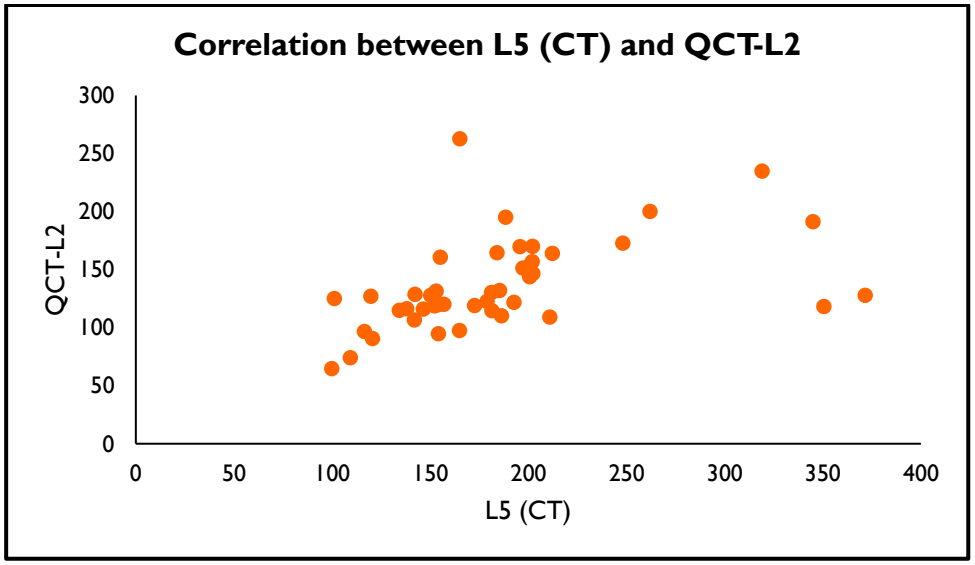

Graph 5.110: The Scatter graph shows correlation between L5 (CT) and QCT-L2

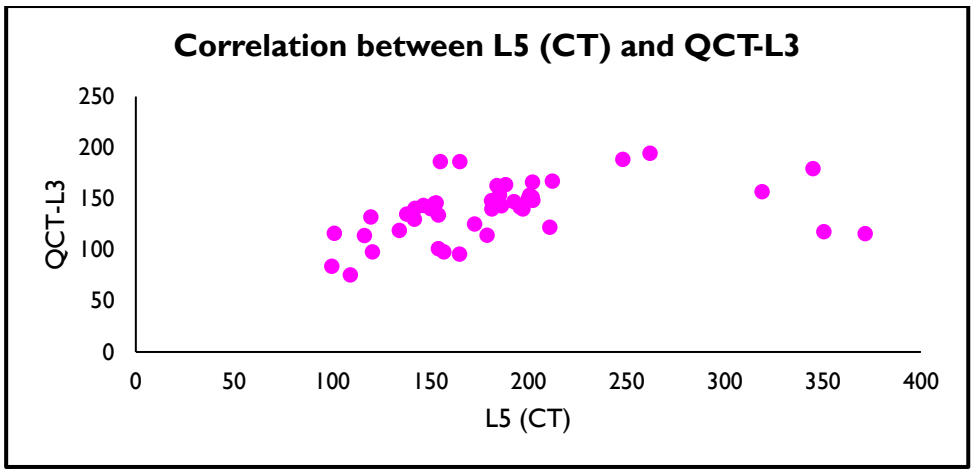

Graph 5.111: The Scatter graph shows correlation between L5 (CT) and QCT-L4

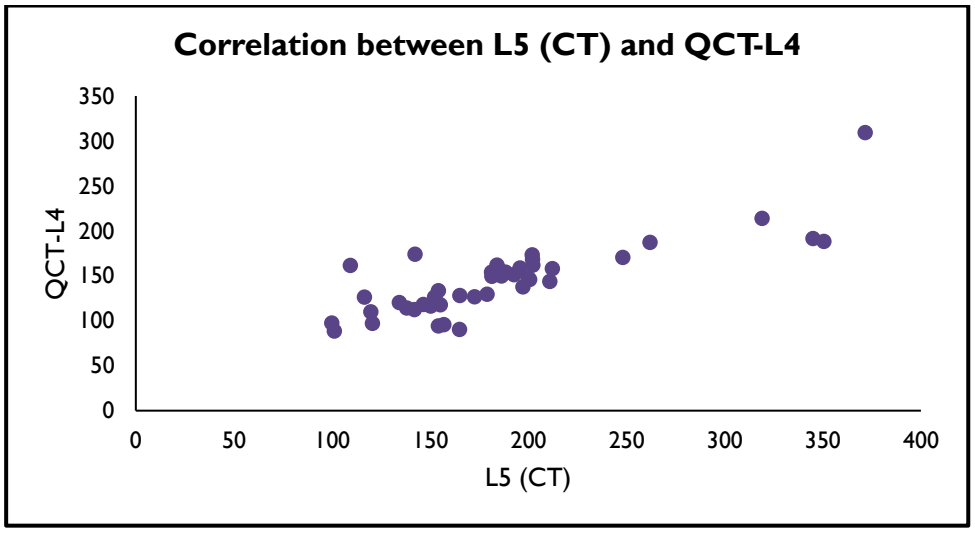

Graph 5.112: The Scatter graph shows correlation between L5 (CT) and QCT-L4

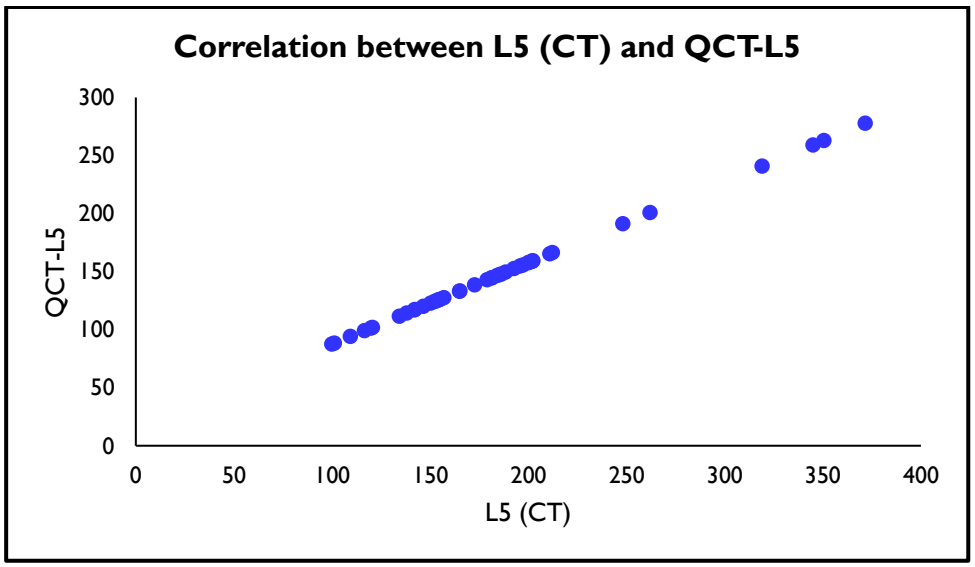

Graph 5.113: The Scatter graph shows correlation between L5 (CT) and QCT-L5

4. DISCUSSION

The objective of this prospective cross-sectional study, which was carried out at Teerthanker Mahaveer Hospital and Research Centre in Moradabad, was to compare computed tomography (CT) and 1.5 Tesla magnetic resonance imaging (MRI) in a population from Western Uttar Pradesh in order to quantitatively estimate bone mineral density (BMD) in the lumbar spine. With an emphasis on diagnosing osteoporosis, the study evaluated imaging parameters (Hounsfield Units [HU], T1-weighted, T2-weighted, and gradient echo [GRE] signal intensities) and their relationship with quantitative computed tomography (QCT)-derived BMD values. The results are analyzed in light of the literature study, emphasizing their parallels, divergences, and additions to the corpus of current knowledge.

Comparison of Imaging Parameters Across Gender

The imaging parameters (T1, T2, GRE, HU) and QCT-derived BMD values throughout lumbar levels (L1-L5) did not differ significantly ($p > 0.05$) between males and females, according to the study. In contrast to previous studies that indicate gender-specific differences, this is consistent with other findings from the literature. In contrast to dual-energy X-ray absorptiometry (DEXA), Xu et al. (2018) reported a higher detection rate of osteoporosis in men using QCT, indicating that the sensitivity of QCT to trabecular bone alterations may show gender-specific patterns not seen in our investigation. Similarly, Hammood et al. (2023) discovered that QCT was better than DEXA at identifying osteoporosis in postmenopausal women, suggesting that there may be gender-related variations in the measurement of bone density. According to the limitations, the small sample size (n=44) or the homogeneity of the regional population may have contributed to the lack of gender differences in our study by failing to detect modest differences observed in larger or more diverse cohorts.

Age-Related Differences in Imaging Parameters and BMD

Imaging parameters (L1-T1, L1-T2, L1-CT, L2-T1, L2-T2, L2-CT, L3-CT, L4-T2, L5-T2) and QCT-derived BMD values (QCT-L1, QCT-L2, QCT-L3) varied significantly ($p < 0.05$) among age groups. Numerous researches in the literature are in agreement with this conclusion. Our finding of age-related reductions in CT-based parameters is supported by Lee et al. (2013), who showed a fall in HU values with increasing age, associated with decreased BMD. In a similar vein, Raghu et al. (2021) discovered that postmenopausal women had a significantly lower bone mineral density (BMD) than premenopausal women. They attributed this to age-related bone loss, specifically after menopause. The age-related variations in MRI parameters (T1 and T2 signal intensities) in our study are consistent with the findings of Shayganfar et al. (2019) and Saad et al. (2019), who showed that age-related decreases in bone density are reflected in the negative correlation between MRI-based M-scores and DEXA T-scores. These results highlight the ability of both CT and MRI to identify age-related bone alterations, with MRI providing a radiation-free option and QCT enabling accurate volumetric BMD measurements.

Correlation Between Imaging Parameters and QCT-Derived BMD

Imaging parameters and QCT-derived BMD were found to be significantly correlated by the study's Pearson correlation analysis. In particular, CT-derived HU values were positively linked with QCT-BMD at all lumbar levels, but T1 and T2 signal intensities exhibited negative correlations with QCT values at different lumbar levels (e.g., L1-T1 with QCT-L1, L3, L4, L5; L2-T2 with QCT-L4, L5). These results are in good agreement with previous research. According to Raushan Kumar et al. (2018), MRI is useful for assessing BMD because it is non-ionizing. They found that T1 and T2 signal intensities rose when BMD decreased. Similarly, Liu et al. (2023) discovered a strong association between fat fraction, MRI R2* values, and QCT-derived BMD, indicating MRI's further use in osteoporosis assessment. Our significant HU-QCT correlations were supported by Choi et al. (2016) and Kim et al. (2019), who showed substantial correlations between HU and DEXA-derived BMD on the CT side, especially in non-degenerative spines. The usefulness of HU in opportunistic osteoporosis screening using abdominal CT scans was further confirmed by Pickhardt et al. (2013), supporting our conclusions that CT-based HU measures are accurate for determining BMD. The negative correlations between MRI signal intensities (T1, T2) and QCT-BMD in our investigation, however, are in contrast to Koyama et al. (2013), who discovered that T1-weighted imaging was quite effective (93.8%) at distinguishing between osteoporotic and normal vertebrae. This disparity could result from variations in MRI procedures (for example, Koyama's study included diffusion-weighted imaging) or our study's emphasis on a wider range of lumbar levels, which could lessen the effects of certain signal intensities. Furthermore, Bandirali et al. (2015) found a strong relationship between MRI signal-to-noise ratio (SNR) and DEXA bone mineral density (BMD), with an M-score threshold that had a 90% specificity rate in identifying osteoporosis. These results are supported by our study's more comprehensive correlation methodology (T1, T2, GRE vs. QCT), which also raises the possibility that particular sequences or scoring techniques may affect how well an MRI can diagnose a patient.

Gender Prediction Accuracy

Based on imaging characteristics and QCT-BMD, the binary logistic regression model demonstrated an overall gender prediction accuracy of 50%, with 0% accuracy for males and 100% accuracy for females. Due to the short sample size or uneven representation of gender-specific bone alterations, this glaring discrepancy raises the possibility of biases in the model or sample features. Though research like Schreiber et al. (2011) and Zou et al. (2019) highlight HU's reliability for BMD assessment without specifically addressing gender prediction, the literature provides few direct comparisons for gender

prediction models. As suggested by Hammood et al. (2023) and Saad et al. (2019), our finding of perfect female prediction accuracy might be the result of greater correlations between imaging parameters and BMD in females, especially postmenopausal women. The male cohort's less noticeable BMD changes or a lack of male-specific data may be the cause of the zero accuracy for men, which calls for more research.

Advantages of MRI Over CT and DEXA

Since MRI doesn't use ionizing radiation, one of its main goals was to examine its contribution to BMD assessment. Our results corroborate those of Raushan Kumar et al. (2018) and Shayganfar et al. (2019), who emphasized the potential of MRI as a secure substitute for CT and DEXA. According to Liu et al. (2023), the negative correlations seen between T1/T2 signal intensities and QCT-BMD imply that MRI can identify bone marrow alterations (such as elevated fat content) linked to osteoporosis. Our favorable HU-QCT correlations, on the other hand, show that QCT's volumetric BMD values are consistent with Yu et al. (2012), who discovered that QCT was more stable than DEXA over a range of body compositions. Although QCT has better sensitivity for trabecular bone (Xu et al., 2018; Hammood et al., 2023), MRI is better for repeated evaluations because it doesn't use radiation, especially for younger patients or those who need long-term monitoring.

5. CONCLUSION

"The study's two main goals were **(1) to use CT and MRI to evaluate the lumbar spine across genders in the Western UP population and (2) to diagnose osteoporosis by comparing MRI T1, T2, and GRE signal intensity values with QCT, Hounsfield Unit (HU), and BMD values of CT"**

"There were no significant gender-based differences ($p > 0.05$) between males and females in the imaging parameters (T1, T2, GRE, HU) or QCT-derived BMD values across lumbar levels (L1-L5) with respect to the first goal. It would appear from this that gender had no discernible effect on lumbar spine BMD measures using CT or MRI in the population under study. However, the gender prediction binary logistic regression model had a 50% overall accuracy, with 100% accuracy for females and 0% for males. This suggests that there may be limitations in identifying variations in BMD that are specific to males, most likely because of the small sample size (n=44) or the homogeneity of the regional population"

"The study showed a strong relationship between QCT-derived BMD values and MRI signal intensities (T1, T2, and GRE) for the second goal. In particular, CT-derived HU values exhibited positive correlations with QCT-BMD across all lumbar levels, but T1 and T2 signal intensities were negatively linked with QCT-BMD at different lumbar levels (e.g., L1-T1 with QCT-L1, L3, L4, L5; L2-T2 with QCT-L4, L5). These results are consistent with the literature, demonstrating the accuracy of CT in measuring BMD using HU and QCT as well as the capacity of MRI to identify bone marrow alterations linked to decreased BMD, such as increased fat content. The inverse relationship between MRI signal intensities and BMD emphasizes how sensitive MRI is to osteoporotic alterations, providing a radiation-free substitute for CT and DEXA in the measurement of BMD"

The impact of aging on bone density and the ability of both modalities to detect these changes were further highlighted by the age-related differences in both imaging parameters (L1-T1, L1-T2, L1-CT, L2-T1, L2-T2, L2-CT, L3-CT, L4-T2, L5-T2) and QCT-BMD (QCT-L1, QCT-L2, QCT-L3).

"The study also examined the necessity of assessing MRI's role in determining BMD because it doesn't use ionizing radiation. Particularly for populations that need frequent evaluations, like younger patients or those undergoing long-term monitoring, the results validate MRI as a feasible and secure substitute for CT and DEXA. Together with QCT's high sensitivity for evaluating trabecular bone, the strong correlations between MRI parameters and QCT-BMD support MRI's diagnostic value in osteoporosis assessment"

"In summary, this study effectively showed that there are no discernible gender variations in the effectiveness of CT and MRI in evaluating lumbar spine BMD in the population of Western Uttar Pradesh. When diagnosing osteoporosis, the T1, T2, and GRE signal intensities from MRI and the HU and QCT-BMD values from CT offer complimentary information, with MRI providing a radiation-free benefit. These results demonstrate the reliability of QCT in volumetric BMD estimation and add to the increasing body of evidence to support the use of MRI in BMD evaluation methods, especially for osteoporosis diagnosis"

The following points summarize the significant differences, relationships, and lack of relationships among imaging parameters and bone mineral density (BMD) in the lumbar spine as derived from the conclusion of the thesis:

Significant Differences:

Age-Related Differences: "Significant differences ($p < 0.05$) were observed in imaging parameters across lumbar levels (L1-T1, L1-T2, L1-CT, L2-T1, L2-T2, L2-CT, L3-CT, L4-T2, L5-T2) and QCT-derived BMD values (QCT-L1, QCT-L2, QCT-L3) among different age groups, indicating age influences bone density measurements"

Significant Relationships:

MRI Signal Intensities and QCT-BMD: "T1 and T2 signal intensities showed significant negative correlations ($p < 0.05$)

with QCT-derived BMD at various lumbar levels (e.g., L1-T1 with QCT-L1, L3, L4, L5; L2-T2 with QCT-L4, L5), suggesting MRI's sensitivity to bone marrow changes associated with osteoporosis"

CT Hounsfield Units (HU) and QCT-BMD: "CT-derived HU values were positively correlated ($p < 0.05$) with QCT-BMD across all lumbar levels (L1-L5), confirming CT's reliability in quantifying BMD"

No Significant Relationships or Differences:

Gender-Based Differences: "No significant differences ($p > 0.05$) were found in imaging parameters (T1, T2, GRE, HU) or QCT-derived BMD values across lumbar levels (L1-L5) between males and females, indicating gender does not significantly affect BMD measurements in this population"

Gender Prediction Limitations: "The binary logistic regression model showed 0% accuracy in predicting male gender based on imaging parameters and QCT-BMD, suggesting no reliable relationship for male-specific BMD variations (though 100% accuracy was achieved for females)"

6. LIMITATIONS

1. Small Sample Size: According to Slovin's formula, there were only 44 participants in the study. The findings may not be as broadly applicable to a larger population due to the very small sample size, especially when it comes to identifying minute variations in bone mineral density (BMD) between age or gender groups.

2. Geographic Restrictions: The study was limited to one location (Teerthanker Mahaveer Hospital, Moradabad) and focused on the people of Western Uttar Pradesh. Given that BMD and osteoporosis prevalence might differ among populations due to genetic, environmental, and lifestyle variables, this geographic restriction may result in regional bias.

3. Convenience Sampling: Selection bias may be introduced when convenient sampling is used to choose participants. The results may be skewed and less applicable to other populations if this non-random sampling technique produces a non-representative sample.

4. Limitations of the Exclusion Criteria: Although the study did not include patients with major spinal pathologies, recent surgeries, or spinal deformities, it did not take into consideration other possible confounders like the use of medications (like corticosteroids) or comorbid conditions (like diabetes, thyroid disorders) that may have an impact on BMD and thus affect the accuracy of the results.

5. Absence of Longitudinal Data: The research used a cross-sectional design, which gives a momentary picture of BMD. This method reduces the study's capacity to forecast long-term results by making it more difficult to evaluate changes in BMD over time or to prove a link between imaging parameters and the onset of osteoporosis.

7. FUTURE SCOPE

1. Integration of sophisticated MRI Techniques: To increase the precision of BMD assessment, future studies could investigate sophisticated MRI sequences such ultra-short echo time (UTE) or zero echo time (ZTE) imaging. These methods might improve the visibility of trabecular and cortical bone structures, thereby providing a more accurate radiation-free substitute for CT and DEXA.

2. Larger and Diverse Population Studies: A very small sample of 44 patients from Western Uttar Pradesh was used in this investigation. The results might be validated and their wider relevance established by expanding the study to encompass bigger and more diverse populations from other geographic locations and ethnic groups, especially in detecting age- and gender-specific BMD differences.

3. Creation of Automated Analysis Tools: Upcoming research may concentrate on creating automated tools for evaluating CT and MRI data in order to calculate BMD. Algorithms using artificial intelligence and machine learning could be trained to recognize minute variations in Hounsfield Units and signal strength, increasing diagnostic effectiveness and lowering interobserver variability.

4. Longitudinal Studies for Disease Progression: By employing both MRI and CT to monitor changes in bone mineral density over time, longitudinal studies may shed light on how osteopenia and osteoporosis develop. This would make it easier to comprehend how predictive MRI-based indicators (such the M-score) are for early intervention when compared to QCT and DEXA.

5. Comparative Studies with Emerging Modalities: Future studies could examine how well MRI and QCT work in comparison to other modalities such as dual-energy CT or high-resolution peripheral quantitative CT (HR-pQCT). These investigations could identify the best imaging method for assessing BMD in terms of precision, economy, and patient safety, especially for high-risk populations like postmenopausal women.

REFERENCES

[1] Imaging C. History of the CT scan [Internet]. Mobile CT Rental - Mobile Imaging Rental And Lease. Catalina Imaging Inc.; 2019 [cited 2025 May 26]. Available from: https://catalinaimaging.com/history-ct-scan/

[2] Honorary Senior Lecturer Medical Imaging and Radiation Sciences Medical Image Optimization and Perception Group Faculty of Health Sciences University of Sydney Sydney Australia Adjunct Associate Professor Department of Radiatio Euclid Seeram. Computed tomography - Elsevier eBook on vitalsource (retail access card): Physical principles, clinical applications, and quality control. 3rd ed. Saunders; 2008.

[3] Kranioti EF, Bonicelli A, García-Donas JG. Bone-mineral density: clinical significance, methods of quantification and forensic applications. Res Rep Forensic Med Sci [Internet]. 2019;9:9–21. Available from: http://dx.doi.org/10.2147/rrfms.s164933

[4] Kenhub.com. [cited 2025 May 26]. Available from: https://www.kenhub.com/en/library/anatomy/bones.

[5] Kenhub.com. [cited 2025 May 26]. Available from: https://www.kenhub.com/en/library/anatomy/histology-of-bone.

[6] Osteopenia [Internet]. Cleveland Clinic. 2021 [cited 2025 May 26]. Available from: https://my.clevelandclinic.org/health/diseases/21855-osteopenia

[7] Sözen T, Özışık L, Başaran NÇ. An overview and management of osteoporosis. Eur J Rheumatol [Internet]. 2017;4(1):46–56. Available from: http://dx.doi.org/10.5152/eurjrheum.2016.048

[8] Engelke K, Adams JE, Armbrecht G, Augat P, Bogado CE, Bouxsein ML, et al. Clinical use of quantitative computed tomography and peripheral quantitative computed tomography in the management of osteoporosis in adults: the 2007 ISCD Official Positions. J Clin Densitom [Internet]. 2008;11(1):123–62. Available from: http://dx.doi.org/10 .1016/j.jocd.2007.12.010

[9] Lorente-Ramos R, Azpeitia-Armán J, Muñoz-Hernández A, García-Gómez JM, Díez-Martínez P, Grande-Bárez M. Dual-energy x-ray absorptiometry in the diagnosis of osteoporosis: a practical guide. AJR Am J Roentgenol [Internet]. 2011;196(4):897–904. Available from: http://dx.doi.org/10.2214/AJR.10.5416

[10] Centre PEDS. T SCORE. In: Available: Providence Endocrine & Diabetes Specialty Centre. 2022.

[11] Americanbonehealth.org. [cited 2025 May 26]. Available from: https://americanbonehealth.org/bone-density/understanding-the-

[12] Gogate Y, Bhadada SK. FRAX: Facts and fantasy. Indian J Endocrinol Metab [Internet]. 2012;16(Suppl 2):S224-6. Available from: http://dx.doi.org/10.4103/2230-8210.104044

[13] Perry S. Magnetic resonance imaging : principles, methods, and techniques. Medical Physics Pub. 2000;173.

[14] Westbrook C, Roth CK. MRI in Practice. 4th ed. Hoboken, NJ: Wiley-Blackwell; 2013.

[15] Schreiber JJ, Anderson PA, Rosas HG, Buchholz AL, Au AG. Hounsfield units for assessing bone mineral density and strength: a tool for osteoporosis management. J Bone Joint Surg Am [Internet]. 2011;93(11):1057–63. Available from: http://dx.doi.org/10.2106/JBJS.J.00160

[16] Yu EW, Thomas BJ, Brown JK, Finkelstein JS. Simulated increases in body fat and errors in bone mineral density measurements by DXA and QCT. J Bone Miner Res [Internet]. 2012;27(1):119–24. Available from: http://dx.doi.org/10.1002/jbmr.506

[17] Koyama H, Yoshihara H, Kotera M, Tamura T, Sugimura K. The quantitative diagnostic capability of routine MR imaging and diffusion-weighted imaging in osteoporosis patients. Clin Imaging [Internet]. 2013;37(5):925–9. Available from: http://dx.doi.org/10.1016/j.clinimag.2013.05.001

[18] Youn I, Lee HY, Kim JK. Correlation between vertebral marrow fat fraction measured using Dixon quantitative chemical shift MRI and BMD value on dual-energy X-ray absorptiometry. J Korean Soc Magn Reson Med [Internet]. 2012;16(1):16. Available from: http://dx.doi.org/10.13104/jksmrm.2012.16.1.16

[19] Pickhardt PJ, Pooler BD, Lauder T, del Rio AM, Bruce RJ, Binkley N. Opportunistic screening for osteoporosis using abdominal computed tomography scans obtained for other indications. Ann Intern Med [Internet]. 2013;158(8):588–95. Available from: http://dx.doi.org/10.7326/0003-4819-158-8-201304160-00003

[20] Emohare O, Cagan A, Morgan R, Davis R, Asis M, Switzer J, et al. The use of computed tomography attenuation to evaluate osteoporosis following acute fractures of the thoracic and lumbar vertebra. Geriatr Orthop Surg Rehabil [Internet]. 2014;5(2):50–5. Available from: http://dx.doi.org/10.1177/2151458514525042

[21] Bandirali M, Di Leo G, Papini GDE, Messina C, Sconfienza LM, Ulivieri FM, et al. A new diagnostic score to detect osteoporosis in patients undergoing lumbar spine MRI. Eur Radiol [Internet]. 2015;25(10):2951–9. Available from: http://dx.doi.org/10.1007/s00330-015-3699-y

[22] Choi MK, Kim SM, Lim JK. Diagnostic efficacy of Hounsfield units in spine CT for the assessment of real bone mineral density of degenerative spine: correlation study between T-scores determined by DEXA scan and Hounsfield units from CT. Acta Neurochir (Wien) [Internet]. 2016;158(7):1421–7. Available from: http://dx.doi.org/ 10.1007/s00701-016-2821-5

[23] Kumar R, Dahiya M, Yadav K, Dahiya R. Comparative study of DEXA and 1.5 Tesla MRI in quantitative estimation of bone mineral density in lumbar spine. 2020 [cited 2025 May 26]; Available from: https://www.ijrrjournal. com/IJRR_Vol.6_Issue.8_Aug2019/IJRR0010.pdf

[24] Xu X-M, Li N, Li K, Li X-Y, Zhang P, Xuan Y-J, et al. Discordance in diagnosis of osteoporosis by quantitative computed tomography and dual-energy X-ray absorptiometry in Chinese elderly men. J Orthop Translat [Internet]. 2019;18:59–64. Available from: http://dx.doi.org/10.1016/j.jot.2018.11.003

[25] Shayganfar A, Khodayi M, Ebrahimian S, Tabrizi Z. Quantitative diagnosis of osteoporosis using lumbar spine signal intensity in magnetic resonance imaging. Br J Radiol [Internet]. 2019;92(1097):20180774. Available from: http://dx.doi.org/10.1259/bjr.20180774

[26] Saad MM, Ahmed AT, Mohamed KE, Habba MR. Role of lumbar spine signal intensity measurement by MRI in the diagnosis of osteoporosis in post-menopausal women. Egypt J Radiol Nucl Med [Internet]. 2019;50(1). Available from: http://dx.doi.org/10.1186/s43055-019-0046-3

[27] Kim KJ, Kim DH, Lee JI, Choi BK, Han IH, Nam KH. Hounsfield units on lumbar computed tomography for predicting regional bone mineral density. Open Med (Warsz) [Internet]. 2019;14(1):545–51. Available from: http://dx.doi.org/10.1515/med-2019-0061

[28] Zou D, Li W, Xu F, Du G. Use of Hounsfield units of S1 body to diagnose osteoporosis in patients with lumbar degenerative diseases. Neurosurg Focus [Internet]. 2019;46(5):E6. Available from: http://dx.doi.org/10.3171/2019.2.focus18614

[29] Raghu SR, Sachin T, ShanKa Ra K, Ran BRS. Evaluation of bone mineral density using quantitative computed tomography in pre- and post-menopausal women: A retrospective cross-sectional study [Internet]. Available from: https://www.ijars.net/articles/PDF/2599/46826_CE[Ra1]_F(SHU)_PF1(AG_SHU)_PFA(SHU)_PB(AG_SHU)_PN(SHU).pdf

[30] Elarjani T, Warner T, Nguyen K, Nguyen S, Urakov TM. Quantifying bone quality using computed tomography Hounsfield units in the mid-sagittal view of the lumbar spine. World Neurosurg [Internet]. 2021;151:e418–25. Available from: http://dx.doi.org/10.1016/j.wneu.2021.04.051

[31] Buenger F, Sakr Y, Eckardt N, Senft C, Schwarz F. Correlation of quantitative computed tomography derived bone density values with Hounsfield units of a contrast medium computed tomography in 98 thoraco-lumbar vertebral bodies. Arch Orthop Trauma Surg [Internet]. 2022;142(11):3335–40. Available from: http://dx.doi.org/10.1007/ s00402-021-04184-5

[32] Liu Z, Huang D, Jiang Y, Ma X, Zhang Y, Chang R. Correlation of R2* with fat fraction and bone mineral density and its role in quantitative assessment of osteoporosis. Eur Radiol [Internet]. 2023;33(9):6001–8. Available from: http://dx.doi.org/10.1007/s00330-023-09599-9

[33] Hammood AH, Ahmed SB, Hassan QA. Comparison between quantitative computed tomography and dual-energy X-Ray absorptiometry in the detection of osteoporosis in postmenopausal women. Al-Kindy Col Med J [Internet]. 2023 [cited 2025 May 26];19(1):90–4. Available from: https://jkmc.uobaghdad.edu.iq/index.php/MEDICAL/article/ view/864

[34] Pu M, Zhang B, Zhu Y, Zhong W, Shen Y, Zhang P. Hounsfield unit for evaluating bone mineral density and strength: Variations in measurement methods. World Neurosurg [Internet]. 2023;180:e56–68. Available from: http://dx.doi.org/10.1016/j.wneu.2023.07.146

[35] Bisht A. Assessment of lumbar disc degeneration in post menopause women's using 1.5t MRI: A review study. African Journal of Biomedical Research [Internet]. 2024 [cited 2025 Jun 12];27(3S):438–42. Available from: https://africanjournalofbiomedicalresearch.com/index.php/AJBR/article/view/2015